ผลของไอออนของสังกะสีต่อการเปลี่ยนแปลงจากเซลล์บุผิวเป็นเซลล์มีเซนไคม์และความเป็นเซลล์มะเร็งต้นกำเนิดของเซลล์มะเร็งปอด

นางสาวชวนพิศ นิลสันเทียะ

วิทยานิพนธ์นี้เป็นส่วนหนึ่งของการศึกษาตามหลักสูตรปริญญาเภสัชศาสตรดุษฎีบัณฑิต
สาขาวิชาเภสัชวิทยาและพิษวิทยา ภาควิชาเภสัชวิทยาและสรีรวิทยา
คณะเภสัชศาสตร์ จุฬาลงกรณ์มหาวิทยาลัย
ปีการศึกษา 2559

EFFECTS OF ZINC ION ON EPITHELIAL TO MESENCHYMAL TRANSITION AND CANCER STEMNESS OF LUNG CANCER CELLS

Miss Chuanpit Ninsontia

A Dissertation Submitted in Partial Fulfillment of the Requirements
for the Degree of Doctor of Philosophy Program in Pharmacology and Toxicology
Department of Pharmacology and Physiology
Faculty of Pharmaceutical Sciences
Chulalongkorn University
Academic Year 2016

Thesis Title	EFFECTS OF ZINC ION ON EPITHELIAL TO MESENCHYMAL TRANSITION AND CANCER STEMNESS OF LUNG CANCER CELLS
By	Miss Chuanpit Ninsontia
Field of Study	Pharmacology and Toxicology
Thesis Advisor	Associate Professor Pithi Chanvorachote, Ph.D.
Thesis Co-Advisor	Professor rerum naturalium Regine Schneider-Stock, Ph.D.

Accepted by the Faculty of Pharmaceutical Sciences, Chulalongkorn University in Partial Fulfillment of the Requirements for the Doctoral Degree

.....Dean of the Faculty of Pharmaceutical Sciences
(Assistant Professor Rungpetch Sakulbumrungsil, Ph.D.)

THESIS COMMITTEE

.....Chairman
(Associate Professor Thongchai Sooksawate, Ph.D.)

.....Thesis Advisor
(Associate Professor Pithi Chanvorachote, Ph.D.)

.....Thesis Co-Advisor
(Professor rerum naturalium Regine Schneider-Stock, Ph.D.)

.....Examiner
(Associate Professor Suree Jianmongkol, Ph.D.)

.....Examiner
(Assistant Professor Rataya Luechapudiporn, Ph.D.)

.....External Examiner
(Siwanon Jirawatnotai, Ph.D.)

ชวนพิศ นิลสันเทียะ : ผลของไอออนของสังกะสีต่อการเปลี่ยนแปลงจากเซลล์บุผิวเป็นเซลล์มีเซนไคม์และความเป็นเซลล์มะเร็งต้นกำเนิดของเซลล์มะเร็งปอด (EFFECTS OF ZINC ION ON EPITHELIAL TO MESENCHYMAL TRANSITION AND CANCER STEMNESS OF LUNG CANCER CELLS) อ.ที่ปรึกษาวิทยานิพนธ์หลัก: รศ. ภก. ดร. ปิติ จันทร์วรโชติ, อ.ที่ปรึกษาวิทยานิพนธ์ร่วม: ศ. ดร. เรจิน่า ชไนเดอร์ สต๊อก, 177 หน้า.

การเปลี่ยนแปลงจากเซลล์บุผิวเป็นเซลล์มีเซนไคม์และความเป็นเซลล์มะเร็งต้นกำเนิดมีบทบาทสำคัญในการดำเนินไปของโรคและการแพร่กระจายของมะเร็ง แม้ว่าทั้งสองกระบวนการนี้จะมีลักษณะและวิถีในการความคุมที่จำเพาะ ความเป็นเซลล์มะเร็งต้นกำเนิดสามารถถูกกระตุ้นได้ในระหว่างกระบวนการเปลี่ยนแปลงจากเซลล์บุผิวเป็นเซลล์มีเซนไคม์ และเซลล์มะเร็งต้นกำเนิดมักแสดงลักษณะเฉพาะที่คล้ายคลึงกับเซลล์ที่มีการเปลี่ยนแปลงจากเซลล์บุผิวเป็นเซลล์มีเซนไคม์ หลักฐานงานวิจัยชี้ให้เห็นว่าในพลาสมาของผู้ป่วยโรคมะเร็งปอดมีระดับไอออนสังกะสีที่ต่ำกว่าคนปกติ ซึ่งแสดงให้เห็นถึงผลของไอออนสังกะสีที่อาจมีต่อโรคมะเร็ง ไอออนสังกะสีมีความสำคัญต่อกระบวนการทำงานของเซลล์และการส่งสัญญาณภายในเซลล์ เนื่องจากในปัจจุบันยังไม่มีหลักฐานเกี่ยวกับบทบาทของไอออนสังกะสีในการควบคุมการเปลี่ยนแปลงจากเซลล์บุผิวเป็นเซลล์มีเซนไคม์และความเป็นเซลล์มะเร็งต้นกำเนิด งานวิจัยนี้ได้แสดงให้เห็นเป็นครั้งแรกว่าไอออนสังกะสีมีผลที่ต่างกันต่อการเปลี่ยนแปลงจากเซลล์บุผิวเป็นเซลล์มีเซนไคม์และความเป็นเซลล์มะเร็งต้นกำเนิดของเซลล์มะเร็งปอด โดยพบว่าไอออนสังกะสีส่งเสริมการเปลี่ยนแปลงจากเซลล์บุผิวเป็นเซลล์มีเซนไคม์แต่ลดความเป็นเซลล์มะเร็งต้นกำเนิดของเซลล์มะเร็งปอด ในเซลล์ที่ได้รับสังกะสีตรวจพบการเพิ่มขึ้นของโปรตีนที่บ่งชี้ว่าเป็นเซลล์มีเซนไคม์ได้แก่ N-cadherin, vimentin, snail และ slug และพบการลดลงของโปรตีน E-cadherin ที่บ่งชี้ว่าเป็นเซลล์บุผิวซึ่งชี้ให้เห็นว่ามีการเหนี่ยวนำให้เกิดการเปลี่ยนแปลงจากเซลล์บุผิวเป็นเซลล์มีเซนไคม์ โดยเซลล์มะเร็งที่ได้รับสังกะสีมีลักษณะรูปร่างของเซลล์คล้ายเซลล์มีเซนไคม์และยังมีความสามารถในการเคลื่อนที่เพิ่มขึ้นอีกด้วย ในอีกแง่มุมหนึ่งไอออนของสังกะสีมีผลยับยั้งการเกิดก้อนมะเร็งในสภาวะแขวนลอย (tumor spheroid) ด้วยการลดระดับของโปรตีน CD133, ALDH1A1, Oct2, Nanog และ Sox2 ที่เป็นตัวบ่งชี้ความเป็นเซลล์มะเร็งต้นกำเนิด ในเชิงกลไกไอออนสังกะสีเหนี่ยวนำให้มีการเพิ่มขึ้นของ superoxide anion ภายในเซลล์ซึ่งส่งผลให้มีการเพิ่มขึ้นของโปรตีนที่บ่งชี้การเปลี่ยนแปลงจากเซลล์บุผิวเป็นเซลล์มีเซนไคม์และส่งเสริมการเคลื่อนที่ของเซลล์มะเร็ง การให้ตัวยับยั้งที่จำเพาะเจาะจงต่อ superoxide anion (MnTBAP) สามารถยับยั้งผลของไอออนสังกะสีในการเหนี่ยวนำการเพิ่มขึ้นของ superoxide anion ภายในเซลล์และการเปลี่ยนแปลงลักษณะของเซลล์จากเซลล์บุผิวเป็นเซลล์มีเซนไคม์ได้ และ MnTBAP ยังสามารถยับยั้งผลของไอออนสังกะสีในการกดการสร้างก้อนมะเร็งในสภาวะแขวนลอยและยับยั้งผลของไอออนสังกะสีในการการลดปริมาณโปรตีนที่บ่งชี้ความเป็นเซลล์มะเร็งต้นกำเนิดได้ นอกจากนี้ยังพบว่า superoxide anion ที่เกิดจากการเหนี่ยวนำของไอออนสังกะสีกดความเป็นเซลล์มะเร็งต้นกำเนิดผ่านทางวิถี PKCα/β-catenin โดย superoxide anion กระตุ้นการทำงานของโปรตีน PKCα ในการเติมหมู่ฟอสเฟสให้กับโปรตีน β-catenin จากนั้น β-catenin จะถูกส่งต่อไปทำลายโดยกระบวนการ ubiquitin-proteasome ไอออนสังกะสียังสามารถเร่งกระบวนการเติม ubiquitin บนโครงสร้างของ β-catenin ซึ่งกระบวนการนี้ถูกยับยั้งได้โดยการให้ตัวยับยั้งที่จำเพาะต่อ PKCα โดยสรุปงานวิจัยนี้ให้ข้อมูลใหม่ที่สำคัญเกี่ยวกับบทบาทของไอออนสังกะสีและกลไกในการควบคุมการเปลี่ยนแปลงจากเซลล์บุผิวเป็นเซลล์มีเซนไคม์และความเป็นเซลล์มะเร็งต้นกำเนิดของเซลล์มะเร็งปอดซึ่งเป็นสองปัจจัยสำคัญในการส่งเสริมให้เซลล์สมะเร็งมีพฤติกรรมก้าวร้าวและเกิดการแพร่กระจาย และการค้นพบนี้ยังช่วยให้เกิดความเข้าใจดีขึ้นในแง่ของชีววิทยาของเซลล์มะเร็งที่เกี่ยวกับแร่ธาตุที่จำเป็นต่อพฤติกรรมก้าวร้าวของเซลล์มะเร็ง

ภาควิชา	เภสัชวิทยาและสรีรวิทยา	ลายมือชื่อนิสิต	.....
สาขาวิชา	เภสัชวิทยาและพิษวิทยา	ลายมือชื่อ อ.ที่ปรึกษาหลัก	.....
ปีการศึกษา	2559	ลายมือชื่อ อ.ที่ปรึกษาร่วม	.....

5676451933 : MAJOR PHARMACOLOGY AND TOXICOLOGY
KEYWORDS: ZINC / EMT / CANCER STEM CELLS / STEMNESS / LUNG CANCER / METASTASIS / REACTIVE OXYGEN SPECIES

CHUANPIT NINSONTIA: EFFECTS OF ZINC ION ON EPITHELIAL TO MESENCHYMAL TRANSITION AND CANCER STEMNESS OF LUNG CANCER CELLS. ADVISOR: ASSOC. PROF. PITHI CHANVORACHOTE, Ph.D., CO-ADVISOR: PROF. RER. NAT. REGINE SCHNEIDER-STOCK, Ph.D., 177 pp.

Epithelial-to-mesenchymal transition (EMT) as well as cancer stem cells (CSCs) play critical roles in cancer progression and metastasis. Although these two events have distinct characteristics and molecular pathways, CSCs could be trigger during EMT process and CSCs were frequently found to possess EMT characteristics. Collective evidence showed that plasma level of zinc ion in the patients with lung cancer has significantly lower than that of normal subjects, suggesting the impact of zinc ion on the disease. Zinc ion implicates in many cellular processes and signaling of the cells; however, the regulatory role of zinc ion on EMT and CSCs are unknown. Herein, the present study has shown for the first time that zinc ion has converse effects on EMT and CSCs of lung cancer cells. While zinc ion enhances EMT phenotypes, it was shown to suppresses CSC program. For EMT, an increase in EMT markers including N-cadherin, vimentin, snail and slug and decrease of E-cadherin was observed in zinc ion-treated cells, indicating the induction of EMT with mesenchymal-like morphology and increased cancer cell motility. In contrast, zinc ion reduced tumor spheroid forming with the decreased expression of CSC markers (CD133 and ALDH1A1) and CSC transcription factors (Oct4, Nanog, and Sox2). For mechanistic approaches, zinc ion generated intracellular superoxide anion that increased the EMT proteins and promoted cell motility. Treatment with the specific superoxide anion inhibitor (MnTBAP) could reverse the effect of zinc ion on superoxide anion and EMT phenotypes. The decrease in tumor sphere formation and CSC markers in zinc ion-treated cells were also reversed by MnTBAP treatment. Moreover, this study found that superoxide anion generated by zinc ion suppressed CSCs through the PKCα/β-catenin dependent mechanism by activating PKCα which subsequently phosphorylated and mediated β-catenin degradation via the ubiquitin-proteasomal mechanism. Zinc ion has a capability to increase the β-catenin-ubiquitin complex which can be blocked by bisindolylmaleimide I (PKC inhibitor). In conclusion, this current study has addressed the novel important regulatory roles of zinc ion and underlying mechanisms in regulation of EMT and CSCs, two major factors facilitating cancer aggressiveness. These findings lead to the better understanding of cancer cell biology regarding this essential endogenous element on cancer aggressive behaviors.

Department:	Pharmacology and Physiology	Student's Signature	.....
Field of Study:	Pharmacology and Toxicology	Advisor's Signature	.....
Academic Year:	2016	Co-Advisor's Signature	.....

ACKNOWLEDGEMENTS

My sincere and heartfelt thanks to my advisor, Associate Professor Dr. Pithi Chanvorachote and my co-advisor Professor Dr. rer. nat. Regine Schneider-Stock for their great understandings, excellent advices, supervision, encouragements, and supporting, which have given me throughout this study. Without his kindness and understanding, this work could not be accomplished.

I would like to express my deep appreciate to my teachers, Assistant Professor Dr. Varisa Pongrakhananon, Dr. Chatchai choatham and Dr. Sudjit Luanpitpong for valuable advices, as well as their kindness and helpfulness.

My special thanks go to all colleagues in my laboratory; Miss Nuttida Yongsanguanchai, Miss Chalamart Pramchu- ema, Miss Punyawee Puchsaka, Miss Tawiwan Sawadsopanon, Miss Premkamol Pengpaeng, Mr. Arnatchai Maiuthed, Miss Kerstin Hübner, Mr. Pablo Lennert, Miss Benardina Ndreshkjana, Miss Sara Steinmann, Dr. rer. nat. Julienne Münzner, Mr. Adrian Koch and Ms. Ingrid Mons for valuable comments and their great friendships I had received.

My thankfulness is also expressed to my best friends, Miss Chayanin Kiratipaiboon, Ms. Preeyaporn Phiboonchaiyanan and Miss Ana Carolina Monteira for their helpful and encouragement. They always motivate me to work to the best of my ability and solve many problems together with me.

I would like to thank to the personals of the Department of Pharmacology and Physiology, Chulalongkorn University, Bangkok, Thailand and the personals of Experimental Tumor Pathology, Institute of Pathology, Friedrich- Alexander University Erlangen- Nürnberg (FAU), Erlangen, Germany. Their advices and helpfulness are also appreciated.

Eventually, the extremely gratitude is expressed to my parents and to my brothers for their love, understanding, helping, supporting and encouraging with care, which enable me to conduct this research successfully.

The present work was partly supported by the Thailand Research Fund through the Royal Golden Jubilee Ph.D. program (Grant No. PHD/0004/2556).

CONTENTS

Page

LIST OF FIGURES

LIST OF TABLES

LIST OF ABBREVIATIONS

%	=	percentage
°C	=	Degree Celsius
$^{\bullet}OH$	=	Hydroxyl radical
µm	=	Micrometer
µM	=	Micromolar
Akt	=	Protein kinase B
ALDH	=	Aldehyde dehydrogenase
CO_2	=	Carbon dioxide
CSCs	=	Cancer stem cells
$DCFH_2$-DA	=	2,7-Dichlorofluorescein diacetate
DHE	=	Dihydroethidium
DMNQ	=	2,3-Dimethox A
EMT	=	Epithelial to mesenchymal transition
et al.	=	et alibi, and others
FAK	=	Focal adhesion kinase
g	=	Gram
h	=	Hour, hours
H_2O_2	=	Hydrogen peroxide
HPF	=	Hydroxyphenyl fluorescein
IC_{50}	=	50% Inhibition concentration
min	=	Minute (s)
ml	=	Milliliter
mM	=	Millimolar

MnTBAP	=	Mn (III) tetrakis (4-benzoic acid) porphyrin chloride
MTT	=	3-(4,5-Dimethylthiazol-2-yl)-2,5-diphenyltetrazolium bromide
NADPH	=	Nicotinamide adenine dinucleotide phosphate
$O_2^{\bullet-}$	=	Superoxide anion radical
Oct4	=	Octamer-binding transcription factor 4
PBS	=	Phosphate-buffered saline
PKC	=	Protein kinase C
Rac1	=	Ras-related C3 botulinum toxin subdtrate 1
RhoA	=	Ras homolog gene family member A
ROS	=	Reactive Oxygen Species
RPMI	=	Roswell Park Memorial Institute's medium
S.D.	=	Standard deviation
SOD	=	Superoxide dismutase
Sox2	=	Sex-determining region Y (SRY)-box containing gene 2
U	=	Unit
Wnt	=	Wingless-type
ZIP	=	Zrt/Irt-like protein
$ZnSO_4$	=	Zinc sulfate

CHAPTER I
INTRODUCTION

Background and Rationale

Zinc is a trace element implicated in many important processes including body growth, brain development and wound repair. In plasma and tissue, zinc is found in form of zinc ion (Zn^{2+}). It is detected in plasma at the concentrations ranging from 10-18 μM (Hajo and Wolfgang, 2010; Wu et al., 2013). Interestingly, the aberrant level of zinc ion has been found in the condition of cancers. The reduced plasma zinc ion level was found in patients with gallbladder, prostate, and lung cancers (Gupta et al., 2005; Gumulec et al., 2014). Zinc ion has been found to be a component of various proteins, enzymes and transcription factors (Hajo and Wolfgang, 2010), which are responsible for structure, function and cell signaling (Hajo and Wolfgang, 2010; Wu et al., 2013). Zinc ion is required for cytoskeleton organization and is an essential component of several proteins involved in migration, invasion and metastasis, such as matrix metalloproteinases (MMPs) (Lansdown, 1996; Lansdown et al., 2007). Additionally, recent study has shown that zinc ion treatment succeeds in sensitizing lung cancer cells for anoikis (Pramchu-Em et al., 2016). Such data has suggested the roles of zinc ion in regulation of cancer cell biology. However, the effect of zinc ion on metastasis and cancer progression remains largely unknown.

Metastasis is one of the life-threatening pathological events and more than ninety percent of the clinical death of cancer patients is due to metastasis (Mehlen and Puisieux, 2006). Numerous attempts have been made to understand the molecular basis, which regulates cancer cell metastasis. Although advanced knowledge about

cancer biology are well developed, cancer has remained to be the major health problem in several parts of the world (Siegel et al., 2015). Accumulating evidences have indicated the roles of epithelial to mesenchymal transition (EMT) in cancer aggressiveness and metastasis; they are being considered as the underlying cause of the high mortality rate of cancer (Mehlen and Puisieux, 2006; Scheel and Weinberg, 2012; Tanaka et al., 2013; da Silva et al., 2015). EMT-phenotypic cancer cells elicit highly metastatic potential, such as aggressive migratory and invasive abilities (Yang and Weinberg, 2008; Thiery et al., 2009; Iwatsuki et al., 2010; Craene and Berx, 2013). In addition, emerging evidence has revealed that CSCs can be triggered during EMT process by many factors and CSCs always found EMT properties (Scheel and Weinberg, 2012; Voon et al., 2013; Zhou et al., 2014; Yongsanguanchai et al., 2015). CSCs have been suggested to be the potential driving force of new tumor initiation and cancer progression due to the self-renewal and tumorigenic abilities, leading to chemoresistance, metastasis and cancer relapse (Hermann et al., 2007; Maitland and Collins, 2008; McDermott and Wicha, 2010; Merlos-Suarez et al., 2011; Perona et al., 2011). In order to improve the approaches of cancer treatment, knowledge about the factors affecting EMT and CSCs have been identified.

Numerous studies have indicated that ROS are involved in many processes of tumor metastasis including migration, invasion and EMT (Wu, 2006; Wang et al., 2010; Wu and Wu, 2010). As signaling mediator, ROS have a capability to oxidize the important target molecules, such as protein kinase C (PKC) and protein tyrosine phosphatases (PTPs), which are relevant to tumor migration and invasion (Carter and Kane, 2004; Sliva, 2004; Wu and Wu, 2010). In addition, ROS-induced expression of snail represses the cellular level of E-cadherin and consequently exhibits EMT characteristics (Lee et

al., 2013; Cichon and Radisky, 2014). Presently, it is not clear about the role of ROS in regulation of CSCs (Shi et al., 2012). To effectively target CSCs, understanding ROS regulatory mechanism in CSCs is necessary.

Previous studies have shown that zinc ion has an effect on cellular redox status of the cells (Noh and Koh, 2000; Rudolf, 2007; Wu et al., 2013). The exogenous zinc ion has a capability to induce reactive oxygen species (ROS) production through NADPH oxidase and mitochondria (Noh and Koh, 2000; Rudolf, 2007; Wu et al., 2013). Such increased ROS level could mediate survival signaling of the cells (Noh and Koh, 2000; Rudolf, 2007; Wu et al., 2013). There is little known about the association between zinc ion-induced ROS in cancer cells and tumor progression. Therefore, this study aims to investigate the effects of zinc ion on lung cancer EMT as well as CSCs and also attempts to clarify the mechanisms involved in zinc ion-induced EMT and CSCs via ROS dependent pathway. This finding can help fulfill the understanding in tumor cell biology and provide the knowledge for improving cancer therapy and using zinc in cancer patients.

Research questions

1. Whether zinc ion has an effect on EMT characteristics in H460 lung cancer cells?
2. Whether zinc ion has an effect on CSC phenotypes in H460 lung cancer cells?
3. Does zinc ion mediate EMT and CSC phenotypes through ROS dependent pathway?

Objectives

1. To investigate the effect of zinc ion on EMT characteristics in H460 lung cancer cells.
2. To investigate the effect of zinc ion on CSC phenotypes in H460 lung cancer cells.
3. To examine the mechanisms involved in the effects of zinc ion on EMT and CSC phenotypes.

Hypothesis

Zinc ion affects EMT and CSC phenotypes through ROS dependent pathway.

Expected benefits

This finding can help fulfill the knowledge regarding role of zinc ion in tumor cell biology that zinc ion plays a key mediator in the regulation of EMT and CSCs. This information is beneficial for finding new drug targets, improving cancer therapy and using zinc in cancer patients.

CHAPTER II
LITERATURE REVIEWS

Cancer metastasis

Cancer has become the major health problem in several parts of the world. For example in the United State, the number of cancer deaths in men (year 1991-2011) and women (year 1992-2011) have continuously increased in each year (Siegel et al., 2015). It has been well known that more than ninety percent of all cancer suffering and death is due to metastasis (Mehlen and Puisieux, 2006; Nguyen et al., 2009). Metastasis, one of the life-threatening pathological, is the process that cancer cells disseminate from the original site of tumor to one or more distant site in the body (Mehlen and Puisieux, 2006; Nguyen et al., 2009). Metastasis is a multistep process beginning with the (1) dissociation of cancer cells from epithelial layer, (2) migration and penetration through the basement membrane into the surrounding connective tissue, (3) intravasation, (4) survival in the circulation, (5) extravasation at the metastatic site and finally (6) initiation of new tumors with stimulation of neovascularization (Mehlen and Puisieux, 2006; Nguyen et al., 2009). The illustration of complicated processes of metastasis is showed in the figure 2.1.

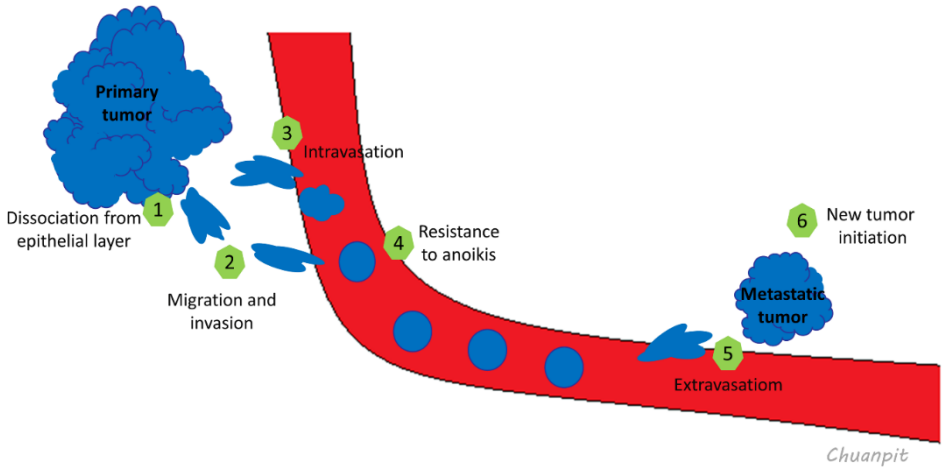

Figure 2.1 Metastatic process

Epithelial-to-mesenchymal transition (EMT)

Epithelial-to-mesenchymal transition or EMT is a biological process, which generally occurs during embryonic development, wound repair and pathological events, such as fibrosis and cancer (Iwatsuki et al., 2010).

EMT is classified into three different subtypes

1) Type 1 EMT: This type occurs during embryonic development and organogenesis
2) Type 2 EMT: This type associates with tissue repair and fibrosis
3) Type 3 EMT: This type associates with cancer progression and metastasis

EMT characteristics can be identified by the change of cell morphology and the expression of EMT marker proteins. During EMT, epithelial cells undergo remarkable morphological conversion from clobble stone-like epithelial morphology to elongated-like mesenchymal morphology. The crucial hallmark of EMT is the loss of E-cadherin, a cellular junction protein typically expressed in epithelial cells. In addition, EMT-

phenotypic cells increase the expression of mesenchymal markers such as N-cadherin and vimentin as well as up-regulate the transcriptional factors, namely snail and slug (Yang and Weinberg, 2008; Thiery et al., 2009; Iwatsuki et al., 2010; Craene and Berx, 2013). The alteration of cell components, including adhesion molecules and cytoskeletons makes the cells loss of cell polarity and acquired high migratory ability, leading to facilitate cancer cell metastasis.

Focusing on cancer metastasis, accumulating evidences have indicated the roles of epithelial to mesenchymal transition (EMT) in cancer aggressiveness and metastasis; it is being considered as the underlying cause of the high mortality rate of cancer (Mehlen and Puisieux, 2006; Tanaka et al., 2013; da Silva et al., 2015). EMT elicits distinct behaviors which leads to facilitate cancer cell metastasis including increased cell motility (migration and invasin) and anoikis resistance. Previous studies have demonstrated that loss of E-cadherin expression has been shown to decrease cell polarity and promote individual cell migration and invasion (Wong and Gumbiner, 2003; Onder et al., 2008). Accordingly, increased expression of N-cadherin results in a less stable cell-cell adhesion, which promotes cell motility and invasion by maintaining the steady-state level of active Rac1 (Nieman et al., 1999; Wheelock et al., 2008). Similar to N-cadherin, vimentin, type III intermediate filament protein, plays a predominant role in the changes in cell shape, adhesion, and motility by maintaining FAK activity and Rac1 activation (Mendez et al., 2010; Havel et al., 2015). Several signaling pathways have been proposed to play an important role in regulating EMT process, including TGF-ß, tyrosine kinase, integrin and Wnt/ß-catenin signaling (Jiang et

al., 2007; Xu et al., 2009; Iwatsuki et al., 2010; Katsuno et al., 2013; Lamouille et al., 2014) as indicated in figure 2.2.

TGF-ß signaling

Previous evidence suggested the role of TGF-ß in EMT during embryogenesis, cancer progression and fibrosis (Miyazono, 2009; Xu et al., 2009; Katsuno et al., 2013). TGF-ß can induce EMT in 2 major pathways, including smad pathway and non-smad pathway (Katsuno et al., 2013). Activation of smad signaling beginning with TGF-b binds to TGF-ß receptor (TßR) subtype II (TßRII). TßRII phosphorylates TßRI, which subsequently activates Smad2 and Smad3. Active Smad2/3 create complexes with Smad4, and translocate into the nucleus. The Smad complexes interact with various transcription factors and transcriptional co-activators, and regulate the transcription of target genes (Miyazono, 2009; Katsuno et al., 2013). On the other hand, non-smad activation pathway, TGF-ß is able to regulate multiple intracellular signaling cascades. Erk, JNK, and p38 MAP kinases, PI3 kinase, and small GTPases such as Cdc42 and Rac are mediated after TGF-ß receptor activation and play a crucial role in TGF-ß-induced EMT (Miyazono, 2009; Katsuno et al., 2013; Lamouille et al., 2014). TGF-ß can induces the expression of several transcription factors involved in EMT, including ZEB1, snail and slug. Ras signaling crosstalk with TGF-b signaling in inducing the expression of transcription factor snail (Miyazono, 2009; Katsuno et al., 2013; Lamouille et al., 2014).

Tyrosine kinase signaling

A number of growth factors have been found to induce EMT by binding to receptor tyrosine kinases, such as fibroblast growth factor (FGF) (Strutz et al., 2002),

epidermal growth factor (EGF) (Cheng et al., 2012), vascular endothelial growth factor (VEGF) (Fantozzi et al., 2014), hepatocyte growth factor (HGF) (Farrell et al., 2014) and insulin-like growth factor (IGF) (Liao et al., 2014). Activation of tyrosine kinase receptor induces nuclear translocation of β-catenin in the present of SRC and and RAS activation (Lamouille et al., 2014). SRC phosphorylates cytoskeletal and focal adhesion proteins (FAK, Cas and paxillin), which mediate the reorganization of cell architecture and focal adhesions. SRC-induced EMT may or may not require downstream transcription factors, depending on the model system (Lamouille et al., 2014). In addition, EMT and scattering in renal MDCK cells is induced by binding of HGF/c-Met (Khoury et al., 2005). Dissection of the signaling pathways downstream of activated c-Met has been conducted by mutagenesis of the relevant phosphotyrosine residues phosphorylated during receptor activation (Khoury et al., 2005).

Integrin signaling

Integrin, an adhesion molecule, which presents at the plasma membrane of the cells, plays a critical role in cell-matrix interaction. In the mesenchymal state, expression of integrin facilitates the formation of focal adhesion enhancing the induction of intracellular signaling-related cell motility. Integrin consists of alpha and beta subunit (Maschler et al., 2005). Extracellular domain of integrins links to extracellular matrix (ECM), whereas intracellular parts are served as signal transduction platform. Integrin functions as a signal intermediary from extracellular to cytoplasm, which regulate cytoskeleton behaviors. The alteration of integrin expression has been found during EMT process (Maschler et al., 2005). Previous studies showed the increased expression of integrin β_1 as well as integrin α_V and display EMT phenotypes

in TGF-ß-treated cells (Mamuya and Duncan, 2012; Ju and Zhou, 2013). Cancer cells which expresses an elevated level of integrin $\alpha_V\beta_3$ have high metastasis and aggressive behaviors (Knowles et al., 2013).

Furthermore, integrin linkage kinase (ILK) is a key component of focal adhesions that always binds to integrin (Gil et al., 2011). ILK can phosphorylate protein kinase B (Akt) and glycogen synthase kinase 3ß (GSk-3ß) (Oloumi et al., 2004; Gil et al., 2011). Overexpression of ILK leads to nuclear translocation of ß-catenin, increased invasiveness and repression of E-cadherin via upregulation of snail transcription (Barbera et al., 2004; Oloumi et al., 2004; Gil et al., 2011). ILK is also involved in the TGF-ß mediated EMT of human keratinocytes (Lee et al., 2004).

Wnt/ß-catenin signaling

There are a lot of evidence have reported that canonical Wnt/ß-catenin pathway plays a crucial role in cancer growth and metastasis (MacDonald et al., 2009; Havel et al., 2015). Lacking of Wnt signals, ß-catenin, a destruction complex consisting of APC, axin GSK-3ß, and ß-catenin is phosphorylated by GSK-3ß and targeted for ubiquitin-proteasome-mediated degradation. In the present of Wnt, Wnt ligands bind Frizzled receptors and activate Disheveled, which inhibits ß-catenin degradation. Excess ß-catenin translocate into the nucleus, in turn associate with the transcription factor TCF/LEF and promote the expression of several target genes (MacDonald et al., 2009). Wnt/ß-catenin signaling induces EMT during developmental process (Larue and Bellacosa, 2005; MacDonald et al., 2009). Wnt/ß-catenin-induced EMT has been shown

to regulate colorectal cancer metastasis (Brabletz et al., 2005) and squamous cell carcinoma progression (Taki et al., 2003). During EMT, Wnt/ß-catenin signaling can promote the level of snail and slug, via inhibition of its phosphorylation and degradation (Newton, 1995; Barbera et al., 2004; Yook et al., 2005). Consistent with these observations, inhibition of GSK-3ß activity results in the increase expression of snail transcription, E-cadherin repression and EMT (Bachelder et al., 2005). In addition, intracellular interaction between E-cadherin and ß-catenin plays an important role on cell adhesion and Wnt signaling (Clevers, 2006). The depletion of E-cadherin by various stimuli leads to the disruption of cell-cell contact, and the release of ß-catenin from the complex which accordingly enters the nucleus (Clevers, 2006). ß-Catenin regulates the transcription of several signaling-participating in cell motility, EMT and stemness properties (Clevers, 2006; Cai and Zhu, 2012). Accordingly, members of wnt family were reported to stabilize ß-catenin in cytosol and enhance its accumulation in nucleus (Clevers, 2006; Cai and Zhu, 2012). Recent study demonstrated that overexpression of Wnt3 activates Wnt/ß-catenin pathway and epidermal growth factor (EGFP), and consequently promote mesenchymal transition (Scheel and Weinberg, 2012; Wu et al., 2012).

RAS pathway

RAS activation plays a crucial role in the downstream activation of receptor tyrosine kinases (Edme et al., 2002; Lamouille et al., 2014). RAS can activate Jun, Fos and other transcription factors regulated EMT, such as slug and snail thought RAF and MEK activation (Edme et al., 2002; Lamouille et al., 2014). Additionally, RAS also affects the activity of the two small GTPases, such as Rac1 and Rho A which is the important

molecules in regulating actin stress fibers, cell adhesion, myosin phosphorylation, and focal adhesions, leading to enhance cell motility and scattering (Edme et al., 2002).

Reactive oxygen species (ROS) signaling

Recently, the role of ROS in EMT has been highlighted (Radisky et al., 2005; Fukawa et al., 2012; Cichon and Radisky, 2014). The transcription of Rho-family proteins, including Rac 1b is induced by treating the mouse mammary epithelial cells with MMP-3 (Radisky et al., 2005). Rac1b facilitrates the production of ROS, which subsequently stimulate snail expression and EMT induction (Radisky et al., 2005). Treatment with *N*-acetyl cysteine, a widely known anti-oxidant, can prevent snail expression and EMT (Radisky et al., 2005). This finding suggests the link between extracellular matrix, oxidative damage and EMT.

PI3K/Akt pathway

A number of evidence have shown that cancer cells with mesenchymal property potentiate metastasis through PI3K/Akt signaling (Larue and Bellacosa, 2005; Lamouille et al., 2014). PI3K/Akt acts as a down-stream signal and crosstalk with several EMT pathway, such as tyrosine kinases, and ß-catenin signaling pathways (Larue and Bellacosa, 2005). Canonical Wnt and PI3/AKT signaling can promote an inhibition of GSK-3ß by regulating the phosphorylation (Larue and Bellacosa, 2005). In addition, ß-catenin can be phosphorylated and increased the transcriptional activation by Akt (Fang et al., 2007)

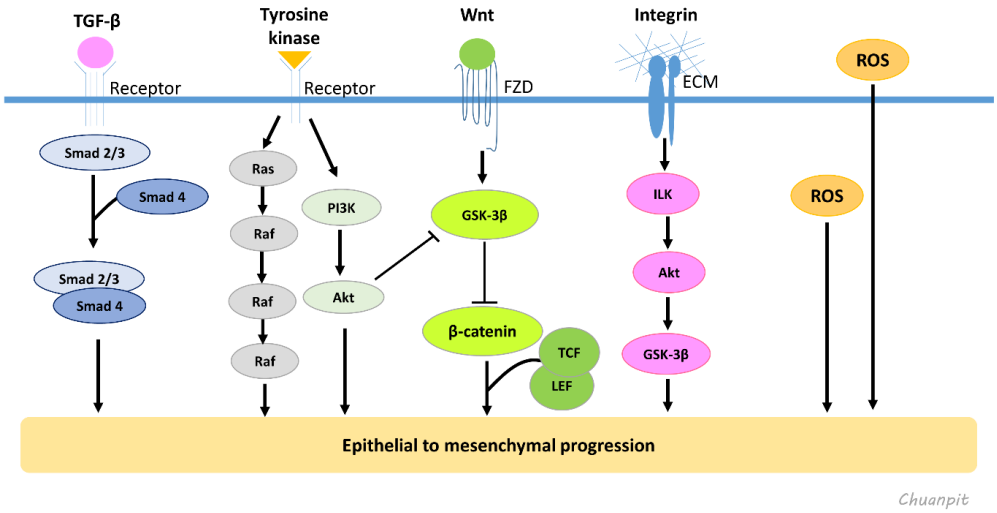

Figure 2.2 Signaling pathways involved in EMT

Cancer stem cells (CSCs)

Increasing evidence has indicated the roles CSCs in cancer aggressiveness, metastasis and cancer relapse; it is being considered as the underlying cause of the high mortality rate of cancer (Mehlen and Puisieux, 2006; Hermann et al., 2007; Merlos-Suarez et al., 2011; Perona et al., 2011; Scheel and Weinberg, 2012). Emerging evidence has revealed that CSCs can be triggered during EMT process by many factors and CSCs always found EMT properties (Scheel and Weinberg, 2012; Voon et al., 2013; Zhou et al., 2014; Yongsanguanchai et al., 2015).

In the past decade, several studies have reported that cancer stem cells (CSCs) or tumor initiating cells are found in various types of solid tumors, including breast, colon, prostate, pancreatic and lung cancers (Hermann et al., 2007; Maitland and Collins, 2008; McDermott and Wicha, 2010; Merlos-Suarez et al., 2011; Perona et al., 2011).

CSCs have been suggested to be the potential driving force of new tumor initiation and cancer progression due to the self-renewal and tumorigenic abilities, leading to chemoresistance, metastasis and cancer relapse (Hermann et al., 2007; Maitland and Collins, 2008; McDermott and Wicha, 2010; Merlos-Suarez et al., 2011; Perona et al., 2011). The distinct abilities of CSCs to increase the expression of various transcription factors regulating self-renewal and pluripotentcy, including Nanog, Sox2 and Oct4, making CSCs different from normal cancer cells (Liu et al., 2013). Besides, CSCs always express the up-regulation of CSC marker proteins, such as CD133 and ALDH1A1 which involves in tumorigenicity and drug resistant properties of CSCs (Bertolini et al., 2009; Li et al., 2010; Perona et al., 2011; Grosse-Gehling et al., 2013).

CSCs are defined by their capacity to self-renew, differentiate and initiate tumor growth that recapitulates features of the original tumor (Lobo et al., 2007). By impairing the control of stem-cell self-renewal, differentiation and increasing tumorigenicity of CSCs, several aberrations in signaling pathways have been proposed to play an important role in CSC induction, including Notch, Hedgehog (Zhao et al.), and Wnt/ ß-catenin pathway (Lobo et al., 2007; Karamboulas and Ailles, 2013; Pattabiraman and Weinberg, 2014) as indicated in figure 2.3.

Notch signaling

Notch signaling begins with binding of the Notch ligands (DLL/JAG) located in the membranes of adjacent cells to the Notch receptor and triggering two proteolytic cleavages by ADAM and **γ**-secretase which in turn releases an active intracellular domain or NICD (Lobo et al., 2007; Bolos et al., 2009; Pattabiraman and Weinberg, 2014). NICD translocates into nucleus and interacts with mastermind-like proteins

(MAML) as well as CBF1/Suppressor of Hairless/LAG1 /RBPJ (CSL) factors to activate transcription of Notch target genes (Lobo et al., 2007; Bolos et al., 2009; Pattabiraman and Weinberg, 2014).

Hedgehog signaling

Sonic Hh (Shh) has been shown to regulate proliferation, migration, and cancer stem cell induction in many cancer types (Zhao et al., 2009; Cochrane et al., 2015) .In the absence of the Hedgehog (Zhao et al.) ligand, Patched (Ptch) seem to inhibit Smoothened (Smo) and prevent signal transduction to Gli factors. Gli1/2 factors interact with Cos2 (Kif7), fused (Fu) and suppressor of fused (Sufu) and are phosphorylated by protein kinase 1 (PKA), cacine kinase-1 (CK1), and GSK3ß leading to ß-TrCP-mediated degradation. Lacking of Hh signaling, truncated Gli3-repressor family member dissociates from Sufu and represses transcriptional activity of Hh target genes. On the other hand, in the presence of Hh ligands, Hh ligands can bind to Ptch to relieve inhibition of Smo by Ptch, causing the activation and dissociation from Sufu/Fu/Cos2 (Kif7) complex. Activated Gli1/2 transcription factors accumulate and translocate to the nucleus where they bind and activate Hh target genes (Lobo et al., 2007; Pattabiraman and Weinberg, 2014; Cochrane et al., 2015).

ß-Catenin signaling

ß-Catenin plays an important role in cadherin-based adhesions and is also an essential co-activator of Wnt-mediated gene expression (Holland et al., 2013). The Wnt/ ß-catenin pathway is activated by Wnt interacting with Frizzled receptors and low-density lipoprotein receptor-related protein 5/6 co-receptor. The signal causes an inhibition of glycogen synthase kinase-3ß (GSK-3ß) (Holland et al., 2013). Regardless of

Wnt signal, GSK-3ß always phosphorylates ß-catenin at ser 33, ser37 and Thr41 and promote ß-catenin degradation via proteasome-dependent manner (Holland et al., 2013). The inhibition of GSK-3ß by Wnt causes an increase in ß-catenin level. Available ß-catenin is translocated into nucleus, where it forms a complex with T-cell factor/lymphocyte enhancer factor (TCF/LEF) family of transcription factor to activate the expression of Wnt/ß-catenin responsive gene, such as Nanog, Oct4 and Sox2, leading to increase stemness of the cells (Cai and Zhu, 2012; Holland et al., 2013).

Activation of ß-catenin appear to maintain the important properties of stem cell, including self-renewal and pluripotency (Cai and Zhu, 2012; Holland et al., 2013). Likewise, PKC is able to phosphorylate ß-catenin at the same position as GSK-3ß and inhibit ß-catenin signaling (Gwak et al., 2006; Luna-Ulloa et al., 2011). Alteration of PCK activation may alter the stem cell properties in stem and cancer stem cells.

PKC is a family of serine/threonine kinase. An amount of evidence has reported that PKC mediates diverse cellular function, such as proliferation, differentiation, cytoskeleton organization, cell migration and apoptosis (Gomez et al., 1999; Luna-Ulloa et al., 2011). Importantly, pro-oxidant exposure can induce aberrant PKC activation, which leads to cancer progression (Gomez et al., 1999). Moreover, previous study indicated that the level of ß-catenin can be regulated by PKC signaling (Gwak et al., 2006; Luna-Ulloa et al., 2011). PKC is able to phosphorylate ß-catenin at the position of serine 33 and 37 and threonine 41, contributing to an inhibition of ß-catenin signaling (Gwak et al., 2006). However, whether PKC mediates lung CSCs is not known.

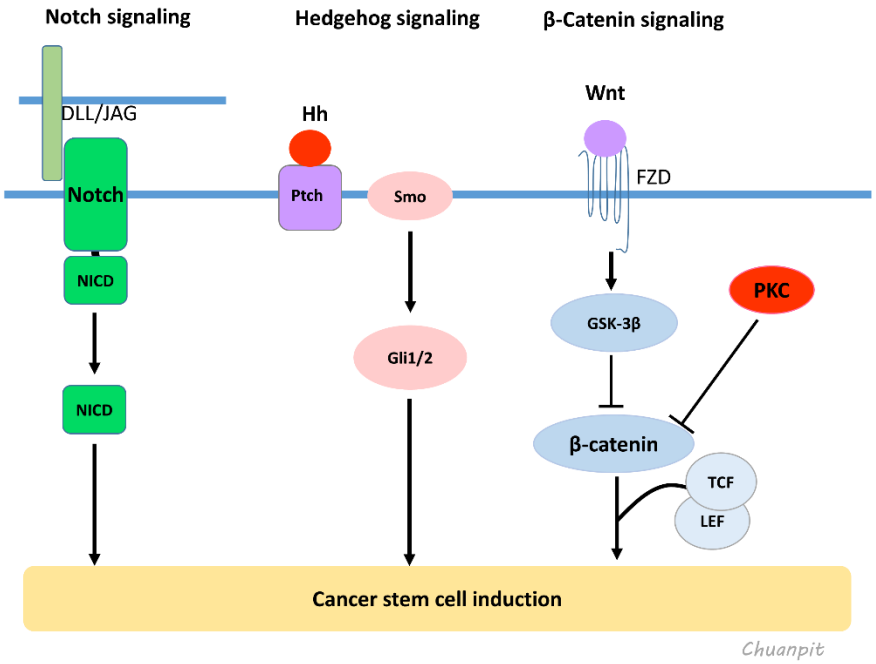

Figure 2.3 Signaling pathways involved in CSCs

Reactive oxygen species (ROS)

A number of studies have indicated that reactive oxygen species (ROS) play a central role in the intracellular signaling pathway for a variety of cellular processes when they present at the low or moderate concentrations in normal condition (Andreoli, 1991). There are two distinct sources of ROS in the body, including mitochondrial respiratory chain and NADPH oxidase system. Superoxide anion ($^{\bullet}O_2^-$) is the first ROS that mainly produced from non-enzymatic process during oxidative phosphorylation of electron transport chain in mitochondria and from oxidation reaction of NADPH oxidase enzyme. Although, superoxide anion lacks an ability to penetrate lipid membranes, with accelerated by superoxide dismutase (Ivanovska et al.), the two molecules of superoxide anion are rapidly dismutated to hydrogen peroxide (H_2O_2) which has a capability to penetrate cell membranes. Because hydrogen peroxide is able to cross the cell membranes, an important function of hydrogen

peroxide is to act as inter- and intracellular signaling molecules. Besides, hydrogen peroxide can be inactivated by antioxidant enzymes, namely catalase and glutathione peroxidase or catalyzed by metal ions (Fe^{2+} or Cu^{+}) to form hydroxyl radical (°OH) called Fenton reaction. In addition to hydrogen peroxide, superoxide anion is another intermediate in the production of hydroxyl radical via reduction of metal ions (Fe^{3+} or Cu^{2+}) which is called Haber-weiss reaction (Andreoli, 1991; Thannickal and Fanburg, 2000; Hancock et al., 2001).

Involvement of ROS and cancer

Numerous studies have indicated that ROS are involved in many processes of tumor metastasis including migration, invasion and EMT (Wu, 2006; Wang et al., 2010; Wu and Wu, 2010). Also, an elevation of oxidative stress has been found in various types of cancer cells, which contributes to carcinogenesis EMT (Wu, 2006; Wang et al., 2010; Wu and Wu, 2010). As signaling mediator, ROS have a capability to oxidize the important target molecules, such as protein kinase C (PKC) and protein tyrosine phosphatases (PTPs), which are relevant to tumor migration and invasion (Carter and Kane, 2004; Sliva, 2004; Wu and Wu, 2010). In addition, snail, one of the EMT transcriptional factors, is previously reported to be regulated by ROS. ROS-induced expression of snail represses the cellular level of E-cadherin and consequently exhibits EMT characteristics (Lee et al., 2013; Cichon and Radisky, 2014).

Zinc ion

Zinc is a trace element implicated in many important processes including body growth, brain development and wound repair. It is detected in plasma at the concentrations ranging from 10-18 μM (Hajo and Wolfgang, 2010; Wu et al., 2013), while

the concentration of zinc ion in plasma or tissues is found to be elevated in pathological condition including cancer (Wright and Dormandy, 1972; Margalioth et al., 1983; Kollmeier et al., 1992; Nimmanon and Taylor, 2014). Zinc ion has been found to be a component of various proteins, enzymes and transcriptional factors (Hajo and Wolfgang, 2010; Fukada et al., 2011), which are responsible for structural, functional and signaling of the cells (Hajo and Wolfgang, 2010; Fukada et al., 2011; Wu et al., 2013). Proteome analysis estimate that approximately 10% of proteins encoded in human genome have potential zinc-binding motif. The other is labile zinc (free zinc ion) (Fukada et al., 2011; Kambe, 2014). The amount of free zinc ions in the cytosol maintains is very low, whereas it is high in zinc ion containing vesicle called zincrosome. Interestingly, recent studies have reported the dynamic role of free zinc ion in diverse biological processes, which highlights the signaling function of zinc ion (Frederickson et al., 2005; Hirano et al., 2008; Fukada et al., 2011). In intracellular zinc signaling, there are a plenty of molecular targets have been identified, including protein tyrosine phosphatases (PTPs), phosphodiesterases (PEDs), caspase, and kinase (Hirano et al., 2008; Wu et al., 2013; Kambe, 2014). Zinc ion has an ability to bind with anionic groups, such as histidyl, aspartyl, glutamyl (Rahuel-Clermont and Dunn, 1998), and thiolate, causing a crucial roles in protein structure and activity in enzymatic function (Rahuel-Clermont and Dunn, 1998; Wu et al., 2013).

Physiological function of zinc

Zinc ion has shown to possess diverse physiological functions including cell replication, tissue or cell growth, immunity, and bone formation. It is a component of various metalloenzymes and proteins which are responsible for structural integrity, enzyme activity and cell signaling. Zinc ion has a capability to bind directly to amino

acid residues at the catalytic site and participates in reaction activity of enzymes in order that zinc ion affect several life processes. The role of zinc ion in controlling cell and tissue growth id associated with its function to regulate protein and nucleic acid synthesis. Regarding of transcription, zinc ion appears to interact with nuclear transcription factors, which can bind to promoter sequences of specific genes on DNA. Therefore, zinc ion may regulate transcription. More than 2,000 transcription factors seem to require zinc ion for structural integrity. Zinc fingers is a term used to indicate the configuration of the proteins, which look like fingers, and the presence of the zinc ion bound to the protein. The finger-like structure caused by the twisting and coiling of the cysteine and histidine residues to which zinc ion binds in that segment of the protein (Kuwahara and Coleman, 1990).

Moreover, the effect of zinc ion on cell membranes may result from direct effects on the conformation of membrane proteins or on protein-protein interactions. Zinc ion seem to affect the functional activity of many enzymes that attached to plasma membranes, including alkaline phosphatase, superoxide dismutase and protein kinase C (Newton, 1995). Zinc ion also stabilizes membrane integrity by blocking free radicals as part of metallothionein and by enhancing the associations between membrane skeletal and cytoskeletal proteins. Zinc ion is intracellularly found to bind to tubulin, a subunit of microtubules which act as a framework for structural support of the cell as well as being needed for cell motility.

It has been known that zinc ion is involved in host defense. Zinc ion affects both cell-mediated and humoral immunity. Zinc ion also appears to regulate the mammalian target of rapamycin (mTor), thereby affecting insulin-signalling as well as

protein- synthesis pathways. Zinc ion participates in regulation of cell survival, especially apoptosis in immature T- and B-cells.

In controlling of cell signal transduction, Zinc ion induces Akt activation in human airway epithelial cells by decreasing the expression of PTEN which is a negative regulation of PI3K/Akt signaling (Wu et al., 2003). Zinc ion causes PTEN depletion by down-regulating PTEN mRNA expression and promoting ubiquitin-proteasome degradation of PTEN (Wu et al., 2003). In addition, non-cytotoxic concentrations of zinc ion cause an induction of MAPK phosphorylation in BEAS cells. Distinct activation of ERK, JNK and p38 are found in zinc ion-exposed BEAS cells (Samet et al., 1998). Consistently, the phosphorylation of transcription factors c-Jun and ATF-2, substrates of JNK and p38, respectively, are clearly increased in response to zinc ion treatment. Consequently, IL-8 protein which is a down-stream target gene of MAPK activation, is found to increase in zinc ion-treated cells (Samet et al., 1998). Another study supports that zinc ion is able to induce MAPK activation and protein tyrosine phosphorylation in mouse fibroblast which is the same effects of growth factor activation (Hansson, 1996). In addition to activations of Akt and MAPK signaling, zinc ion seems to induce a phosphorylation of IκB-α, causing the activation and nuclear translocation of NFκB (Bao et al., 2007). Likewise, zinc ion also activates NFκB and subsequently increase IL-2 as well as IL-2Rα expression in human malignant lymphoblastoid HUT-78 cells (Prasad et al., 2001). These finding suggests the role of zinc ion in NFκB activation via IκB pathway. On the other hand, activation of NFκB is found in zinc ion-exposed human airway epithelial cells (BEAS-2B cells) (Kim et al., 2007). 50 μM of zinc ion increases the transcriptional activity of NFκB independent of IκB inhibition. The phosphorylation of p65/Rel A, NFκB subunit, on ser 276, ser 592, and ser 536 are found in zinc ion-treated

cells (Kim et al., 2007). Importantly, phosphorylation at ser 536 of NFκB in response to zinc ion causes an increase in NFκB transactivation in BEAS-2B cells. Also, zinc ion reduces IKKα and IKKβ in regulation of this event (Kim et al., 2007). Some studies indicate the role of zinc ion in protein tyrosine phosphatases (PTPs) (Brautigan et al., 1981; Haase and Maret, 2003). Zinc ion acts as insulin/insulin-like growth factor-1 by enhancing the phosphorylation of insulin receptor. Zinc ion also causes an inhibition of PTP1B which is a key phosphatase regulating the phosphorylation of insulin receptor (Haase and Maret, 2003). Zinc ion is found to be the potent inhibitor of PTP by interacting with cysteines in the active site (Brautigan et al., 1981). The effect of zinc ion on epidermal growth factor receptor (EGFR) has been found in many cells. Zinc ion induces the phosphorylation of EGFR at tyr 845, 1068, and 1173 without EGFR dimerization (Samet et al., 2003) and also induces c-src phosphorylation at try 416. Interestingly, the phosphorylation of EGFR at try 845and 1086 induced by zinc ion can be inhibited by c-src kinase inhibitor PP2, suggesting the role of zinc ion in regulation of EGFR phosphorylation via c-src activation in human epidermoid A431 cells. In mouse B826 fibroblast cells, zinc ion induces the phosphorylation of the EGFR at try 845 via src dependent activation (Wu et al., 2002). Moreover, the roles of zinc ion in regulating protein kinase C (PKC) pathway are characterized in various studies. Translocation of PKC to membranes has been accepted as a critical event in PKC activation (Forbes et al., 1990; Newton, 1995). Zinc ion has been shown to be the essential component of PKC structure and induce an activation of PKC and also promote the translocation of PKC into plasma membrane (Forbes et al., 1990). Such event increases an interaction between PKC and actin filament (Forbes et al., 1990). Zinc ion is necessary for binding activity of phorbol ester and zinc finger domain of PKC. The activation of PKC in

response to phorbol ester can be blocked by treating with chelator (Csermely et al., 1988). The structure of PKC contains two identical zinc-binding domain at the regulatory region and this zinc figure domain is required for the binding of phorbol ester and PKC acgtivation (Parker et al., 1986). This evidence provides the important role of zinc ion in PKC activity.

Zinc homeostasis

The recommended dietary allowance (Maschler et al.) of zinc is 11 mg for men and 8 mg for women. The absorption efficiency of zinc is less than 50%. In plasma, 98% of zinc ion binds to albumin and other proteins (Hajo and Wolfgang, 2010). Zinc ion transportation is controlled by two major proteins, including Zrt/Irt-like protein (ZIP) and zinc transporter protein (ZnT). ZIP transports extracellular zinc ion to the cytosol, while ZnT transports cytosolic zinc ion out of the cells or moves it into vesicle or organelle (Haase and Maret, 2003; Cousins et al., 2006). The cellular level of zinc ion is controlled by metal-response element-binding transcription factor-1 (MTF-1) transcription factor and metallothionine (MT) protein (Haase and Maret, 2003; Cousins et al., 2006). High concentration of zinc ion is able to induce an increased in MTF-1 expression. MTF-1 is then translocate into nucleus and enhance the expression of thionein as well as zinc transporter ZnT-1, resulting in decreasing the level of free zinc ion (Haase and Maret, 2003; Cousins et al., 2006).

In the cells, zinc ion always binds to MT. Zinc in MT are bound exclusively to the sulfur donor of cysteine that have characteristic thiolate ligand bridges between zinc ion (Haase and Maret, 2003; Cousins et al., 2006). MT structure consists of 20 reduced cystenyl residues which able to bind with seven molecules of zinc ions inside

the protein (Haase and Maret, 2003; Cousins et al., 2006). Besides, zinc ion may be intracellular collected in vesicle called zincrosome (Hajo and Wolfgang, 2010).

Role of zinc ion in cellular oxidative status

Previous studies have shown that zinc ion has an impact on cellular redox status of the cells (Noh and Koh, 2000; Rudolf, 2007; Wu et al., 2013) The exogenous zinc ion has a capability to induce reactive oxygen species (ROS) production and NADPH oxidase as well as mitochondria are relevant targets of zinc ion-induced ROS. Zinc ion exposure is found to induce translocation of NADPH oxidase subunits to plasma membrane, which is the signature event for NADPH oxidase activation and this event is inhibited by the addition of NADPH oxidase inhibitor (Link and von Jagow, 1995; Noh and Koh, 2000; Rudolf, 2007; Rudolf and Cervinka, 2010; Wu et al., 2013). In addition to activate of NADPH oxidase, an elevation of intracellular zinc ion also inhibits tricarboxylic acid cycle and complex III of electron transport chain, resulting in mitochondria dysfunction and increased ROS production (Link and von Jagow, 1995; Brown et al., 2000; Dineley et al., 2005; Rudolf and Cervinka, 2010)

Roles of zinc in cancer

Having shown that the concentration of zinc ion in plasma or tissues is found to be elevated in some cancer tissues, such as liver and breast cancers (Wright and Dormandy, 1972; Margalioth et al., 1983; Kollmeier et al., 1992; Nimmanon and Taylor, 2014). In contrast, the reduced plasma zinc ion level is found in patients with gallbladder, prostate, and lung cancers (Gupta et al., 2005; Gumulec et al., 2014). Zinc ion is required for cytoskeleton organization and is an essential component of several proteins involved in migration, invasion and metastasis, such as matrix

metalloproteinases (MMPs) (Lansdown, 1996; Lansdown et al., 2007). Aberrations in zinc ion status may play a significant role in cellular dysfunction, including the development and/or progression of cancer (Wright and Dormandy, 1972; Margalioth et al., 1983; Kollmeier et al., 1992; Nimmanon and Taylor, 2014). Accumulating evidence support the idea that, zinc ion is known to be an essential for cell proliferation (Hajo and Wolfgang, 2010), and is important for tumor growth cancers (Wright and Dormandy, 1972; Margalioth et al., 1983; Kollmeier et al., 1992).

Previous study has shown that migration ability of breast cancer cells was inhibited by zinc ion depletion in response to zinc ion chelator TPEN treatment (Kagara et al., 2007). Besides, the increased expressions of zinc influx transporters such as ZIP6 (Hogstrand et al., 2013), ZIP7 (Taylor et al., 2012) and ZIP10 (Kagara et al., 2007) has been observed in breast cancer, leading to change in tumor zinc levels and such aberrant expressions of those is correlated with aggressive behaviors and poor prognosis of breast cancer (Kagara et al., 2007; Levenson and Somers, 2008; Taylor et al., 2012; Hogstrand et al., 2013). This evidence indicates the role of zinc in cancer metastasis.

As mentioned, zinc ion has shown to participate in a wide range of physiological activities and many signaling (Nimmanon and Taylor, 2014), such as oxidative stress induction and PKC activation also play a critical role in EMT and CSC regulation (Radisky et al., 2005; Gwak et al., 2006; Fukawa et al., 2012; Cichon and Radisky, 2014). This study therefore investigates the effect of zinc ion on EMT and CSC phenotypes.

CHAPTER III
MATERIALS AND MEDTHODS

Materials

1. Chemicals and reagents

Zinc sulfate ($ZnSO_4$), dimethyl sulfoxide (DMSO), A23187 (PKCα activator), 2,7-dichlorofluorescein diacetate (hydrogen peroxide specific probe; $DCFH_2$-DA), dihydroethidium (superoxide anion specific probe; DHE), hydroxyphenyl fluorescein (hydroxyl redical; HPF), 2,3-dimethoxy-1,4-naphthoquinone (superoxide anion donor; DMNQ), 3-(4,5-Dimethylthiazol-2-yl)-2,5-diphenyltetrazolium bromide (MTT), clasto-lactacystin ß-lactone (Larue and Bellacosa), Hoechst 33342 were obtained from Sigma Chemical, Inc. (St. Louis, MO, USA). Mn (III) tetrakis (4-benzoic acid) porphyrin chloride (superoxide anion inhibitor; MnTBAP) and Bisindolylmaleimide I (PKCα inhibitor; BIM) were obtained from Calbiochem (San Diego, CA, USA). Antibodies for N-cadherin, E-cadherin, vimentin, snail, slug, phosphorylated FAK (Y397), FAK, Nanog, Oct4, Sox2, ALDH1A1, phosphorylated PKCα (Thr638), PKCα, ß-catenin and ß-actin and peroxidase-labeled secondary antibodies were obtained from Cell Signaling Technology, Inc. (Denver, MA, USA). Antibody for ALDH1A1 was Santa Cruz Biotechnology, Inc. (Texas, USA). Mouse monoclonal antibodies for active RhoA-GTP and Rac1-GTP were obtained from New East Biosciences (Malvern, PA, USA). Antibody for CD133 was Cell Applications (San Diego, CA). Immobilon Western chemiluminescent HRP substrate was obtained from Millipore, Corp (Billerica, MA, USA) and Thermo Fisher Scientific Inc. (Rockfort, IL, USA). Alexa Fluor 488-conjugated goat anti-rabbit IgG (H^+L) secondary antibody was obtained from Life Technologies (Eugene, OR).

2. Equipments

Laminar flow cabinet, carbon dioxide incubator, autopipette: 2-10 µl, 10-100 µl, 20-200 µl and 200-1,000 µl, pipette tips for 2-10 µl, 10-100 µl, 20-200 µl and 200-1,000 µl, cell culture plate: 96-well and 6-well (Nunc), conical tube: 15 ml and 50 ml (Neptune), bottle: 100 ml, 250ml, 500 ml and 1,000 ml (Duran) disposable pipette: 1ml and 5ml, hemocytometer, pH meter, vertex mixer, balance, microplate reader (Anthros, Durham, NC, USA) flow cytometer (FACSort; Becton Dickinson, Rutherford, NJ) and fluorescence microscope (Olympus IX 51 with DP70, Olympus America Inc., Center valley, PA).

Methods

1. Cell culture

Since lung cancer has become the leading cause of cancer-related death in male and female worldwide and the death of lung cancer patients tightly relates to metastasis (Siegel et al., 2015, 2017), this study then uses human non-small cell lung cancer (NSCLC) NCI-H460, NCI-H292, and NCI-H23 cell lines as a model. All cell lines obtained from the American Type Culture Collection (ATCC, Manassas, VA). Every types of cells were cultured in RPMI 1640 medium in a 5% CO_2 environment at 37°C. The media was supplemented with 2 mmol/L l-glutamine, 10% fetal bovine serum and 100 units/ml of penicillin/streptomycin (Gibco, Gaithersburg, MA, USA).

2. Cytotoxicity assay

Cell viability was determined by MTT colorimetric assay. Briefly, cells in 96-well plate were incubated with 500 µg/mL of MTT for 4 hours at 37°C. The supernatant was then removed and DMSO was added to dissolve the formazan product. The intensity

was spectrophotometrically measured at 570 nm using an ELISA reader (Anthros, Durham, NC, USA). As viable cells can convert yellow MTT to purple formazan by mitochondria reductase, the absorbance of crystal formazan was referred to amount of living cells.

Cell viability was calculated as follow:

$$\text{Cell viability} = \frac{\text{A570/620 with treatment}}{\text{A570/620 without treatment}} \times 100$$

3. Apoptosis assay

Apoptotic cell death was detected by Hoechst 33342 and staining. After specific treatments, cells were stained with 10 μM of the Hoechst for 30 min at 37°C and analyzed under a fluorescence microscope using blue filter. The apoptotic cells having condensed chromatin and/or fragmented nuclei stained by Hoechst 33342 were visualized and scored under a fluorescence microscope (Olympus IX 51 with DP70, Olympus America Inc., Center valley, PA).

4. Cell Morphology characterization assay

Cell morphology was investigated by seeding the cells at a density of $5x10^4$ cells/well onto a 12-well plate for 48h. The cells were treated with various concentrations of zinc ion for 24 h. The cells were then washed with PBS, fixed with 4% paraformaldehyde in PBS for 10 min at 37℃, rinsed 3 times with PBS, and mounted with 50% glycerol. Cell morphology was then assessed by a phase contrast microscope (Eclipse Ti-U, Nikon, Tokyo, Japan).

5. Immunofluorescene

Cells were seeded at a density of 1 × 10^5 cells/well onto coverslips in 6-well plate and incubated overnight. After the treatment, the cells on coverslips were fixed with 4% paraformaldehyde for 30 min and permeabilized with 0.1% Triton-X for 20 min. Thereafter, the cells were incubated with 3% bovine serum albumin (BSA) for 30 min to prevent nonspecific binding. The cells were washed and incubated with rabbit anti-Vimentin antibody for 1 h at room temperature. Primary antibody was removed and the cells were washed and subsequently incubated with Alexa Fluor 488 (Invitrogen) conjugated goat anti-rabbit IgG (H+L) secondary antibody for 1h at room temperature. Samples were washed with PBS then visualized and imaged by fluorescence microscope (Olympus IX 51 with DP70, Olympus America Inc., Center valley, PA).

6. Western blot analysis

After specific treatments, cells were incubated in lysis buffer containing 20 mM Tris-HCl (pH 7.5), 1% Triton X-100, 150 mM sodium chloride, 10% glycerol, 1 mM sodium orthovanadate, 50 mM sodium fluoride, 100 mM phenylmethylsulfonyl fluoride, and a protease inhibitor cocktail (Roche Molecular Biochemicals) for 90 minutes on ice. The cell lysates were collected, and the protein content was determined using the BCA protein assay kit (Thermo scientific, IL, USA). Equal amounts of proteins from each sample (60 µg) were denatured by heating at 95°C for 5 min with Laemmli loading buffer and subsequently loaded onto a 10% SDS-PAGE. After separation, proteins were transferred onto 0.45 µM nitrocellulose membranes (Bio-Rad, Hercules, CA). The transferred membranes were blocked for 1 hour in 5% nonfat dry

milk in TBST (25 mM Tris-HCl pH 7.5, 125 mM NaCl, and 0.05% Tween 20) and incubated with the appropriate primary antibodies at 4°C overnight. Then, the membranes were washed twice with TBST for 10 min and incubated with horseradish peroxidase-labeled isotype-specific secondary antibodies for 2 h at room temperature. The immune complexes were detected by enhancement with chemiluminescence substrate (Supersignal West Pico; Pierce, Rockfore, IL) and quantified the level of proteins using imageJ software.

7. Flow cytometry analysis

The cells were collected, washed and blocked. Then the cells were incubated on ice with mouse anti-CD133 (Cell Applications) and ALDH1A1 (Cell Signaling Technology) antibody for 1 h. The primary antibody was removed and the cells were incubated on ice for 30 min with Alexa Fluor 488-conjugated goat anti-rabbit IgG (H+L) secondary antibody (Life Technologies, Eugene, OR). Fluorescence intensity was detected by flow cytometry using a 488-nm excitation beam and a 519-nm band-pass filter (FACSort; Becton Dickinson, Rutherford, NJ). The mean fluorescence intensity was quantified by CellQuest software (Becton Dickinson).

8. Migration assay

Migration was determined by wound healing and transwell assays. For the wound healing assay, a monolayer of the treated cells was cultured in a 96-well plate, and a wound space was made with a 1-mm-wide tip. After rinsing with PBS, the cell monolayers were incubated with the indicated treatments and allowed to migrate for 24 h. Micrographs were taken under a phase contrast microscope (Olympus DP70, Melville, NY), and the wound spaces were measured from 10 random fields of view

using Olympus DP controller software. Quantitative analysis of cell migration was performed using an average wound space from those random fields of view, and the percentage of change in the wound space was calculated using the following formula: % change = (average space at time 0 h) - (average space at time 24 h)/(average space at time 0 h)x100. Relative cell migration was calculated by dividingthe percentage change in the wound space of treated cells by that of the control cells in each experiment.

For the transwell assay, the treated cells were seeded at a density of 5×10^4 cells/well onto the upper chamber of a transwell (8 μm pore size) in a 24-well plate in serum-free medium. RPMI medium containing 10% FBS was added to the lower chamber. Following the incubation, the non-migrated cells in the upper chamber were removed by cotton-swab wiping, and the cells that migrated to the underside of the membrane were stained with 10 μg/ml of Hoechst 33342 for 10 min and visualized and scored under a fluorescence microscope (Olympus IX51 with DP70).

9. Invasion assay

An invasion assay was performed using a 24-well transwell unit with polycarbonate (PVDF) filters (8 μm pore size). The membrane was coated with 0.5% matrigel on the upper surface of the chamber overnight at 37°C in a humidified incubator. The cells were plated at a density of 2×10^4 cells per well into the upper chamber of the transwell unit in serum-free medium. Medium containing 10% FBS was added to the lower chamber of the unit. After incubation with specific test agents for 24 h at 37°C, the medium in the upper chamber was aspirated, and the cells on the upper side of the membrane were removed with a cotton swab. The cells that invaded

to the underside of the membrane were stained with 10 µg/ml of Hoechst 33342 for 10 min, visualized and scored under a fluorescence microscope.

10. In vitro 3D tumorigenesis assay

In vitro 3D tumorigenesis was performed in a matrigel-coated 96-well plate. A plate was coated with 0.5% agarose and left for solidification. The cells were suspended in culture medium containing 4% matrigel, and plated at a density of $3x10^2$ cells/well onto an agarose-coated plate. Fresh medium was replaced every 3 days. After 10 days, the cells were visualized and scored by image analyzer under microscope (Olympus IX51 with DP70). Whole area of each well was captured in one picture and the colonies with more than 25 µm of diameter were quantified.

11. Spheroid formation assay

A spheroid formation assay was performed under nonadherent and serum-free conditions as previously described by Yongsanguanchai et al (2015). Approximately $5×10^3$ cells/well were suspended in RPMI serum free medium and plated onto a 24-well ultralow attachment plate. Cells were cultured for 14 days and then primary spheroids were resuspended into single cells, and again $5×10^3$ cells/well were plated onto a 24-well ultralow attachment plate using RPMI serum free medium. Cells were cultured for anorther 14 days and visualized under a light microscope. Characterization of stem cell phenotype-rich population was performed at *day 28* of spheroid culture.

12. ROS detection

Intracellular ROS were determined by fluorescence microplate reader and by flow cytometry using the ROS-specific probe, superoxide anions, hydrogen peroxide and hydroxyl radicals were determined by dihydroethidium (DHE), dichlorofluorescein

diacetate ($DCFH_2$-DA) or hydroxyphenyl fluorescein (HPF), respectively. For fluorescence microplate reader, cells were seeded overnight in 96-well plate. Before zinc ion treatment cells were incubated with 10 μM of DHE, $DCFH_2$-DA and HPF for 30 min at 4°C, after which they were washed and treated with various concentrations of zinc ion (0-50 μM) for 1 and 3 h. After incubation, the fluorescence intensity was immediately analyzed by fluorescence microplate reader (SpectraMax M5, Molecular Devices Corp., Sunnyvale, CA, USA) using a 488-nm excitation beam and a 610-nm band-pass filter for DHE, using a 480-nm excitation beam and a 530-nm band-pass filter for detecting DCF fluorescence or using a 490-nm excitation beam and a 515-nm band-pass filter for HPF.

For flow cytometry, cells were seeded overnight in 6-well plate. Before zinc ion treatment cells were incubated with 10 μM of DHE, $DCFH_2$-DA or HPF for 30 min at 4°C, after which they were washed and treated with 50 μM of zinc ion for 1 and 3 h. After incubation, cells were washed, resuspended in phosphate-buffered saline (PBS), and immediately analyzed for fluorescence intensity by FACScan flow cytometer (Beckton Dickinson, Rutheford, NJ) using a 488-nm excitation beam and a 610-nm band-pass filter for DHE, using a 480-nm excitation beam and a 530-nm band-pass filter for detecting DCF fluorescence or using a 490-nm excitation beam and a 515-nm band-pass filter for HPF. Mean fluorescence intensity was quantified by CellQuest software (Becton–Dickinson) analysis of the recorded histograms. Relative fluorescence was calculated as a ratio of the treated to the non-treated control fluorescence intensity.

13. Immunoprecipitation assay

Anti-β-catenin antibodies was first incubated with protein A-conjugated Sepharose (Santa Cruz Biotechnology) overnight at 4°C to obtain anti-β-catenin-agarose bead. Cells were washed after treatments with ice-cold PBS and lysed in lysis buffer (containing 50 mM Tris-HCl (pH 7.5), 1% Triton X-100, 150 mM NaCl, 20 mM EDTA, 50 mM NaF, 1 mM phenylmetylsulfonyl fluoride (PMSF), and a commercial protease inhibitor mixture (Roche)) at 4°C for 30 min. After centrifugation at 14,000 g for 15 min at 4°C, the supernatants were collected and determined for protein content. Protein content was determined by the Bradford method (Bio-Rad). Cell lysates containing 60 μg proteins were incubated with 12 μl of anti-β-catenin-agarose bead diluted with 12 μl sepharose for 6 h at 4°C. The immune complexe was then washed 5 times with 20 volumes of lysis buffer, resuspended in 2x Laemmli sample buffer and boiled at 95°C for 5 min. Immunoprecipitates containing approximately 20 μg protein equivalent were separated by 10% SDS-PAGE and analyzed by Western blot using anti-ubiquitin antibody as described.

14. Statistical analysis

All data were expressed as the means ± S.E.M. from three or more independent experiments. Multiple comparisons were examined for significant differences of multiple groups, using analysis of variance (ANOVA), followed by individual comparisons with the Scheffe's post-hoc test. Statistical significance was set at $P<0.05$.

Conceptual framework

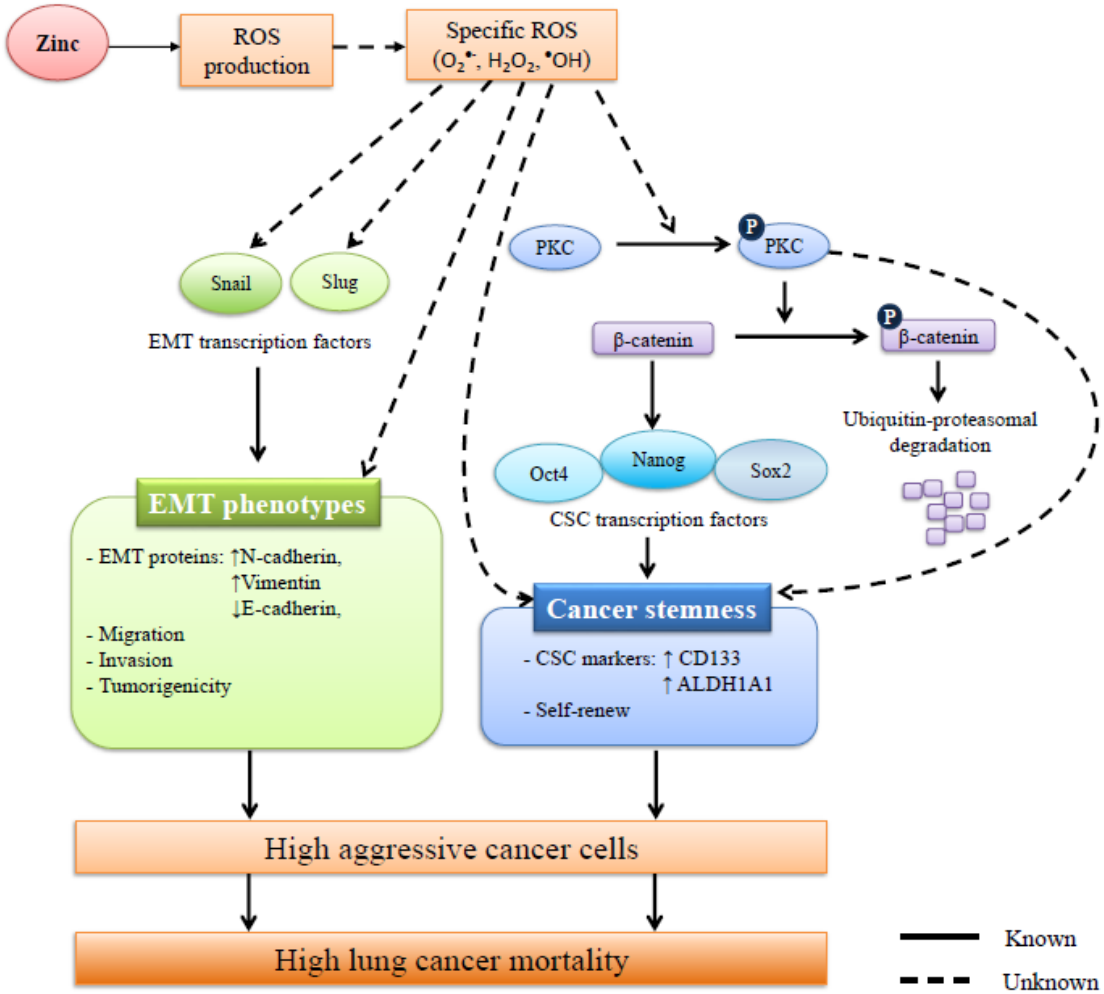

Experimental designs

Part I Investigation on cytotoxic effect of zinc ion on human lung cancer cells

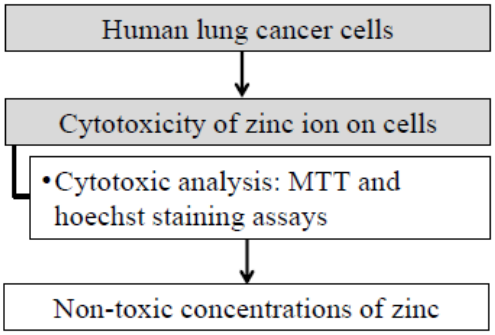

Part II Investigation on effects of zinc ion on EMT and CSC phenotypes

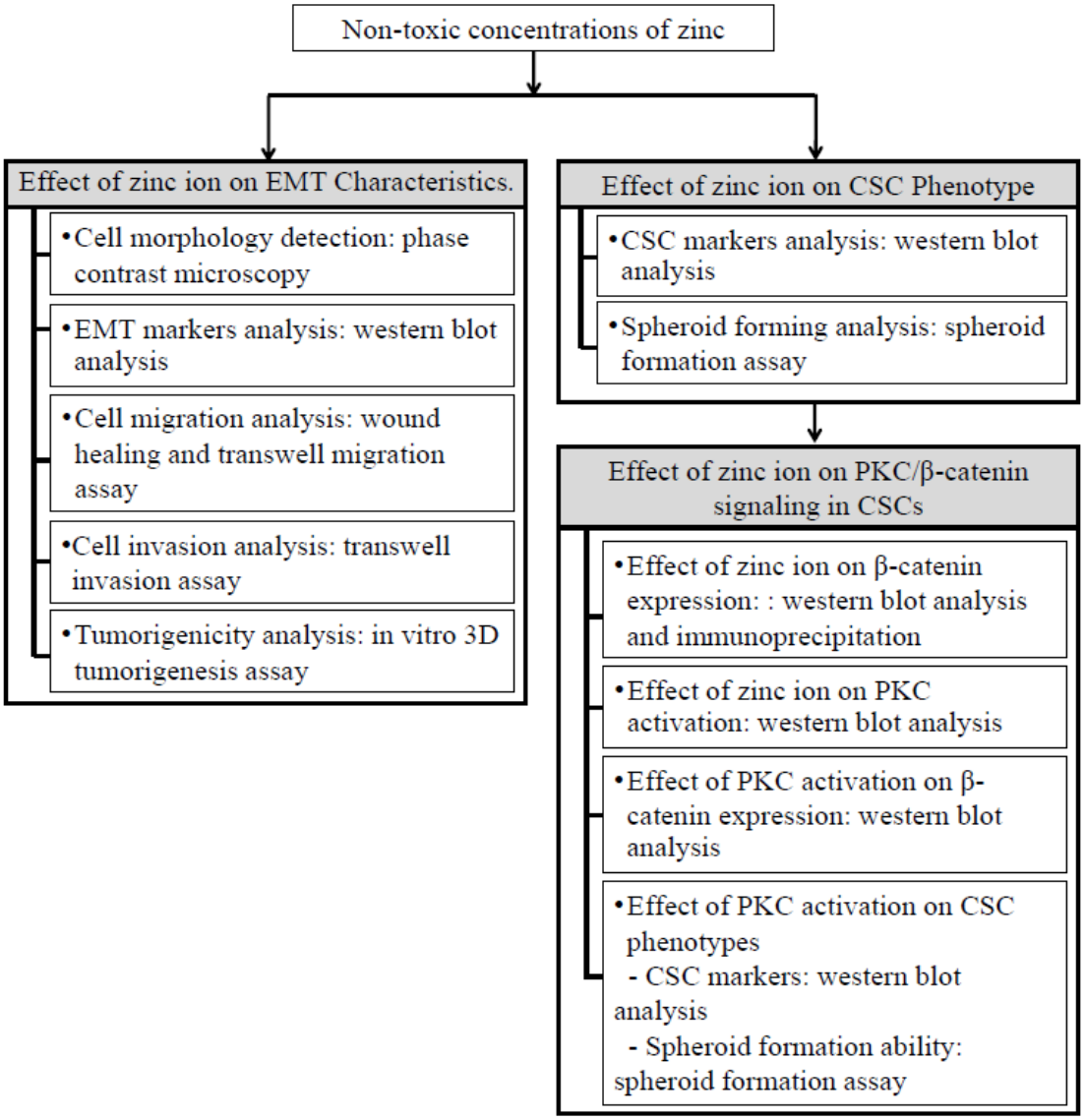

Part III Investigation on the underlying mechanisms involved zinc ion mediated EMT and CSCs

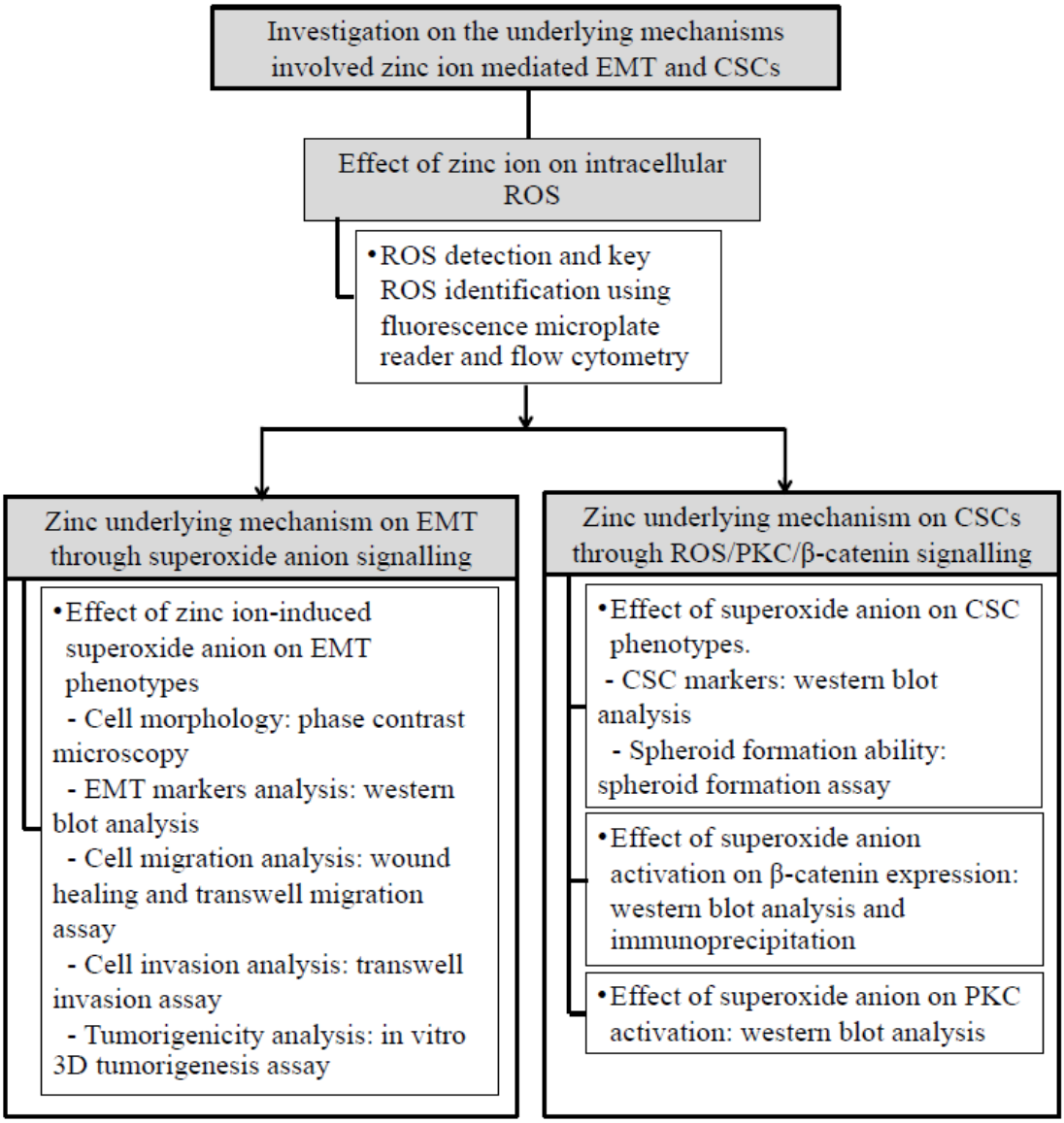

1. Cytotoxic and proliferative effects of zinc ion on lung cancer H460 cells.

1.1 Cytotoxic effects of zinc ion on H460 cells.

Having shown that the level of zinc ion in plasma was found at the concentrations ranging from 10-18 μM (Hajo and Wolfgang, 2010; Wu et al., 2013) and An aberrant intracellular zinc ion level has been found in the condition of cancer (Gupta et al., 2005; Gumulec et al., 2014). The toxic level of zinc ion in lung cancer H460 cells was first investigate.

Cells were treated with various concentrations of zinc ion (0-100μM) and incubated at 37°C for 24 h. Cell viability and apoptosis were determined by MTT and Hoechst staining assay. Non-toxic concentrations of zinc ion which cause no significant effect and not less than 80% on cell viability were used in further experiments.

1.2 Proliferative effects of zinc ion on H460 cells.

Because zinc ion has been generally known to regulate cell division in many cell types (MacDonald, 2000; Kambe, 2014), the proliferative effect of zinc ion on lung cancer H460 cells was investigate.

Approximately $2x10^3$ cells/well were seeded onto 96-well plate and treated with various non-toxic concentration of zinc ion (0-50μM) and incubated at 37°C for 24, 48 and 72 h. Cell viability was determined by MTT. Relative cell proliferation was calculated as a ratio of the treated to the non-treated control cell viability.

2. Effect of zinc ion on EMT characteristics in lung cancer H460 cells.

As zinc ion was required for cytoskeleton organization and was an essential component of several proteins involved in cell motility and metastasis, such as matrix metalloproteinases (MMPs) (Lansdown, 1996; Lansdown et al., 2007) and previous study reported that migration ability of breast cancer cells was inhibited by zinc ion depletion in response to zinc ion chelator TPEN treatment (Kagara et al., 2007), whether zinc ion has an impact on lung cancer H460 cell motility and EMT.

2.1 Effect of zinc ion on cell morphology.

During EMT, epithelial cells undergo remarkable morphological conversion from cobble stone-like epithelial morphology to elongated-like mesenchymal morphology (Yang and Weinberg, 2008; Thiery et al., 2009; Iwatsuki et al., 2010; Craene and Berx, 2013). Therefore, the morphology alteration of lung cancer H460 cells in response to zinc ion treatment was examined.

Cells were seeded at a density of $5x10^4$ cells/well onto a 12-well plate and treating the cells with various non-toxic concentrations of zinc ion (0-50μM) for 24 h. The treated cells were processed as described in *Materials and Methods* and cell morphology was then examined by a phase contrast microscope (Eclipse Ti-U, Nikon, Tokyo, Japan).

2.2 Effect of zinc ion on EMT markers.

The hallmark of EMT is the loss of E-cadherin, a cellular junction protein typically expressed in epithelial cells. In addition, EMT-phenotypic cells increase the expression of mesenchymal markers such as N-cadherin and vimentin as well as up-regulate the transcriptional factors, namely snail and slug (Yang and

Weinberg, 2008; Thiery et al., 2009; Iwatsuki et al., 2010; Craene and Berx, 2013). We further investigate the expression level of EMT markers in response to zinc ion treatment.

Cells were seeded at a density of $2x10^5$ cells/well onto a 6-well plate and treated with various non-toxic concentrations of zinc ion (0-50μM) for 24 h. After 24 h of incubation, the expression of EMT-related proteins, including E-cadherin, N-cadherin, vimentin, snail and slug were determined by western blot analysis.

2.3 Effect of zinc ion on cell migration.

Increased migration and invasion were considered to be the aggressiveness of cancer and the principal characteristics of EMT (Yang and Weinberg, 2008; Thiery et al., 2009; Iwatsuki et al., 2010; Craene and Berx, 2013).

To investigate the effect of zinc ion on cell migration, cells were left pretreated with zinc ion at various non-toxic concentrations (0-50μM) for 24 h and the migration ability was then assessed using wound healing and transwell migration assay as describe in *Materials and Methods*. The result of cell migration ability was represented as relative cell migration comparing to control.

2.4 Effect of zinc ion on cell invasion.

For invasion, cells were left pretreated with zinc ion at various non-toxic concentrations (0-50μM) for 24 h and cell invasion ability was then determined by matrigel-cloted transwell invasion assay as describe in *Materials and Methods*. The result of cell invasion ability was represented as relative cell invasion comparing to control.

2.5 Effect of zinc ion on motility-related proteins.

To identify the underlying mechanism of cell motility mediated by zinc ion in lung cancer H460 cells, the expression of migratory-related proteins, such as activated FAK (phosphorylated FAK, Tyr 397), FAK, active Rac1 (Rac1-GTP) and active RhoA (RhoA-GTP) were evaluated by western bolt analysis after treatment the cells with various non-toxic concentrations of zinc ion for 24 h.

2.6 Effect of ion on tumorigenicity.

It is well known that the EMT process facilitate tumor formation at the metastatic site (Hwang et al., 2011; Voon et al., 2013; Zhou et al., 2014) and this potential is responsible for cancer progression (Hwang et al., 2011; Voon et al., 2013; Zhou et al., 2014).

Therefore, the tumorigenicity in response to zinc ion treatment was evaluated by pretreating the cell with various non-toxic concentrations of zinc ion (0-50μM) for 24 h. The treated cells were subjected to 3D in vitro tumorigenesis assay as mentioned in *Materials and Methods*.

3. Effect of zinc ion on intracellular ROS in lung cancer H460 cells and specific type of ROS identification.

Previous studies have indicated that zinc ion has an impact on cellular redox status of the cells and exerts the pro-oxidant activity to generate ROS in various normal and cancer cells (Link and von Jagow, 1995; Brown et al., 2000; Noh and Koh, 2000; Dineley et al., 2005; Rudolf, 2007; Rudolf and Cervinka, 2010; Wu et al., 2013).

To prove the ability of zinc ion to generate ROS and identify the specific type of ROS induced by zinc ion in lung cancer H460 cells, cells were pre-incubated with ROS-specific probes using DHE for superoxide anions, $DCFH_2$-DA for hydrogen peroxide and HPF for hydroxyl radicals at 4°C for 30 min. After that the cells were treated with various non-toxic concentrations of zinc ion for 0-3 h and the fluorescent intensity which represents the intracellular ROS levels were determined by fluorescence microplate reader and by flow cytometry as described in *Materials and Methods*.

In addition, having shown in this study that zinc ion caused an increase in intracellular superoxide anion level (The detail was further described in chapter IV). To confirm that superoxide anion is the key ROS induced by zinc ion treatment, standard superoxide anion inhibitors, namely MnTBAP was used to block the signal of intracellular superoxide anion by pretreatment the cells with MnTBAP (50 μM) for 1 h before zinc ion treatment. After incubation with zinc ion for 3 h, the fluorescent intensity was determined by fluorescence microplate reader and by flow cytometry using DHE probes as described in *Materials and Methods*.

Moreover, as DMNQ was used as a superoxide anion donor, the level of superoxide anion in response to DMNQ treatment should be determined. Cells were pre-incubated with DHE at 4°C for 30 min. After that the cells were treated with 5 μM of DMNQ for 3 h and the fluorescent intensity which represents the intracellular superoxide anion level was determined by flow cytometry as described in *Materials and Methods*.

4. Effect of superoxide anion on EMT phenotypes.

Numerous studies have indicated that ROS were involved in many processes of tumor metastasis including migration, invasion and EMT (Wu, 2006; Wang et al., 2010; Wu and Wu, 2010). Previous evidence deeply indicated the roles of hydrogen peroxide in EMT regulation (Cheng et al., 2010; Kim et al., 2013); however, there is no evidence providing those information about EMT regulated by superoxide anion.

4.1 Effect of superoxide anion on cell morphology.

To examine the role of superoxide anion in morphological alteration, cells were treated with MnTBAP (50 μM) in the present and absence of zinc ion (50 μM) treatment for 24 h or treated with DMNQ (5 μM), and morphology of the cells was examined by a phase contrast microscope (Eclipse Ti-U, Nikon, Tokyo, Japan).

4.2 Effect of superoxide anion on EMT markers.

To investigate the role of superoxide anion in the expression of EMT markers, for evaluation of EMT markers, cells were treated with MnTBAP (50 μM) in the present and absence of zinc ion (50 μM) treatment or treated with DMNQ (5 μM) for 24 h and EMT markers were evaluated by western blot analysis.

4.3 Effect of superoxide anion on cell migration.

To investigate the role of superoxide anion in cell migration, cells were treated with MnTBAP (50 μM) in the present and absence of zinc ion (50 μM) treatment or treated with DMNQ (5 μM) for 24 h and cell migration was assessed by wound healing assay.

4.4 Effect of superoxide anion on cell invasion.

To investigate the role of superoxide anion in cell invasion, cells were treated with MnTBAP (50 μM) in the present and absence of zinc ion (50 μM) treatment or treated with DMNQ (5 μM) for 24 h, and invasion ability was determined by transwell invasion assay.

4.5 Effect of superoxide anion on tumorigenicity.

To investigate the role of superoxide anion in tumorigenicity, cells were treated with MnTBAP (50 μM) in the present and absence of zinc ion (50 μM) treatment or treated with DMNQ (5 μM) for 24 h, and tumorigenicity was analyzed by 3D in vitro tumorigenesis assay.

5. Effect of zinc ion on CSC phenotypes in lung cancer H460 cells.

CSCs have been suggested to be the potential driving force of new tumor initiation and cancer progression due to the self-renewal and tumorigenic abilities, leading to chemoresistance, metastasis and cancer relapse (Mehlen and Puisieux, 2006; Hermann et al., 2007; Merlos-Suarez et al., 2011; Perona et al., 2011; Scheel and Weinberg, 2012). Whether zinc ion has an ability to induce stemness in lung cancer H460 cells. This study next investigated the effect of zinc ion in CSC induction.

5.1 Effect of zinc ion on CSC markers.

The distinct abilities of CSCs to increase the expression of various transcription factors regulating self-renewal and pluripotentcy, including Nanog, Sox2 and Oct4, making CSCs different from normal cancer cells (Liu et al., 2013). Besides, CSCs always express the up-regulation of CSC marker proteins, such as

CD133 and ALDH1A1 which involves in tumorigenicity and drug resistant properties of CSCs, respectively.

To investigate the expression of CSC marker proteins, cells were seeded at a density of $1x10^5$ cells/well onto a 6-well plate and treated with various non-toxic concentrations of zinc ion (0-50 μM) for 72 h. After incubation, the expression of CSC-related proteins, including CD133, ALDH1A1, Nanog, Oct4 and Sox2 were determined by western blot analysis.

5.2 Effect of zinc ion on spheroid formation.

Since spheroid or tumor sphere formation under non-attached and serum-starved conditions was used to determine the CSC self-renewal capability (Luanpitpong et al., 2014; Yongsanguanchai et al., 2015), this study next investigated the effect of zinc ion on spheroid formation in lung cancer H460 cells.

Firstly, to confirm the potential of a model to differentiate the distinct population of CSC-rich phenotype, the spheroid formation model was characterized. Lung cancer H460 cells were grown in single cells-suspended condition to form primary and secondary spheroids (14 + 14 days). The secondary spheroids were collected and determined for the CSC markers by western blot analysis in comparison to their parental cells.

To examine the effect of zinc ion on spheroid formation, cells were pretreated with various non-toxic concentrations of zinc ion (0-50 μM) for 72 h and subjected to spheroid formation assay as described in *Materials and Methods*.

6. Effect of zinc on CSC regulatory proteins

It is widely accepted that β-catenin is a key mediator in regulation of CSCs (Cai and Zhu, 2012; Holland et al., 2013; Mao et al., 2014). β-catenin is able to translocate into nucleus and increase transcriptional activation of β-catenin target genes, which regulate the expression of transcription factors regulating self-renewal and pluripotency, such as Nanog, Oct4 and Sox2 (Cai and Zhu, 2012; Holland et al., 2013). Therefore, the expression of β-catenin was highlighted in this study.

6.1 Effect of zinc ion on β-catenin expression

To determine the expression of β-catenin protein, cells were treated with various non-toxic concentration of zinc ion (0-50 μM) for 24 and 72 h, the expression level of β-catenin was examined by western blot analysis.

6.2 Effect of zinc ion on β-catenin degradation

Having shown that the degradation of β-catenin is mainly mediated by ubiquitin-dependent proteasome complex (Holland et al., 2013). To investigate the effect of zinc ion on β-catenin degradation via proteasome degradation pathway, cells were treated with zinc ion (50 μM) in the present and absence of clasto-lactacystin β-lactone (Lac; 10 μM), a proteasome inhibitor. After 24 h of incubation, the level expression of β-catenin was detected by western blot analysis.

In addiotion, the immunoprecipitation was conducted to confirm the role of zinc ion in regulation of ubiquitin-proteasome degradation, cells were treated with various concentrations of zinc ion in the present of clasto-lactacystin β-lactone

(10 μM) to inhibit proteasome degradation. After 0-3 h of incubation, cell lysates were prepared and immunoprecipitated using anti-ß-catenin antibody as described in *Materials and Methods*. The resulting immume complex was then analyzed for ubiquitin by western blot analysis using anti-ubiquitin antibody.

6.3 Effect of zinc ion on PKCα activation.

Evidence showed that the regulation of ß-catenin degradation is considered to be the determining step in ß-catenin signaling (Holland et al., 2013). The level of ß-catenin can be regulated by PKCα signaling (Gwak et al., 2006; Luna-Ulloa et al., 2011). PKCα is able to phosphorylate ß-catenin at the position of serine 33 and 37 and threonine 41 and subsequently subjected proteasome degradation system (Gwak et al., 2006). However, the effect of zinc ion on PKCα signaling is unknown.

To investigate the effect of zinc ion on PKCα activation, cells were treated with various concentrations of zinc ion (0-50 μM) for 12 h and the expression of phosphorylated PKCα (p-PKCα) and total PKCα were evaluated by western blot analysis.

6.4 Effect of PKCα on spheroid formation

Although previous study reported the effect of PKCα on ß-catenin signaling (Gwak et al., 2006; Luna-Ulloa et al., 2011), the role of PKCα in regulation of CSC program is unknown. To investigate weather PKCα regulates CSC phenotypes in lung cancer cells, PKCα activator (A23187) and PKCα inhibitor (bisindolylmaleimide I; BIM) were utilized.

The effect of PKCα on tumor sphere formation was characterized by leaveing the cells treated with A23187 (0.1 μM) or zinc ion (50 μM) in the present and absence of BIM (5 μM) treatment for 72 h. After incubation, the treated cells were subjected to spheroid formation assay as described in *Materials and Methods*.

6.5 Effect of PKCα on CSC markers

Besides, the expression levels of ß-catenin and CSC markers were characterized. Cells were treated with A23187 (0.1 μM) or zinc ion (50 μM) in the present and absence of BIM (5 μM) treatment for 72 h, the expression levels of ß-catenin and CSC markers were determined by western blot analysis.

7. Effect of superoxide anion on CSC phenotypes

Although the role of ROS in regulation of CSCs was not clear (Shi et al., 2012), to effectively target CSCs, understanding ROS regulatory mechanism in CSCs is necessary. This study therefore investigates the role of superoxide anion in controlling of CSC characteristics of lung cancer cells.

7.1 Effect of superoxide anion on spheroid formation

To investigate the role of superoxide anion in tumor sphere formation, cells were treated with DMNQ (5 μM) or zinc ion (50 μM) in the present and absence of MnTBAP (50 μM) for 72 h, and tumor sphere formation was analyzed by spheroid formation assay.

7.2 Effect of superoxide anion on CSC markers

To investigate the role of superoxide anion in the expression of CSC markers, cells were treated with DMNQ (5 μM) or zinc ion (50 μM) in the present and absence of MnTBAP (50 μM) for 72 h and CSC markers were evaluated by western blot analysis.

7.3 Effect of superoxide anion on β-catenin expression

To investigate the effect of superoxide anion on β-catenin expression, cells were treated with DMNQ (5 μM) or zinc ion (50 μM) in the present and absence of MnTBAP (50 μM) for 24 h, the level expression of β-catenin was determined by western blot analysis. Also, the β-catenin-ubiquitin complex was evaluated by immunoprecipitation as described in *Materials and Methods* to confirm the effect of superoxide anion on β-catenin degradation.

8. Effect of superoxide anion on PKCα activation

It is shown that ROS as a signaling messenger have a capability to oxidize the crucial target molecules, including PKCα (Wu and Wu, 2010). PKCα contains multiple cysteine residues that can be oxidized and activated by ROS (Gomez et al., 1999). This study next investigated the effect of superoxide anion on PKCα activation.

Cells were treated with zinc ion (50 μM) in the present and absence of MnTBAP for 12 or 24 h, and the expression level of phosphorylated PKCα (p-PKCα) and total PKCα were determined by western blot analysis.

9. Effect of zinc ion on other different lung cancer cells

To confirm the effects of zinc ion in CSC program, lung cancer H292 and H23 cells were utilized and the key experiments, such as the expression of CSC markers, spheroid forming ability, superoxide anion production, and p-PKCα/PKCα expressions were conducted in other two cell lines according to the instructions of each experiments as mentioned before.

CHAPTER IV
RESULTS

1. Cytotoxic and proliferative effects of zinc ion on lung cancer H460 cells.

1.1 Cytotoxic effects of zinc ion on H460 cells.

An aberrant intracellular zinc ion level has been found in the condition of cancer (Gupta et al., 2005; Gumulec et al., 2014). In order to investigate the effect of zinc ion on EMT and CSC phenotypes in human lung cancer cells, the non-cytotoxic concentrations of zinc ion were firstly evaluated.

Cells were cultured in the presence or absence of zinc ion (0-100 μM) for 24 h, and cell viability was determined by MTT assay at 24 h. The results indicated that treatment of the cells with zinc ion at the concentrations ranging from 5-50 μM caused no significant cytotoxicity as shown in figure 4.1A. The significant decrease in cell viability was first detected in response to 100 μM of zinc ion treatment with approximately 86% of the cells remaining viable.

In addition, to confirm the effect of zinc ion on cell toxicity, cells were similarly treated with zinc ion for 24 h, and apoptosis was evaluated by Hoechst 33342 staining assay. Figures 4.1B and C show that apoptotic cells containing condensed and/or fragmented nuclei were not detectable in response to zinc ion treatment at the concentrations of 5-50 μM. A significant number of apoptotic cells appreoximately 20% was detected at 100 μM of zinc ion treatment.

A

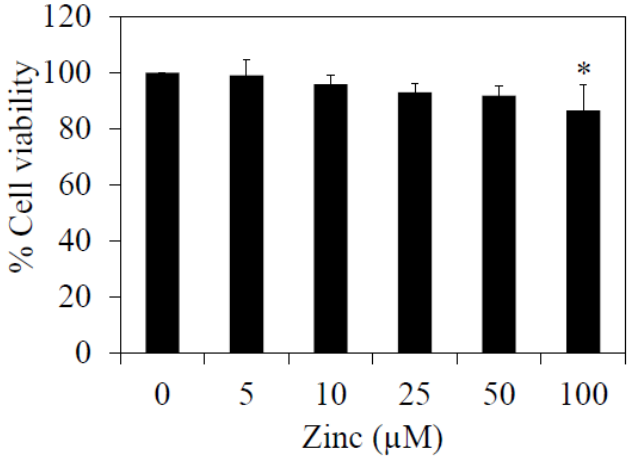

B

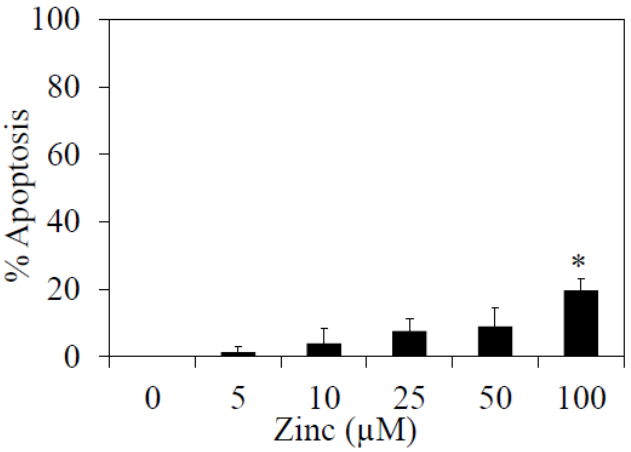

C

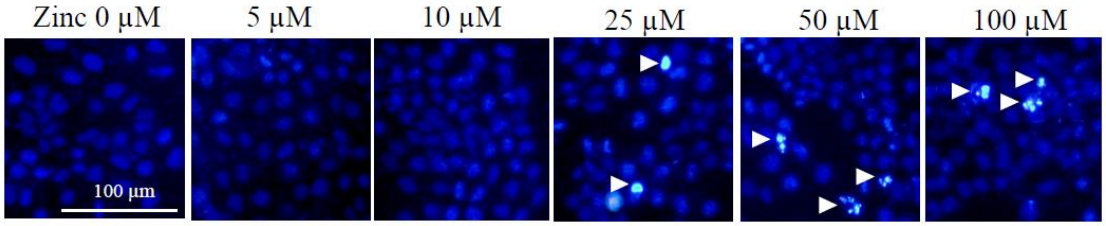

Figure 4.1 Cytotoxic effects of zinc ion on lung cancer H460 cells. (A) Effect of zinc ion on H460 cell viability. Cells were treated with various concentrations of zinc ion (0-100 µM) for 24 h. Percentage of cell viability was determined by the MTT assay. Values are means ± S.E.M. of the independent triplicate experiments. * $p<0.05$ versus non-treated

control. (B) Apoptotic cells were detected by Hoechst33342 staining after 24 h of zinc ion treatment. Values are means of independent triplicate experiments ± S.E.M. * $p<0.05$ versus non-treated control. (C) Nuclear morphology of the cells stained with Hoechst 33342 and visualized under a fluorescence microscope. White arrow indicates the apoptotic cells having condensed chromatin and/or fragmented nuclei.; scale bar = 100 μm.

1.2 Proliferative effects of zinc ion on H460 cells.

Proliferative effect of zinc ion at 0-50 μM was further evaluated by treating the cells with zinc ion for 0-72 h. Figure 4.2 indicates that zinc ion at the concentrations of 0-50 μM had no inductive effect on cell proliferation.

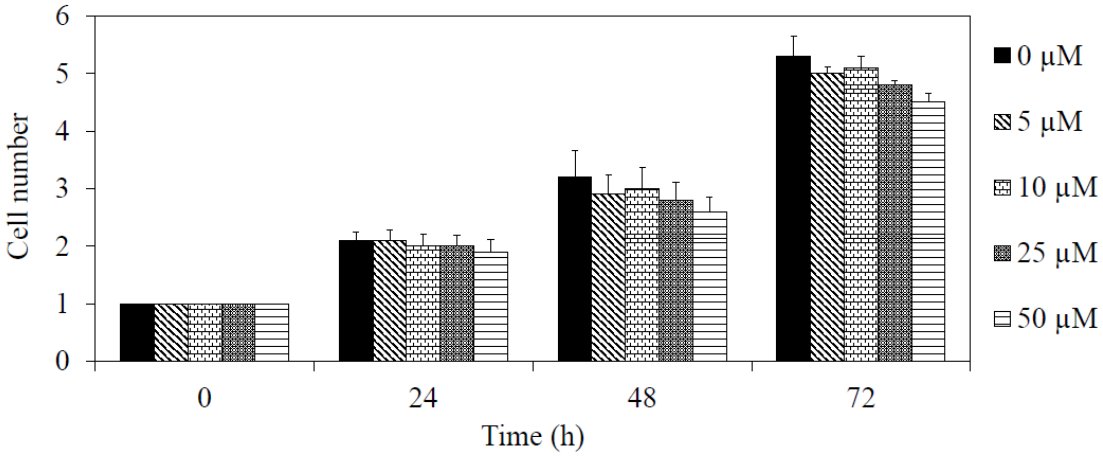

Figure 4.2 Proliferative effects of zinc ion on lung cancer H460 cells. Cells were treated with zinc ion (0-50 μM) for 0-72 h and analyzed by MTT assay. Relative cell proliferation was calculated by divided the percentage of cell viability in the treated group by those of control group. Values are means ± S.E.M. of independent triplicate experiments. * $p<0.05$ versus non-treated control.

2 **Effect of zinc ion on EMT characteristics in lung cancer H460 cells.**

The effect of zinc ion on EMT in H460 cells was next investigated. The alteration of cell morphology as well as hallmarks of EMT were used to monitor the effect of zinc ion on EMT process in lung cancer cells.

2.1 Effect of zinc ion on cell morphology.

Cells were treated with zinc ion at non-toxic concentrations for 24 h. The morphology of the cells was captured and presented in figure 4.3. The results showed that the zinc ion -treated cells exhibited morphology of mesenchymal-like cells with the elongated shape and loss of cell polarity. These results also suggested that the mesenchymal-like morphology is somehow dose-dependent as the more elongated cells could be found in the cells treated with high concentrations of zinc ion.

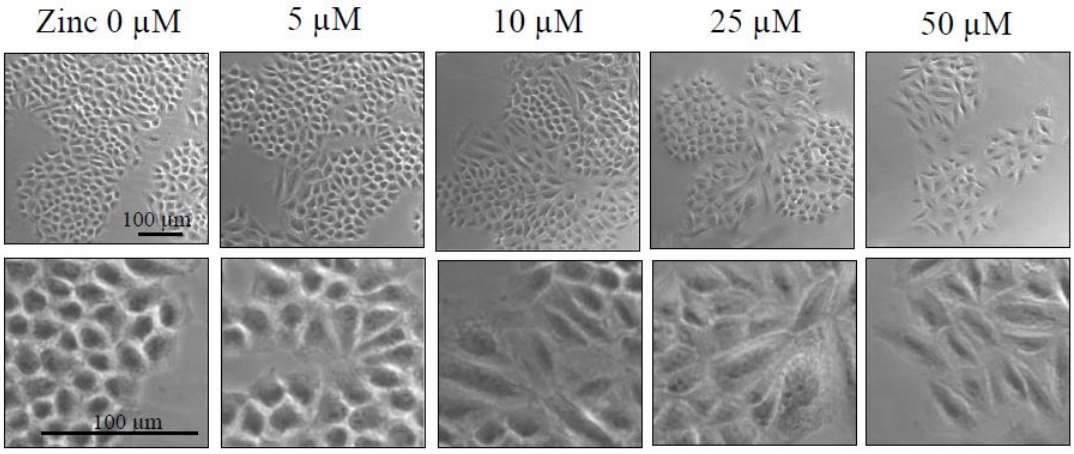

Figure 4.3 Effect of zinc ion on cell morphology. Zinc ion caused an alteration of cell morphology. Cells were treated with various concentrations of zinc ion (0-50 µM) for 24 h. Cells morphology was examined by phase-contrast microscope; scale bar = 100 µm.

2.2 Effect of zinc ion on EMT markers.

The switch of E-cadherin to N-cadherin and increase of EMT proteins including vimentin, slug, and snail have been shown to be important hallmarks of EMT in cancer cells (Yang and Weinberg, 2008; Thiery et al., 2009; Iwatsuki et al., 2010; Craene and Berx, 2013). We next determined such cellular EMT markers in the lung cancer cells treated with zinc ion by western blot analysis and Immunofluorescence.

Obviously, treatment of the cells with zinc ion could reduce E-cadherin in a dose-dependent manner. Together with the fact that the significant increase of N-cadherin was found when treating the cells with 5-50 μM of zinc ion, these data strongly indicated that zinc ion could be able to mediate E-cadherin to N-cadherin switching in these cells as shown in figure 4.4A and B.

In addition, the upstream transcription factors of EMT namely snail and slug were determined in the zinc ion-treated cells. These factors were shown to bind to E-box elements in the promoter region of E-cadherin, resulting in the transcriptional repression of E-cadherin and induction of mesenchymal markers (Yang and Weinberg, 2008; Iwatsuki et al., 2010; Craene and Berx, 2013). The result in figures 4.4A and B indicate that zinc ion significantly increased the expression levels of slug and snail.

Also, the results of western blot analysis (Figure 4.4A and B) and immunofluorescence (Figure 4.4C) indicate the EMT protein vimentin was found to be induced by zinc ion. Taken together, these results suggested that zinc ion could induce EMT in lung cancer cells.

A

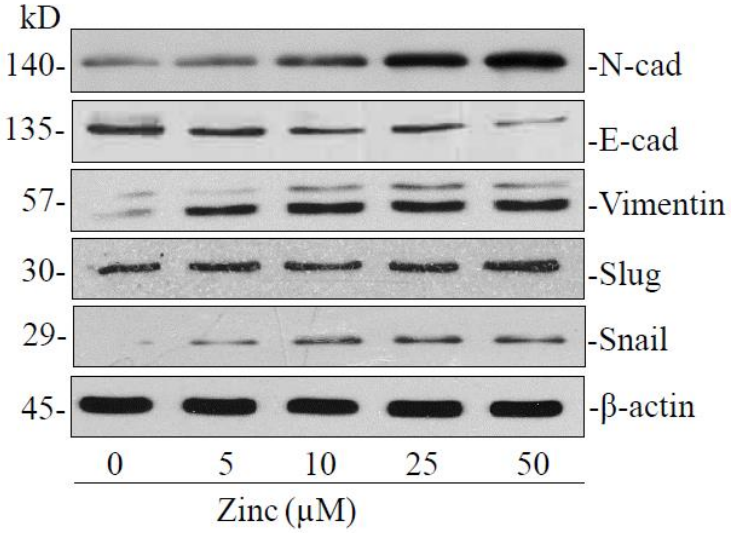
kD
140-
135-
57-
30-
29-
45-
-N-cad
-E-cad
-Vimentin
-Slug
-Snail
-β-actin
0
5
10
25
50
Zinc (μM)

B

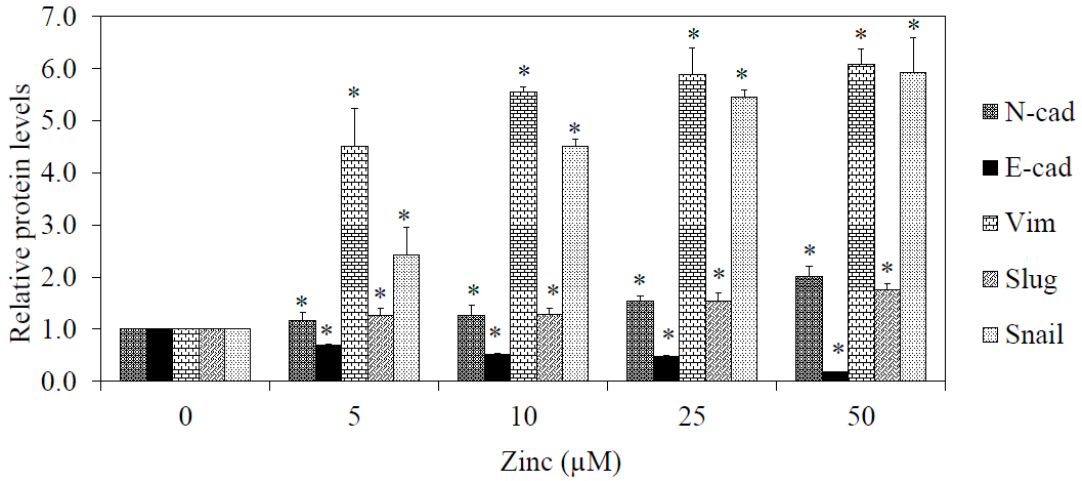
Relative protein levels
7.0
6.0
5.0
4.0
3.0
2.0
1.0
0.0
0
5
10
25
50
Zinc (μM)
N-cad
E-cad
Vim
Slug
Snail

C

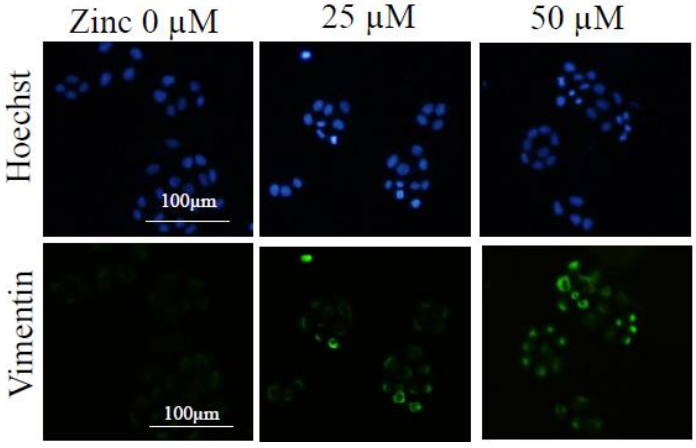
Zinc 0 μM
25 μM
50 μM
Hoechst
Vimentin
100μm
100μm

Figure 4.4 Effect of zinc ion on EMT markers. Cells were treated with various concentrations of zinc ion (0-50 μM) for 24 h. (A) The expression levels of EMT protein markers were determined by western blotting. The blots were re-probed with β-actin to confirm equal loading of the samples. (B) The blots were quantified by densitometry and mean data from three independent experiments were normalized to the results. The bars are the means ± S.E.M. of independent triplicate experiments. *$p<0.05$ versus untreated control (C) Expression of vimentin was analyzed by immunofluorescence staining; scale bar = 100 μm.

2.3 Effect of zinc ion on cell migration.

One important phenotype of EMT cells is the increase in cell motility. Studies have demonstrated that EMT could enhance aggressiveness of tumor cells by increasing their ability to migrate and invade (Yang and Weinberg, 2008; Iwatsuki et al., 2010; Craene and Berx, 2013).

To evaluate the effect of zinc ion on cancer cell motility, cells were left untreated or pretreated with zinc ion at non-toxic concentrations for 24 h and subjected to migration and invasion assays as described in the *Materials and Methods*. Wound healing migratory assay showed that zinc ion significantly facilitated migratory activity of the cells with the relative cell migration increased approximately 1.3-1.8-fold in comparison to that of non-treated control cells (Figure 4.5A and B).

Also, the transwell migration assay was performed to confirm the migratory effect of zinc. Figure 4.6A and B shows that zinc ion treatment significantly

increased the number of cells passed through the membrane of well, suggesting that such element induced cell migration.

2.4 Effect of zinc ion on cell invasion.

Next, we performed experiments to test the ability of the cancer cells in invading through matrigel. The transwell was pre-coated with matrigel and the zinc ion-treated cells were seeded on top. The cells were allowed to invade for 24 h and the invaded cells at the lower part of the membrane were determined.

Figure 4.7A and B shows the significantly higher number of invading cells was found in zinc ion-treated group, suggesting that zinc ion promoted the invasion of H460 cells in a dose-dependent manner.

A

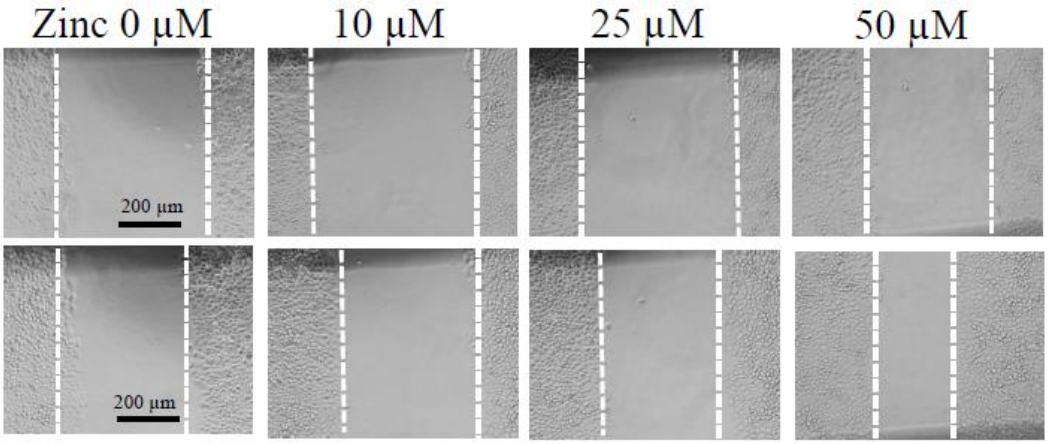

B

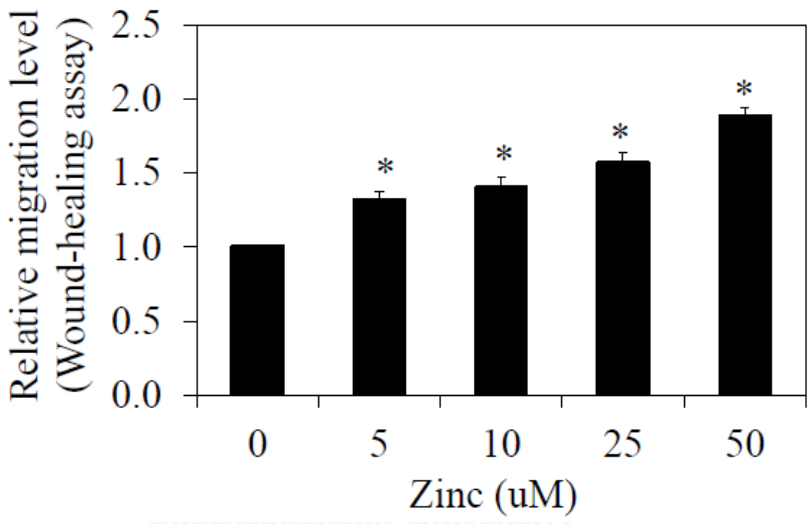

Figure 4.5 Effect of zinc ion on lung cancer cell migration by wound healing assay. Cells were pre-treated with zinc ion (0-50 µM) for 24h. The treated cells were subjected to migration assays. (A) For wound healing assay, the confluent monolayers of the cells were wounded by using a 1 mm-wide tip and cultured with the fresh medium. After 24 h of incubation, wound spaces were analyzed and represented as a relative migration level. (B) The relative migration level was determined by comparing the relative change of zinc ion-treated cells to non-treated control cells. Values are means ± S.E.M. of independent triplicate experiments. *$p<0.05$ versus non-treated control.

A

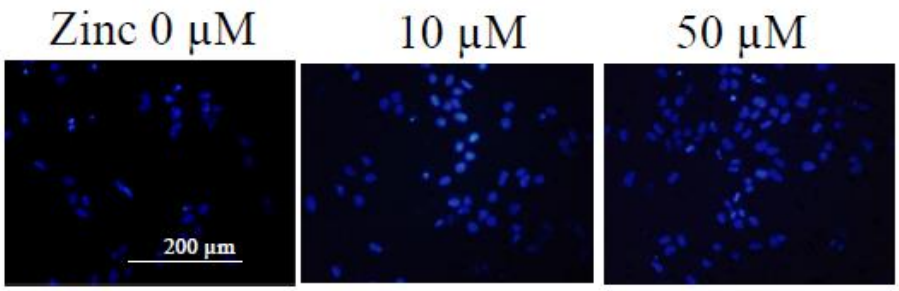

B

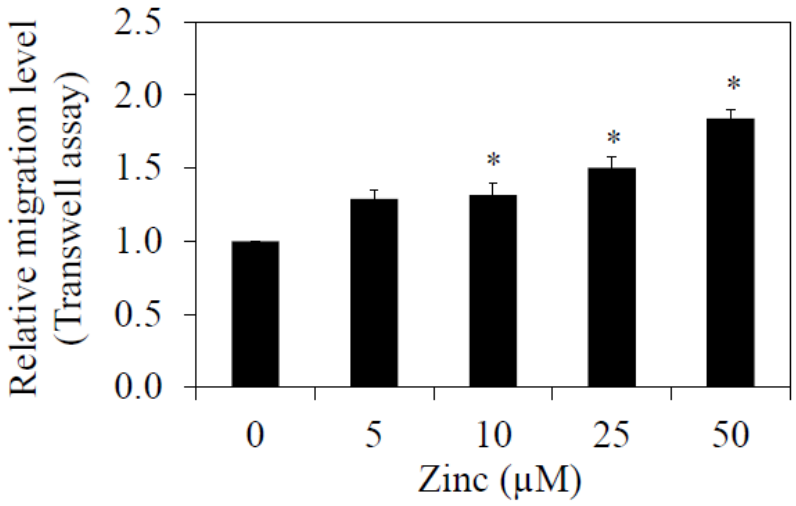

Figure 4.6 Effect of zinc ion on lung cancer cell migration by transwell migration assay. Cells were pre-treated with zinc ion (0-50 µM) for 24 h. The treated cells were subjected to migration assays. (A) For transwell migration assay, migratory cells were stained with Hoechst 33342 for 30 min, determined under a fluorescence microscope. (B) The number of migratory cells was quantified and represented as average number of migratory cells in each field relatively to control cells. The bars are the means ± S.E.M. of independent triplicate experiments. *p<0.05 versus untreated control.

A

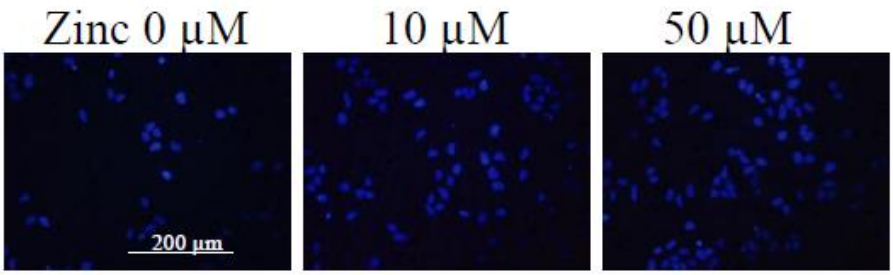

B

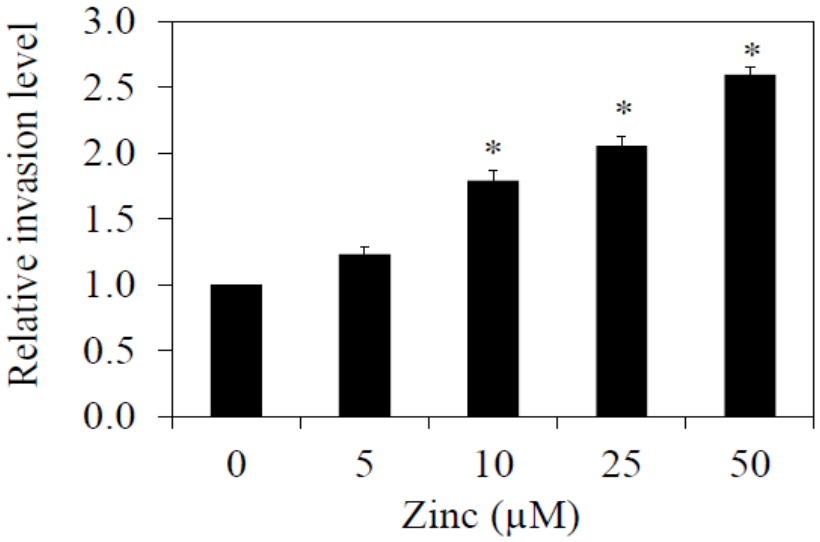

Figure 4.7 Effect of zinc ion on lung cancer cell invasion. Cells were pre-treated with zinc (0-50 µM) for 24h and the treated cells were subjected to invasion assays. (A) Cell invasion was evaluated using a transwell coated with matrigel as described under *Materials and Methods*. After 24 h, the cells that invaded across the membrane were stained with Hoechst 33342 for 30 min and visualized under a fluorescence microscope. (B) Value was represented as average number of invaded cells in each field relatively to control. Values are means ± S.E.M. of independent triplicate experiments *p<0.05 versus untreated control.

2.5 Effect of zinc ion on motility-related proteins.

Enhanced tumor cell migration and invasiveness are shown to be down-stream behaviors of FAK signal (Nieman et al., 1999; Wheelock et al., 2008; Mendez et al., 2010; Havel et al., 2015). This study next determined the effect of zinc ion treatment on motility regulatory proteins including FAK, activated (phosphorylated at Try397) FAK, active forms of RAC1, and RhoA by western blot analysis. The results showed that treatment of the cells with 0-50 μM of zinc ion for 24 h dramatically increased the activation of FAK (Figure 4.8). Also, its down-stream functioning proteins active Rac1 and RhoA were found to increase, accordingly. These results suggested that zinc ion treatment increase EMT-associated cell behaviors trough FAK-dependent pathway.

A

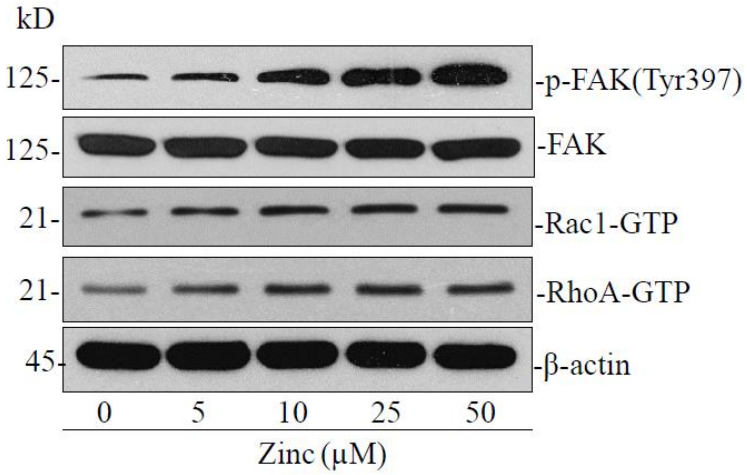

B

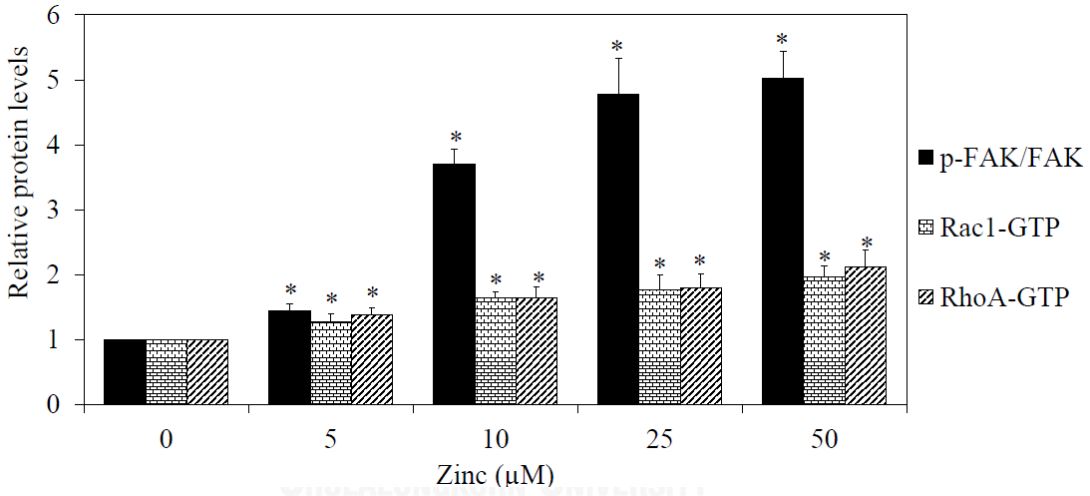

Figure 4.8 Effect of zinc ion on motility-regulatory proteins. (A) Cells were pre-treated with zinc ion (0-50 μM) for 24 h. The treated cells were subjected to western blot analysis to determine the expression levels of motility-regulatory proteins. The blots were re-probed with β-actin to confirm equal loading of the samples. (B) The blots were quantified by densitometry and mean data from three independent experiments were normalized to the results. The bars are the means ± S.E.M. of independent triplicate experiments. *$p<0.05$ versus untreated control.

2.6 Effect of zinc ion on tumorigenicity.

It is well known that the EMT process facilitate tumor formation at the metastatic site (Hwang et al., 2011; Voon et al., 2013; Zhou et al., 2014) and this potential is responsible for cancer progression (Hwang et al., 2011; Voon et al., 2013; Zhou et al., 2014). Having shown that zinc ion affected the expressions of EMT regulatory proteins, we next tested whether zinc ion may augment the ability of cancer cell to initiate a new tumor.

Previous studies have shown that *in vitro* 3D tumorigenesis assay reflexes ability of the cancer cells in *in vivo* cancer condition (Kimlin et al., 2013). *Therefore, in vitro* 3D tumorigenesis assay was utilized to evaluate tumorigenic potential in response to zinc ion treatment.

Cells were left un-treated or pre-treated with various concentrations of zinc ion (0-50 μM) for 24 h and subjected to tumorigenesis assay as described in *Materials and Methods*. After 10 days of 3D culturing, the colony number and diameter were determined. Figure 4.9A and B shows that zinc treatment enhances tumorigenic ability of the lung cancer cells as indicated by the significant increase in the number and size of colonies in zinc-treated groups. The number of colonies increased approximately 1.38-fold and 1.76-fold in response to zinc at 25 and 50 μM, respectively (Fig. 4.9B). The result suggested that zinc ion could enhance tumorigenic potential of lung cancer H460 cells.

A

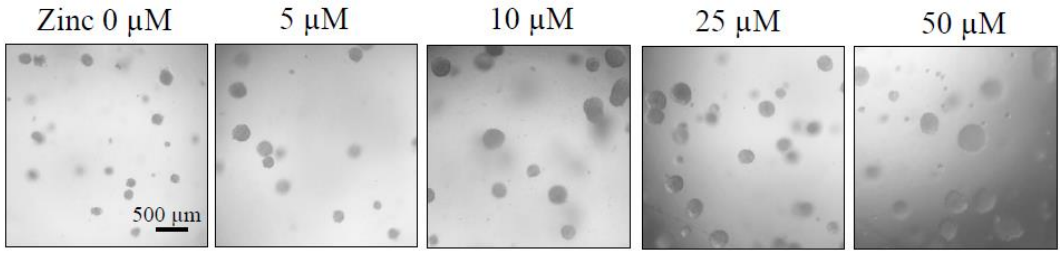

B

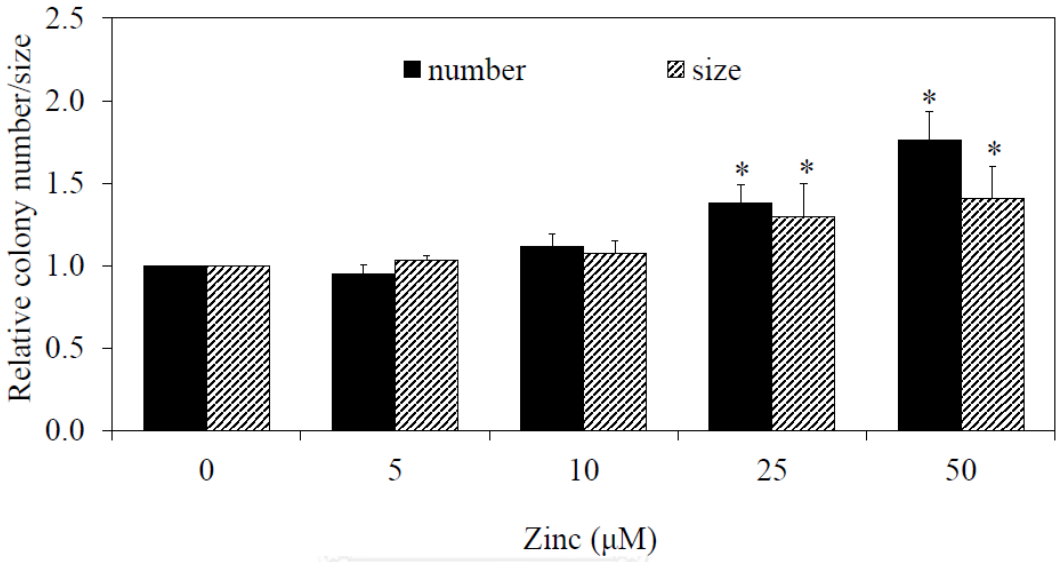

Figure 4.9 Effects of zinc ion on tumorigenic potential of H460 lung cancer cells. (A) H460 cells were pre-treated with zinc (0-50 µM) for 24h. The treated cells were subjected to 3D tumorigenesis assay. The cells were suspended in RPMI medium containing 4% Matrigel and zinc ion (0–50 µM) and plated onto agarose-coated plate. After 10 days, whole area of each well was captured in one picture under microscope and the colonies with more than 25 µm of diameter were quantified; scale bar = 500 µm. (B) Value was represented as average diameter and number of colonies in all field of each well relatively to control cells using image analyzer. Values are means ± S.E.M. of independent triplicate experiments. *p<0.05 versus untreated control.

3. Effect of zinc ion on intracellular ROS in lung cancer H460 cells and specific type of ROS identification.

Studies have demonstrated the roles of ROS on cancer EMT phenotypes (Wu, 2006; Wang et al., 2010; Wu and Wu, 2010). Because zinc ion has been previously shown to affect the redox balance of the cells and exhibit the pro-oxidant activity in normal and cancer cells (Noh and Koh, 2000; Rudolf et al., 2005; Rudolf, 2007; Wu et al., 2013), we next evaluated whether the effect of zinc ion in regulation of EMT in these lung cancer cells is through ROS-dependent mechanism.

To examine the specific ROS levels induced by zinc ion, cells were incubated with various ROS specific probes as mentioned in *Material and Methods* for 30 min before treatment with various concentrations of zinc ion (0-50 μM) and intracellular ROS levels were determined by flow cytometry and fluorescence microplate reader after 0-3 h of incubation.

Figures 4.10A and 4.11A show that zinc ion significantly increased cellular superoxide anion, while it had minimal effect on hydrogen peroxide (Figure 4.10B and 4.11B) and hydroxyl radical (Figure 4.10C and 4.11C). Consistent with microplate reader determination, flow cytometric analysis revealed that intracellular superoxide anion significantly increased up to 2-fold in response to zinc ion treatment (Figure 4.12A and B) and zinc ion had no detectable effect on hydrogen peroxide and hydroxyl radical (Figure 4.12A, C and D).

A

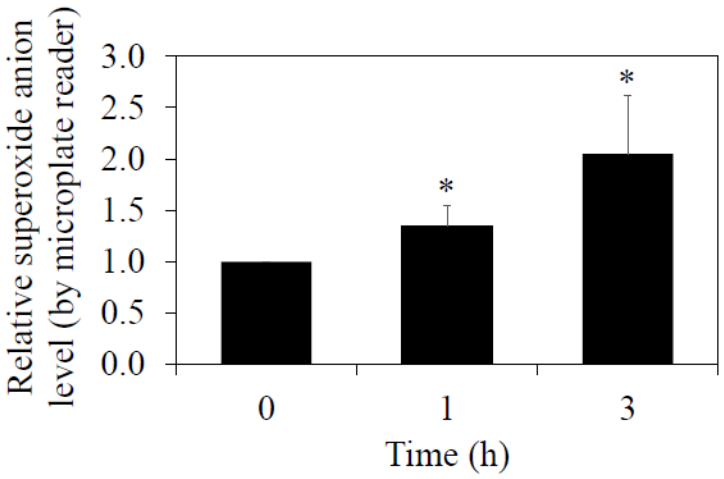
Relative superoxide anion level (by microplate reader)
3.0
2.5
2.0
1.5
1.0
0.5
0.0
*
*
0
1
3
Time (h)

B

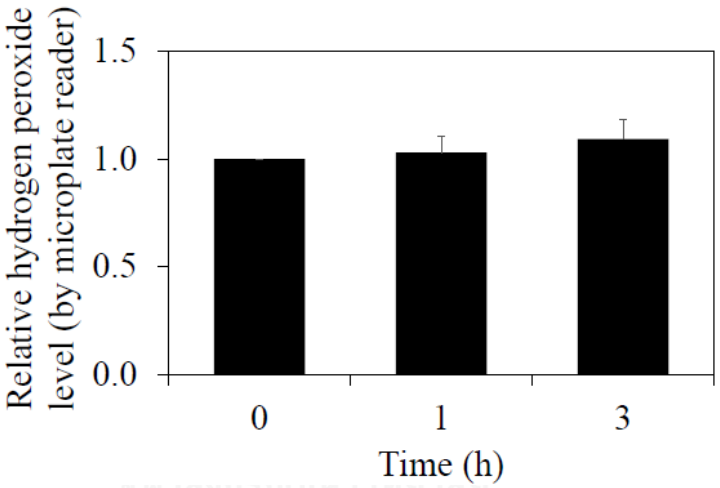
Relative hydrogen peroxide level (by microplate reader)
1.5
1.0
0.5
0.0
0
1
3
Time (h)

C

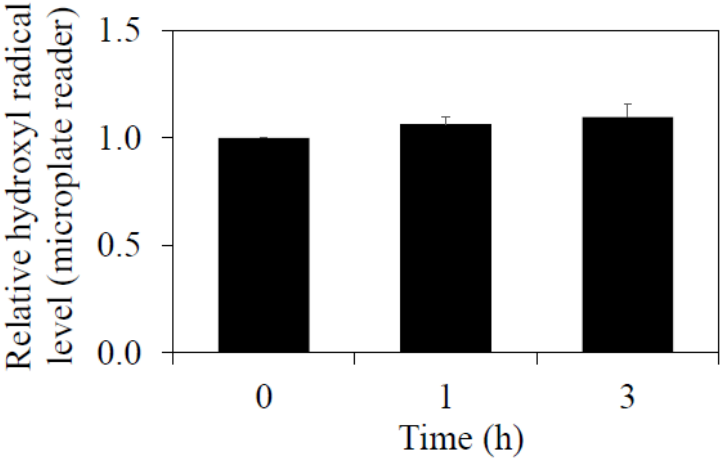
Relative hydroxyl radical level (microplate reader)
1.5
1.0
0.5
0.0
0
1
3
Time (h)

Figure 4.10 Effects of zinc ion on ROS generation in H460 cells in time-dependent manner analyzed by microplate reader. The cells were incubated with specific ROS probes, namely, DHE, $DCFH_2$-DA, or HPF for superoxide anion, hydrogen peroxide and hydroxyl radical, respectively at 4°C for 30 min prior to the treatment with zinc ion (50 μM) for 0-3 h and the fluorescence intensity was analyzed by a microplate reader. Mean intensity was normalized to untreated control cells and represented as relative ROS levels. (A) Effects of zinc ion on superoxide anion generation. (B) Effects of zinc ion on hydrogen peroxide generation. (C) Effects of zinc ion on hydroxyl radical generation. Values are means ± S.E.M. of independent triplicate experiments. *$p<0.05$ versus untreated control.

A

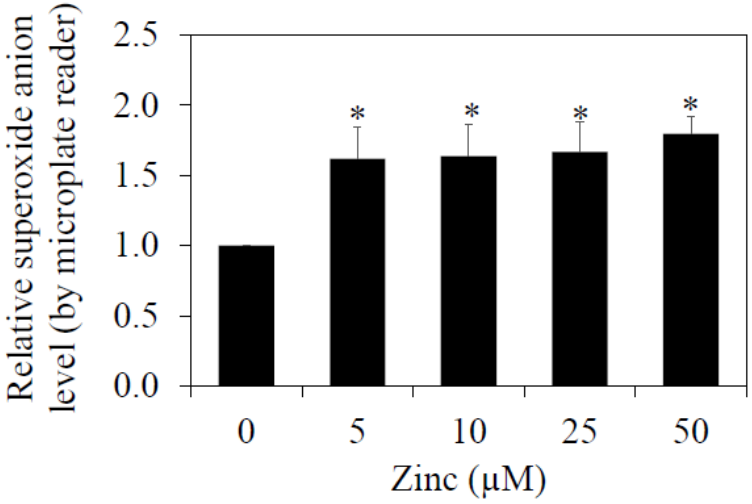
Relative superoxide anion level (by microplate reader)
2.5
2.0
1.5
1.0
0.5
0.0
*
*
*
*
0
5
10
25
50
Zinc (µM)

B

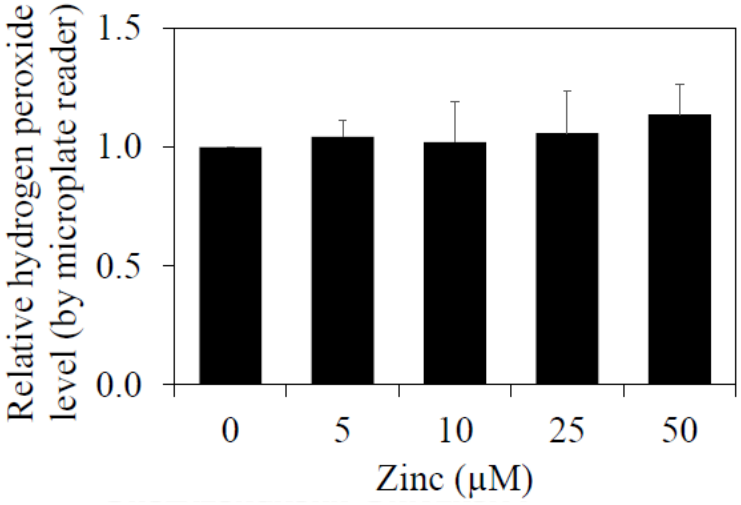
Relative hydrogen peroxide level (by microplate reader)
1.5
1.0
0.5
0.0
0
5
10
25
50
Zinc (µM)

C

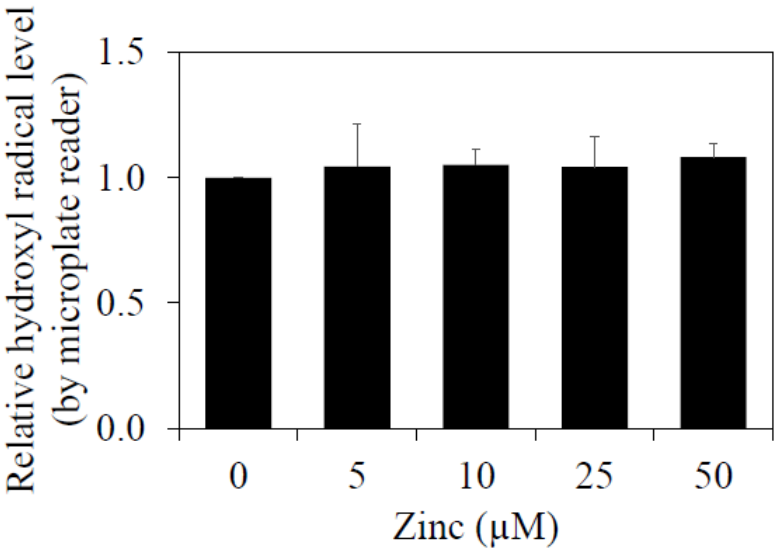
Relative hydroxyl radical level (by microplate reader)
1.5
1.0
0.5
0.0
0
5
10
25
50
Zinc (µM)

Figure 4.11 Effects of zinc ion on ROS generation in H460 cells in dose-dependent manner analyzed by microplate reader. The cells were incubated with specific ROS probes, namely, DHE, $DCFH_2$-DA, or HPF for superoxide anion, hydrogen peroxide and hydroxyl radical, respectively at 4°C for 30 min prior to the treatment with zinc ion (0–50 μM) for 3 h and the fluorescence intensity was analyzed by a microplate reader. Mean intensity was normalized to untreated control cells and represented as relative ROS levels. (A) Effects of zinc ion on superoxide anion generation. (B) Effects of zinc ion on hydrogen peroxide generation. (C) Effects of zinc ion on hydroxyl radical generation. Values are means ± S.E.M. of independent triplicate experiments. *p<0.05 versus untreated control.

A

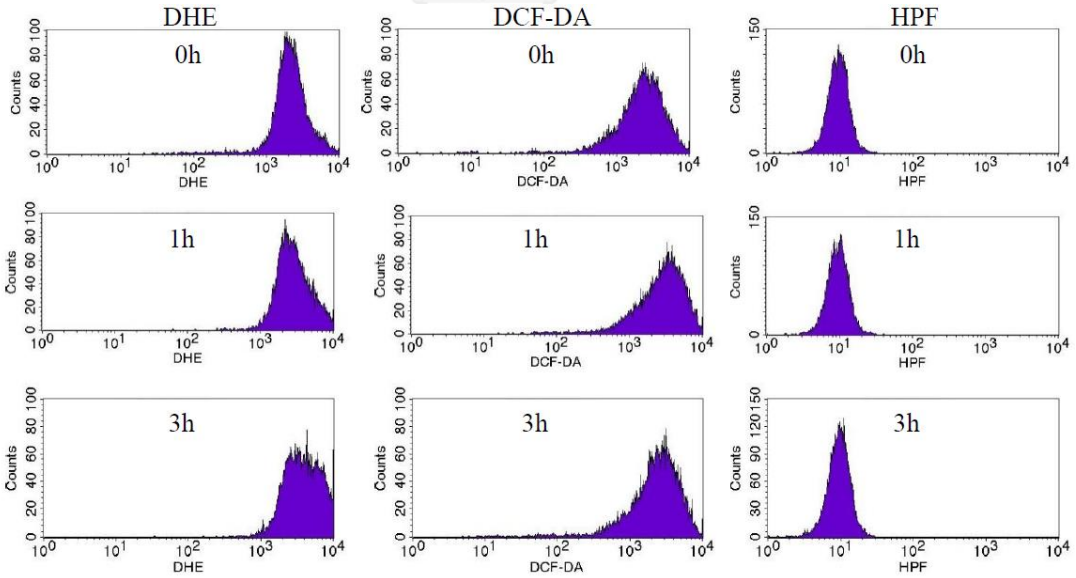

B

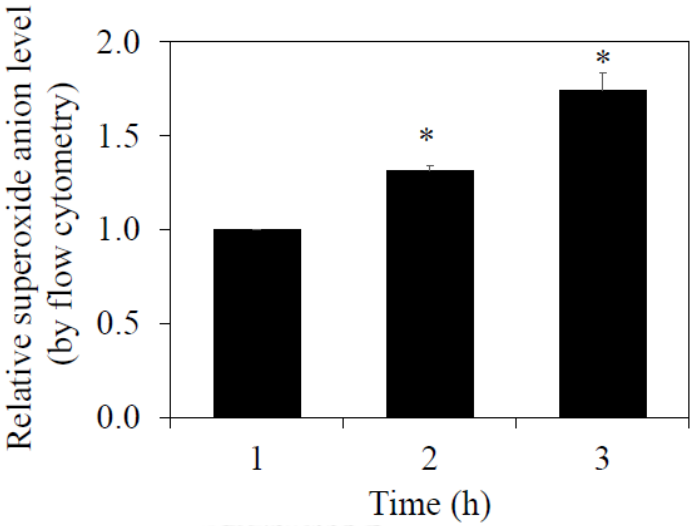
Relative superoxide anion level
(by flow cytometry)
2.0
1.5
1.0
0.5
0.0
*
*
1
2
3
Time (h)

C

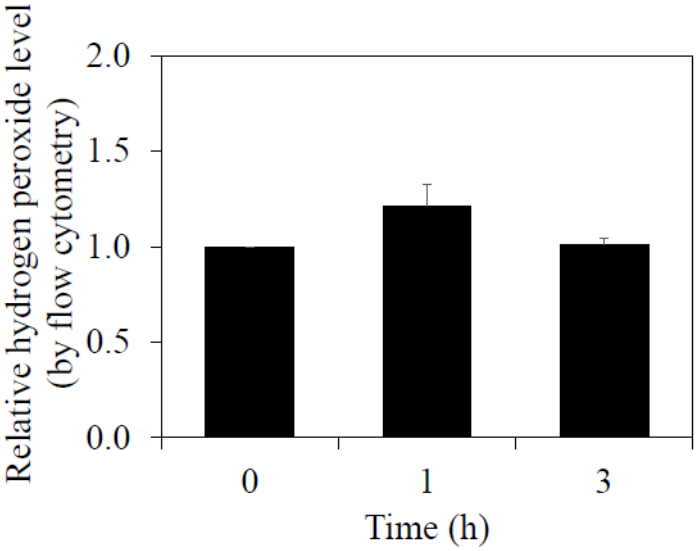
Relative hydrogen peroxide level
(by flow cytometry)
2.0
1.5
1.0
0.5
0.0
0
1
3
Time (h)

D

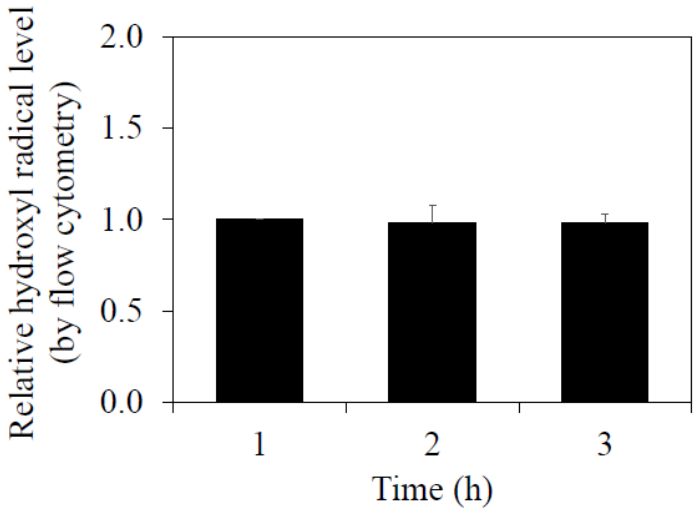
Relative hydroxyl radical level
(by flow cytometry)
2.0
1.5
1.0
0.5
0.0
1
2
3
Time (h)

Figure 4.12 Effects of zinc ion on ROS generation in H460 cells in time dependent manner analyzed by flow cytometry. (A) The cells were incubated with specific ROS probes, namely, DHE, $DCFH_2$-DA, or HPF for superoxide anion, hydrogen peroxide and hydroxyl radical, respectively at 4°C for 30 min prior to the treatment with zinc ion (50 μM) for 0-3 h and the fluorescence intensity was analyzed by flow cytometry. Mean intensity was normalized to untreated control cells and represented as relative ROS levels. (B) Effects of zinc ion on superoxide anion generation. (C) Effects of zinc ion on hydrogen peroxide generation. (D) Effects of zinc ion on hydroxyl radical generation. Values are means ± S.E.M. of independent triplicate experiments. *$p<0.05$ versus untreated control.

We further confirmed the superoxide anion-inducing effect of zinc ion using specific superoxide anion inhibitor MnTBAP. Results indicated that treatment with the zinc ion caused the superoxide anion up-regulation in the cells and such event could be abolished by the addition of MnTBAP as shown in figure 4.13, confirming that the major ROS induced by zinc treatment in our system was superoxide anion.

A

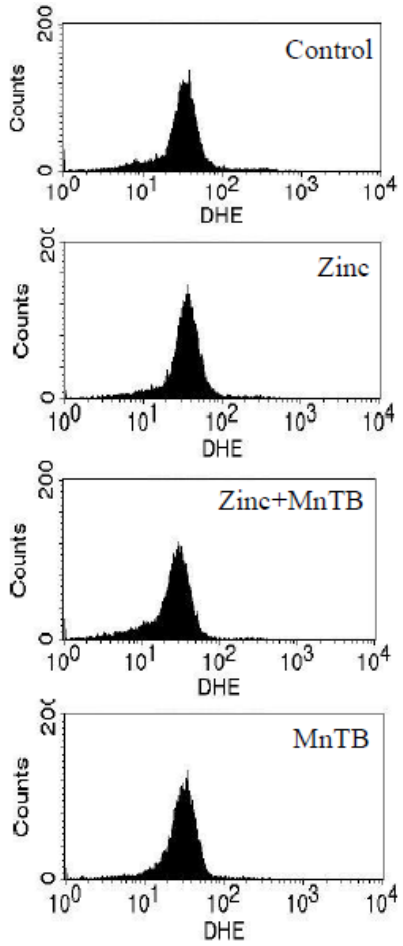
Control
Zinc
Zinc+MnTB
MnTB
Counts
DHE
0
200
10^0
10^1
10^2
10^3
10^4

B

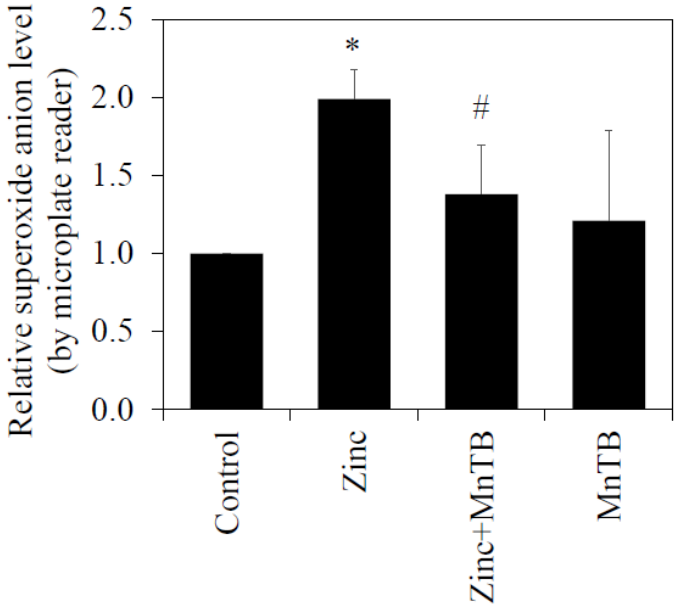
Relative superoxide anion level
(by microplate reader)
2.5
2.0
1.5
1.0
0.5
0.0
*
#
Control
Zinc
Zinc+MnTB
MnTB

Figure 4.13 Effects of zinc ion on superoxide anion generation in H460 cells analyzed by flow cytometry. (A) The cells were incubated with DHE at 4°C for 30 min prior to pre-treatment with 50 μM MnTBAP (superoxide anion inhibitor) for 1 h in the presence or absence of zinc ion (50 μM) for 3 h and the fluorescence intensity was analyzed by flow cytometry. (B) Mean intensity was normalized to untreated control cells and represented as relative superoxide anion levels. Values are means ± S.E.M. of independent triplicate experiments. *$p<0.05$ versus non-treated control cells, #$p<0.05$ versus zinc ion-treated group.

4. Effect of superoxide anion on EMT characteristics.

In order to investigate the role of superoxide anion on EMT induction, cell morphology, EMT markers, migratory behaviors, and tumorigenic assay were evaluated in the cells treated with zinc ion and specific inhibitor of superoxide anion.

4.1 Effect of superoxide anion on cell morphology of H460 cells

For EMT marker evaluation, cells were cultured in the presence or absence of MnTBAP for 1 h prior to zinc ion (50 μM) treatment and EMT phenotypes were determined. Also, to clarify role of superoxide anion, the superoxide anion inducer DMNQ was used. The results show that treatment of the cells with DMNQ or zinc ion alone was able to switch the morphology of lung cancer cells from epithelial to fibroblast-liked mesenchymal feature (Figure 4.14). Addition of MnTBAP to the zinc ion-treated cells could be able to attenuate such morphologic transformation.

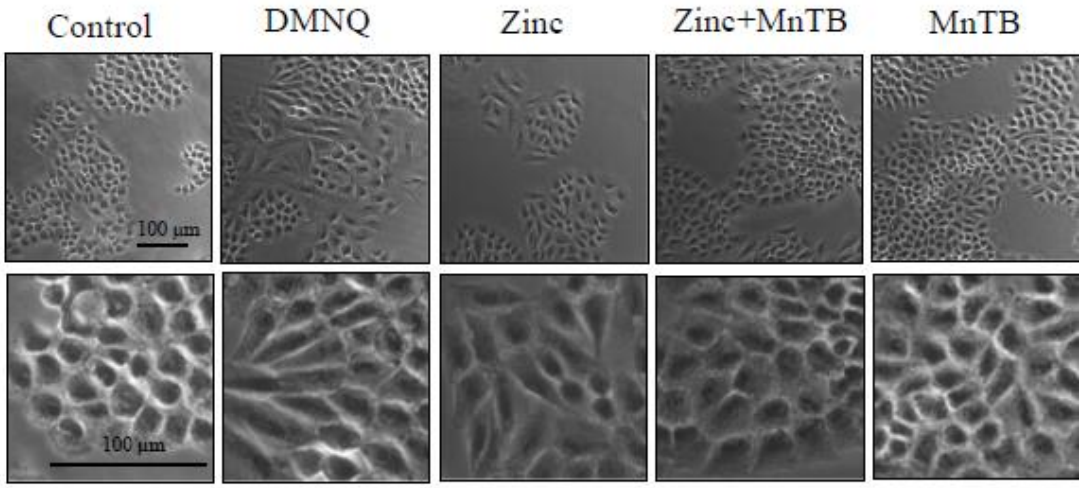

Figure 4.14 Effect of superoxide anion on cell morphology. H460 cells were incubated with 5 µM of DMNQ (superoxide anion inducer) or 50 µM of zinc ion, in the presence or absence of MnTBAP (superoxide anion inhibitor; 50 µM) for 24 h prior to morphology examination using phase contrast microscope; scale bar=100 µm.

4.2 Effect of superoxide anion on EMT markers.

Consistently, the results of western blot analysis revealed that EMT markers including N-cadherin, vimentin, snail, and slug were found to be significantly increased in response to DMNQ and zinc ion treatment and such phenomenon could be reversed by the addition of MnTBAP (Figure 4.15A and B).

In addition, immunocytochemistry showed the increased vimentin found in DMNQ- and zinc ion- treated cells. And the increased vimentin signal induced by zinc ion was suppressed by the addition of MnTBAP (Figure 4.15C).

A

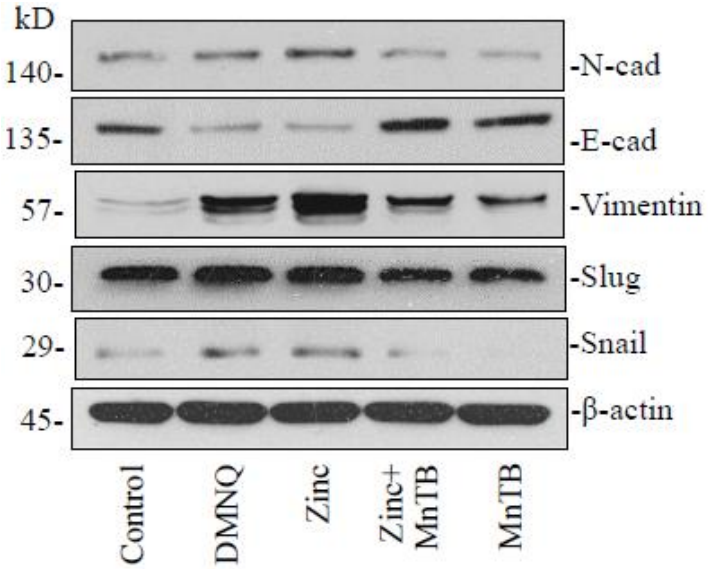
kD
140-
135-
57-
30-
29-
45-
-N-cad
-E-cad
-Vimentin
-Slug
-Snail
-β-actin
Control
DMNQ
Zinc
Zinc+ MnTB
MnTB

B

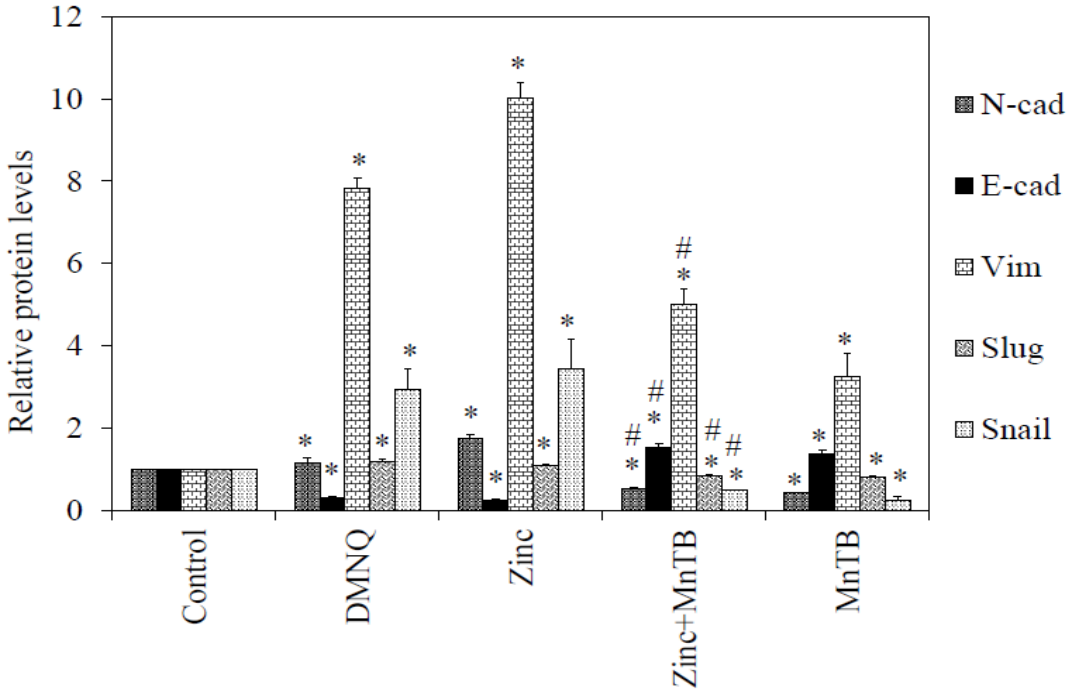
Relative protein levels
0
2
4
6
8
10
12
N-cad
E-cad
Vim
Slug
Snail
Control
DMNQ
Zinc
Zinc+MnTB
MnTB

C

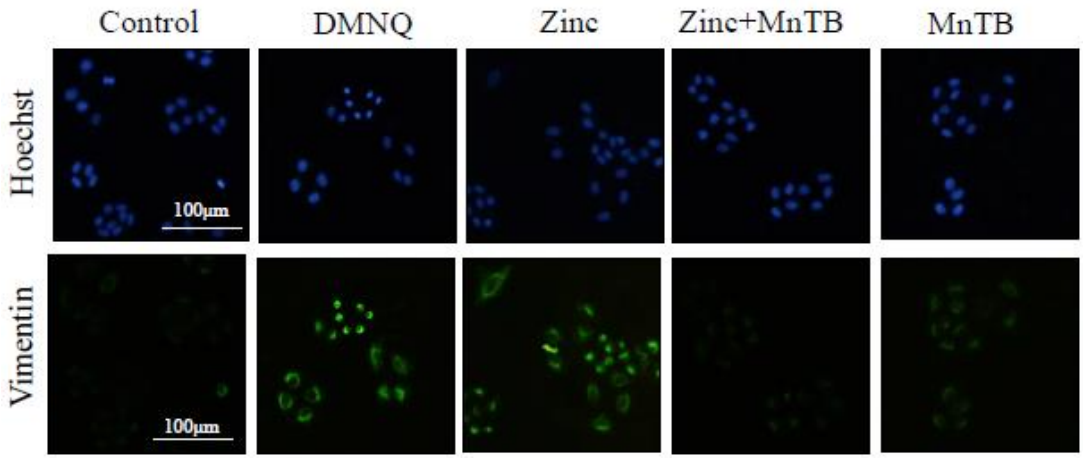

Figure 4.15 Effect of superoxide anion on EMT markers. (A) Cells were treated with 5 μM of DMNQ or 50 μM of zinc ion, in the presence or absence of MnTBAP (50 μM) for 24 h. The cells were collected and analyzed for EMT markers by Western blotting. The blots were re-probed with β-actin to confirm equal loading. (B) The immunoblot signals were quantified by densitometry and mean data from independent experiments were normalized to the results. The bars are the means ± S.E.M. of independent triplicate experiments. *p<0.05 versus non-treated control cells, #p<0.05 versus zinc ion-treated group. (C) The expression of vimentin was analyzed by immunofluorescence staining; scale bar = 100 μm.

4.3 Effect of superoxide anion on cell motility.

The migration and invasion of the cells were further evaluated. The results were consistent with the expression levels of EMT proteins that DMNQ and zinc ion could be able to induce cell migration and invasion and such inductions could be abolished by superoxide anion inhibitor (Figure 4.16 and 4.17).

4.4 Effect of superoxide anion on tumorigenicity.

Tumorigenic potential in response to superoxide anion was also investigated. The result indicated that the colony size and number which were increased in response to DMNQ and zinc ion treatment were found to be significantly attenuated by the treatment of MnTBAP (Figure 4.18).

Taken together, these results pointed out that zinc ion induces EMT process, migratory behaviors, and tumorigenic potential in the lung cancer cells via superoxide anion-dependent mechanism.

A

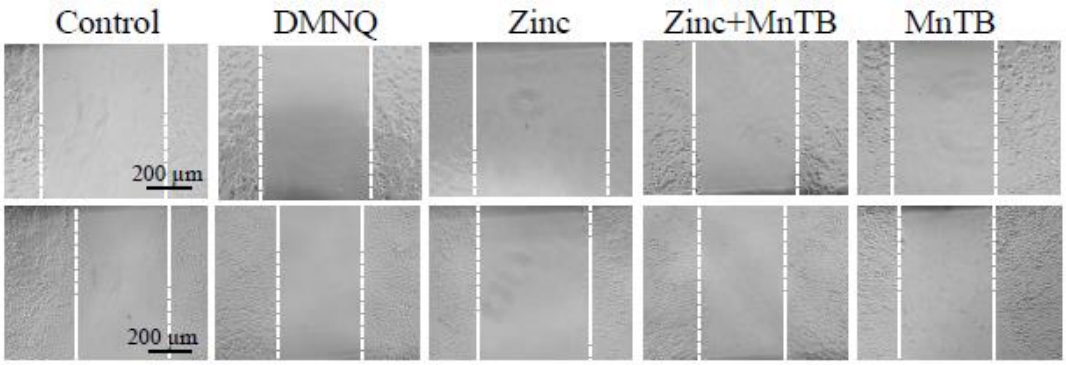

B

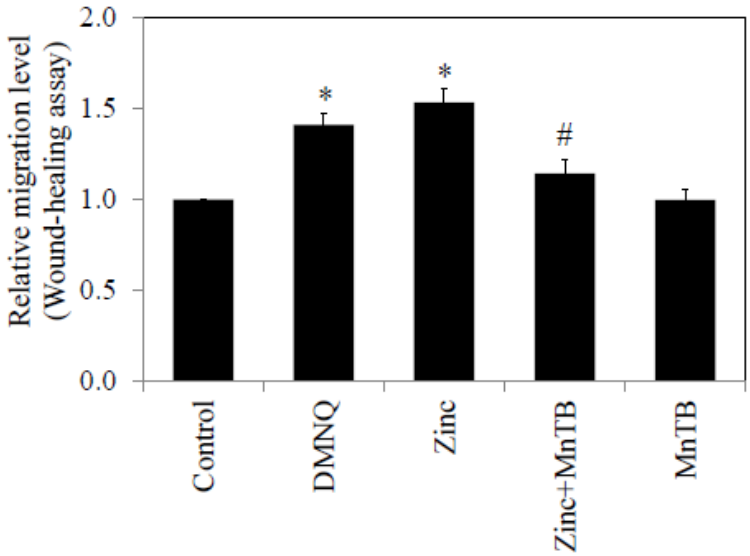

Figure 4.16 Effect of superoxide anion on cell migration in H460 cells. H460 cells were treated with 5 µM of DMNQ or 50 µM of zinc ion, in the presence or absence of MnTBAP (50 µM) for 24 h. The treated cells were subjected to migration assays. (A) For wound healing assay, the confluent monolayers of the cells were wounded by using a 1 mm-wide tip and cultured with the fresh medium. After 24 h of incubation, wound spaces were analyzed and represented as a relative migration level. (B) The relative migration level was determined by comparing the relative change of zinc ion-treated cells to untreated control cells. Values are means ± S.E.M. of independent triplicate experiments. *p<0.05 versus non-treated control cells, #p<0.05 versus zinc ion-treated group.

A

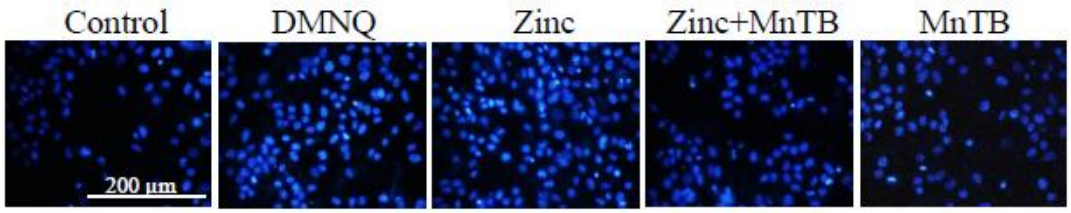

B

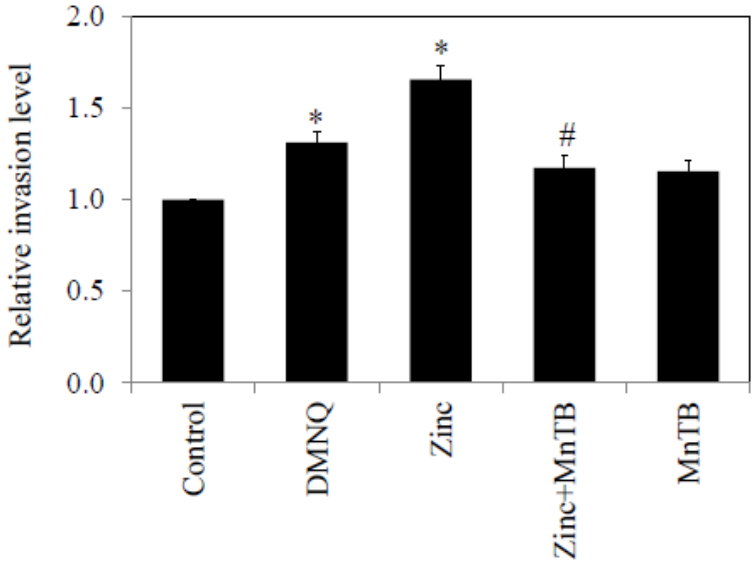

Figure 4.17 Effect of superoxide anion on cancer cell invasion in H460 cells. H460 cells were treated with 5 µM of DMNQ or 50 µM of zinc ion, in the presence or absence of MnTBAP (50 µM) for 24 h. The treated cells were subjected to invasion assays. (A) Cell invasion was evaluated using a transwell coated with matrigel as described under *Materials and Methods*. After 24 h, the cells that invaded across the membrane were stained with Hoechst 33342 for 30 min and visualized under a fluorescence microscope. (B) Value was represented as average number of invaded cells in each field relatively to control. Values are means ± S.E.M. of independent triplicate experiments. *p<0.05 versus non-treated control cells, #p<0.05 versus zinc ion-treated group.

A

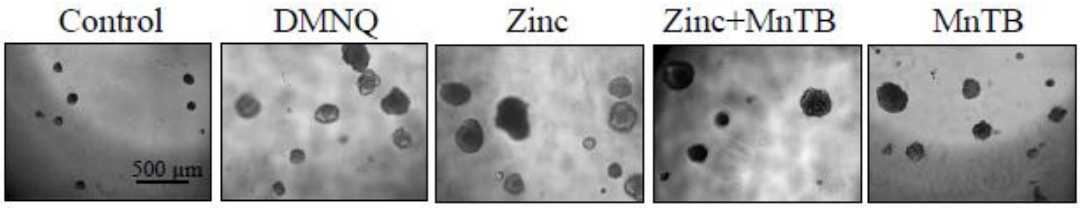

B

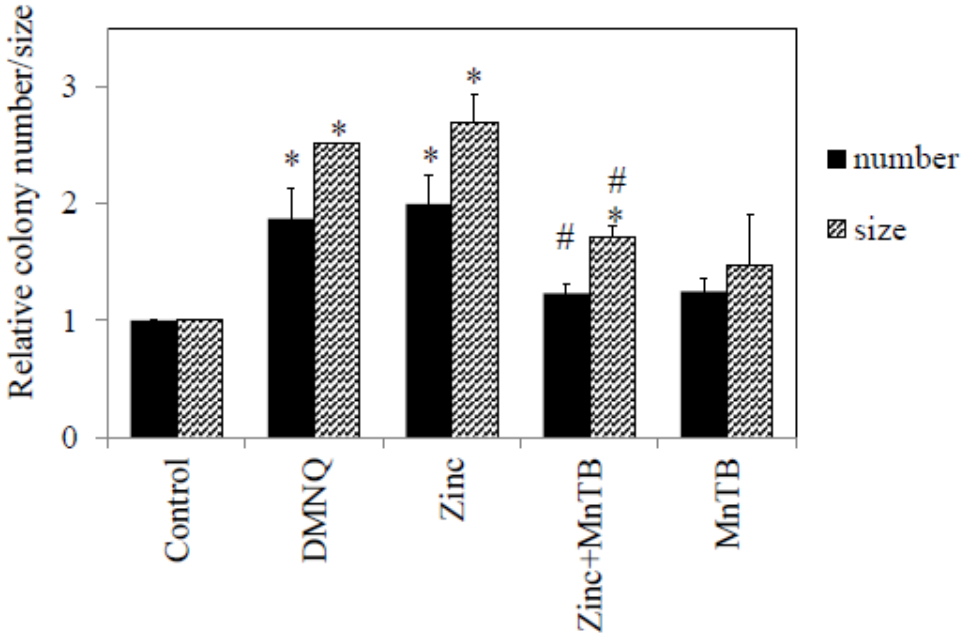

Figure 4.18 Effect of superoxide anion on tumorigenicity of H460 cells. (A) H460 cells were treated with 5 µM of DMNQ or 50 µM of zinc ion, in the presence or absence of MnTBAP (50 µM) for 24 h. The treated cells were subjected to 3D tumorigenesis assay. The cells were suspended in RPMI medium containing 4% Matrigel and plated onto agarose-coated plate. After 10 days, whole area of each well was captured in one picture under microscope and the colonies with more than 25 µm of diameter were quantified; scale bar = 500 µm. (B) Value was represented as average diameter and number of colonies in all field of each well relatively to control cells using image analyzer. Values are means ± S.E.M. of independent triplicate experiments. *$p<0.05$ versus non-treated control cells, #$p<0.05$ versus zinc ion-treated group.

4.5 Effect of DMNQ on superoxide anion generation in H460 cells

As DMNQ was used as a superoxide anion donor, the intracellular superoxide anion generated by DMNQ was determined. Cells were incubated with DHE as mentioned in *Material and Methods* for 30 min and treated with 5 μM of DMNQ. DHE intensity was determined by flow cytometry. The result indicated the 1.5-fold superoxide induction in DMNQ-treated cells as shown in Figure 4.19.

A

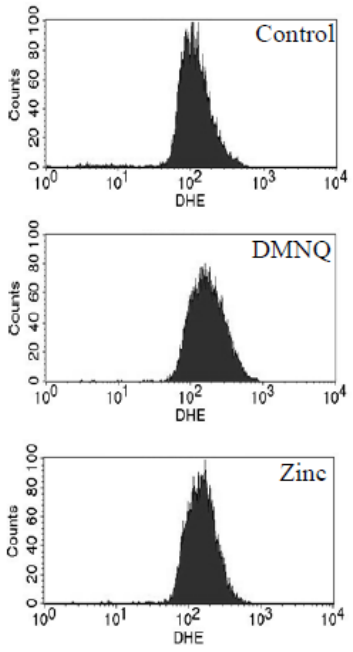

B

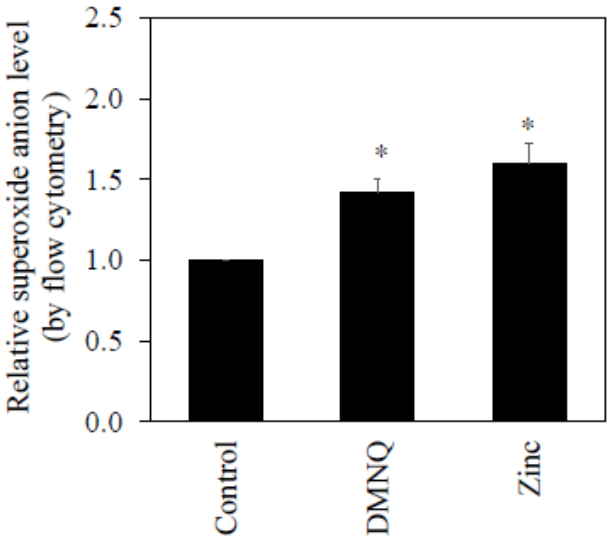

Figure 4.19 Effects of DMNQ on superoxide anion generation in H460 cells analyzed by flow cytometry. (A) Cells were incubated with DHE at 4°C for 30 min prior to the treatment of DMNQ (5 μM) or zinc ion (50 μM), and the fluorescence intensity was analyzed by flow cytometry at 3 h. (B) Mean intensity was normalized to untreated control cells and represented as relative superoxide anion levels. Values are means ± S.E.M. of independent triplicate experiments. *p<0.05 versus non-treated control cells.

5. Effect of zinc ion on CSC phenotypes in lung cancer H460 cells.

Cancer stem cells (CSCs) as well as epithelial-to-mesenchymal transition (EMT) play critical roles in cancer progression and metastasis. Although these two events have distinct characteristics and molecular pathways, EMT were frequently found to possess CSC characteristics**.** Next, the effects of zinc ion on CSC phenotypes was investigated**.**

5.1 Effect of zinc ion on CSC markers.

Previous evidence has stated self-renewal and pluripotency properties of CSCs were regulated by distinct transcription factors, including Nanog, Sox2 and Oct4 (Liu et al., 2013). Additionally, well-accepted indicators for CSCs, in particular in lung cancer CSCs, such as CD133 and ALDH1A1 are often up-regulated (Ginestier et al., 2007; Eramo et al., 2008; Jiang et al., 2009). And these CSC markers have a significant prognostic value strongly related to poor survival in non-small cell lung cancer (Alamgeer et al., 2013).

Therefore, CSC markers were determined in this study using western blot analysis and flow cytometry. Cells were treated with various concentrations of zinc ion (0-50 μM) for 72 h and the expression levels of lung CSC markers (CD133

and ALDH1A1) were determined. The results of western blot analysis and flow cytometry consistently indicated that zinc ion significantly decreased cellular levels of CD133 and ALDH1A1 in a dose-dependent manner (Figure 4.20).

In addition, the transcription factors regulating CSCs, namely Oct4, Nanog, and Sox2 were determined as described. The results indicated that zinc ion dramatically reduced cellular levels of Oct4, Nanog, and Sox2 (Figure 4.20A and B).

A

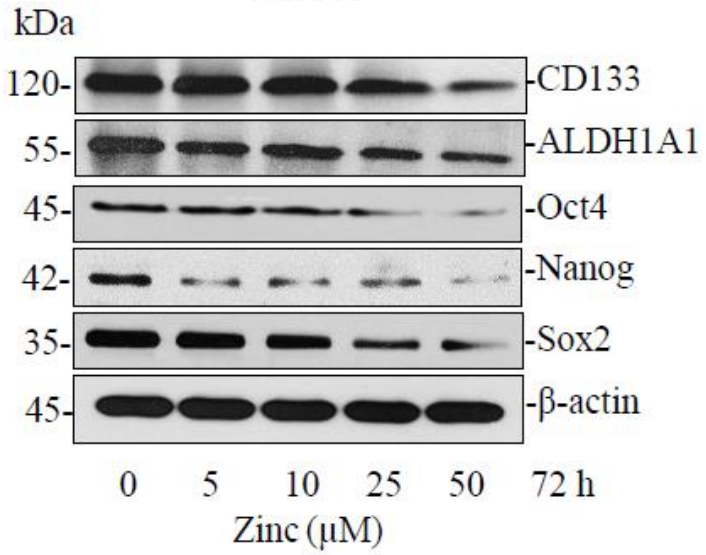

B

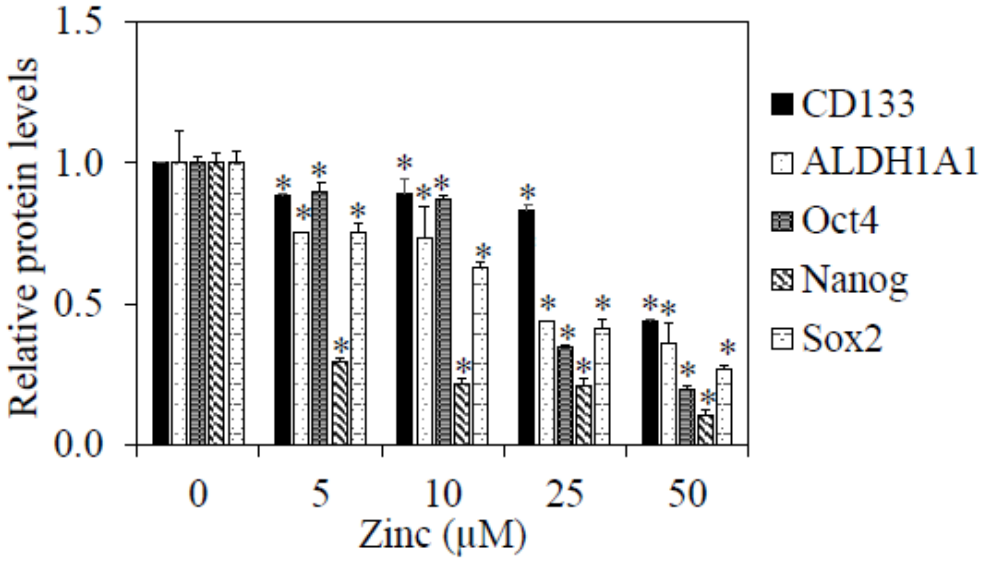

C

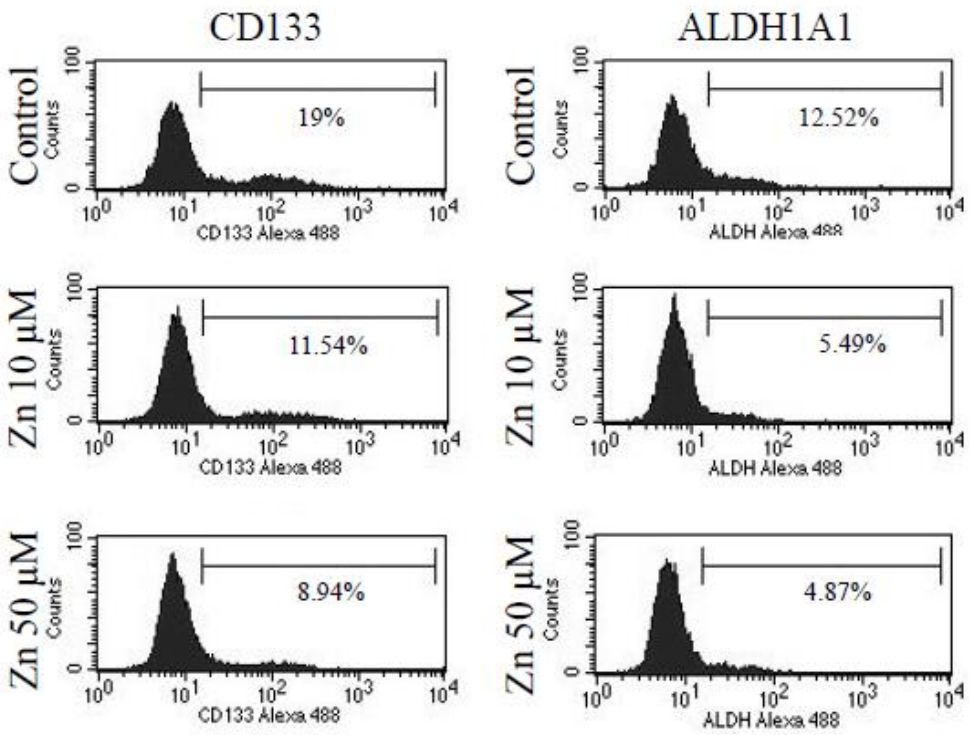

Figure 4.20 Effect of zinc ion on CSC markers of lung cancer H460 cells**.** Zinc ion-exposed cells (0-50 µM) for 3 days were analyzed for the expression levels of CSC markers (A) Expression levels of CSC markers were analyzed by western blotting. The blots were re-probed with ß-actin to confirm equal loading of the samples. (B) The blots were quantified by densitometry and mean data from three independent experiments were normalized to the results. The bars are the means ± S.E.M. of independent triplicate experiments. *P<0.05 versus non-treated control. (C) The expression of CD133 and ALDH1A1 was measured by flow cytometry for zinc ion-treated and non-treated cells at 72 h. Flow cytometry was performed using rabbit anti-CD133 and ALDH1A1 monoclonal antibodies followed by Alexa Fluor 488-labeled secondary antibody to visualize CD133 and ALDH1A1 expressions.

5.2 Effect of zinc ion on spheroid formation.

According to established knowledge of stem cell characteristics of cancer cells, spheroid type cells grown under suspension culture conditions have CSC phenotype-enrich population presented self-renewal ability in a number of cancers (Levina et al., 2010; Cao et al., 2011; Singh et al., 2012; Kantara et al., 2014; Condello et al., 2015; Chanvorachote and Luanpitpong, 2016; Grun et al., 2016; Luanpitpong et al., 2016; Zhou et al., 2016).

To proof the presence of CSC phenotype-rich population in the model which was used in this study, lung cancer cells were grown in single cells-suspended condition to form primary and secondary spheroids (in total the cells were suspended 28 days (14 + 14 days). The secondary spheroids were collected and characterized for the well-known CSC markers.

Figure 4.21A and B, shows that the expressions of CD133 and ALDH1A1 were dramatically increased in stem cell phenotype-rich population in comparison with their parental cells, confirming the exitance of CSC population in this model.

A

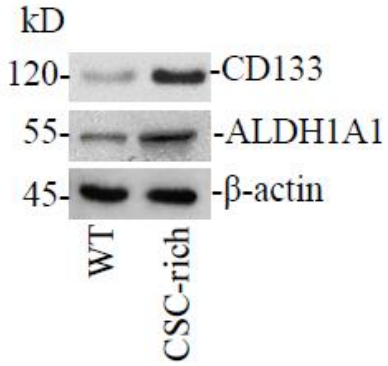

B

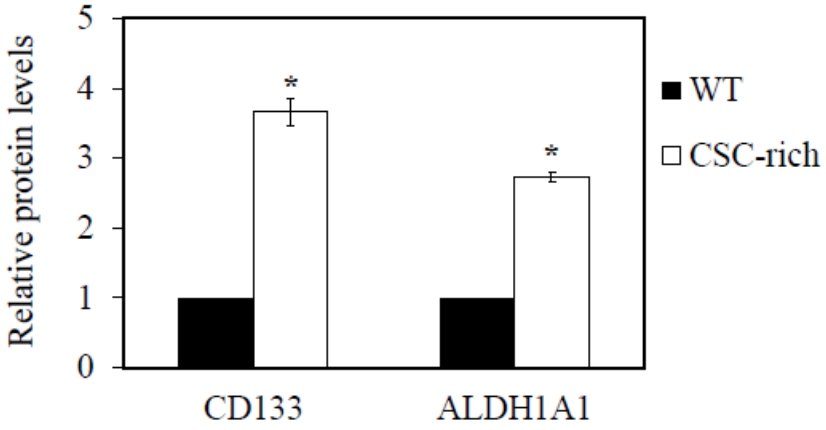

Figure 4.21 The expression of CD133 and ALDH1A1 in CSC-rich population. (A) Cells were grown in suspended condition in serum free RPMI medium to form the primary and secondary spheroid as described in *Materials and Methods* for 28 days in total. Cell lysate was prepared and well-known lung CSC markers were determined by western blot analysis comparing to attached-cultured parental cells. The blots were re-probed with β-actin to confirm equal loading of the samples. (B) The blots were quantified by densitometry and mean data from three independent experiments were normalized to the results. The bars are the means ± S.E.M. of independent triplicate experiments. *P<0.05 versus non-treated control.

To test the effect of zinc ion on CSC regulation in lung cancer cells, H460 cells were similarly incubated with various non-toxic concentrations of zinc (0-50 μM) for 72 h and subjected to spheroid formation assay.

Consistent with the western blot results figure 4.22 show that zinc ion-treated cells formed a reduced number of secondary tumor spheres in comparison to that of passage-matched control cells. Such a finding indicates the existence of CSC phenotype-rich population in H460 cell counterpart and the loss of CSC properties in zinc ion-treated cells. At the treatment doses of 5-50 μM, zinc ion-treated cells exhibited a 50-75% reduction in numbers of spheroids (Figure 4.22B); however, the size of the spheroids formed was only found to be slightly different (Figure 4.22C).

Taken together, these results revealed that zinc ion could attenuate CSC phenotypes of these lung cancer cells.

A

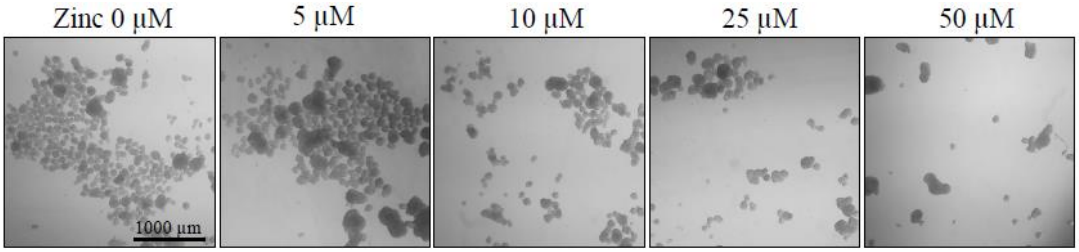

B

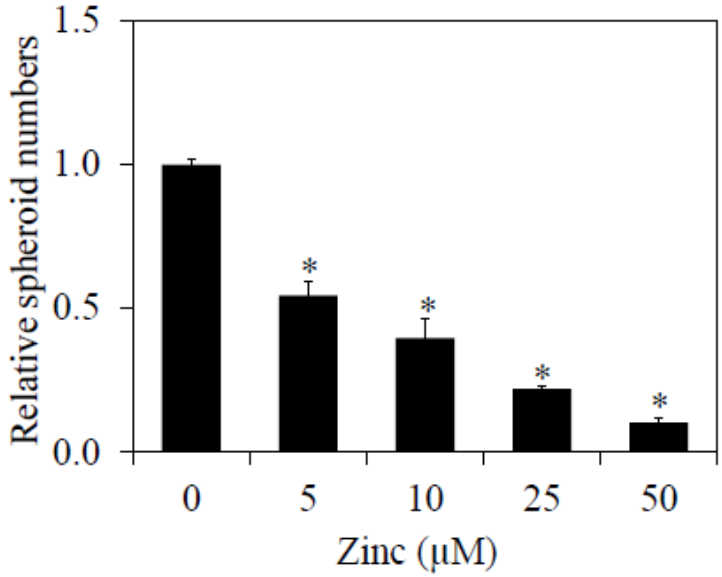

C

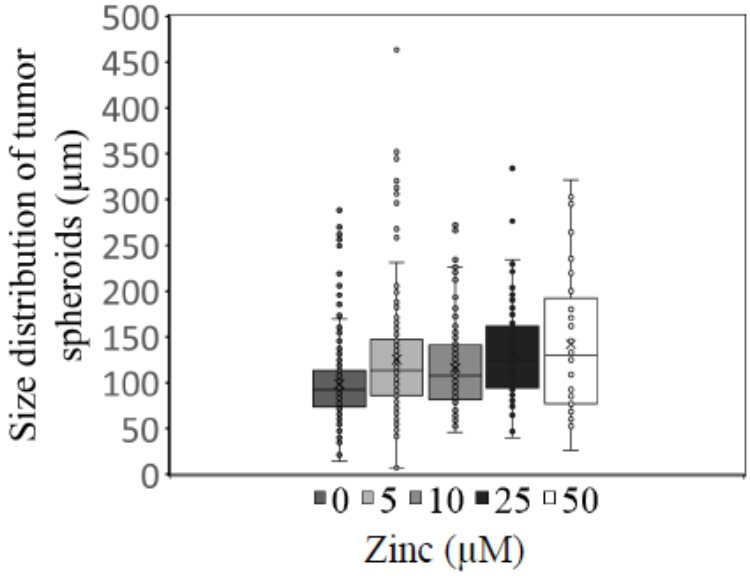

Figure 4.22 Effects of zinc ion on tumor spheroid formation in H460 cells. (A) Zinc ion-exposed cells (0-50 µM) for 3 days were analyzed for tumor sphere formation. Tumor

spheroids were visualized under a phase contrast microscope after 4 weeks of culture; scale bar = 1000 μm. (B-C) Quantitative analysis of tumor spheroids. Values are means ± S.E.M of triplicate independent experiments. *P<0.05 versus non-treated control.

6. Effect of zinc ion on CSC regulatory proteins.

ß-catenin is known to play a central role in the maintenance of CSCs in many cancers including lung cancer (Cai and Zhu, 2012; Holland et al., 2013; Mao et al., 2014).

6.1 Effect of zinc ion on ß-catenin expression.

To investigate whether zinc ion suppresses CSC features of lung cancer cells through a ß-catenin-dependent mechanism, the cells were treated with various concentrations of zinc ion (0-50 μM) for 24 and 72 h, and the cellular level of ß-catenin was determined by western blot analysis.

Figure 4.23 shows that the ß-catenin levels were depleted in dose-dependent manner both at 24 and 72 h post zinc ion treatment.

A

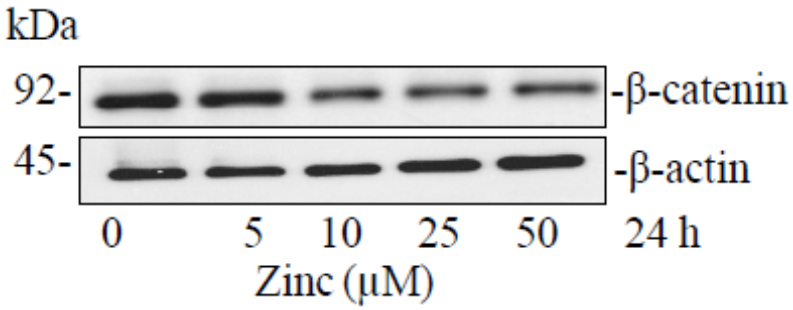
kDa
92-
-β-catenin
45-
-β-actin
0
5
10
25
50
24 h
Zinc (μM)

B

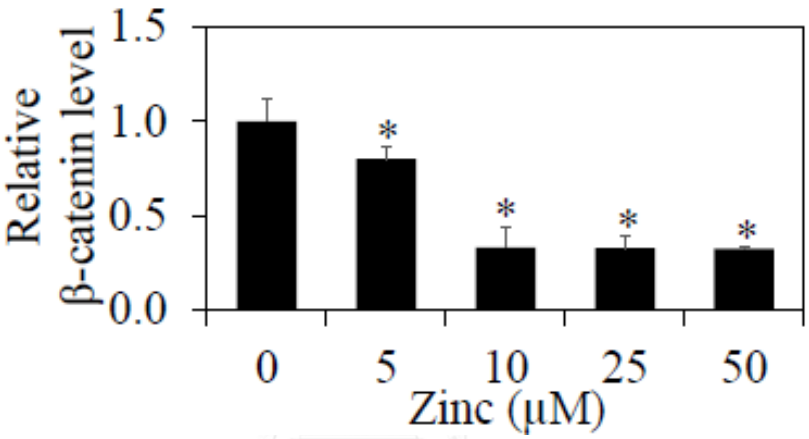
Relative
β-catenin level
1.5
1.0
0.5
0.0
*
*
*
*
0
5
10
25
50
Zinc (μM)

C

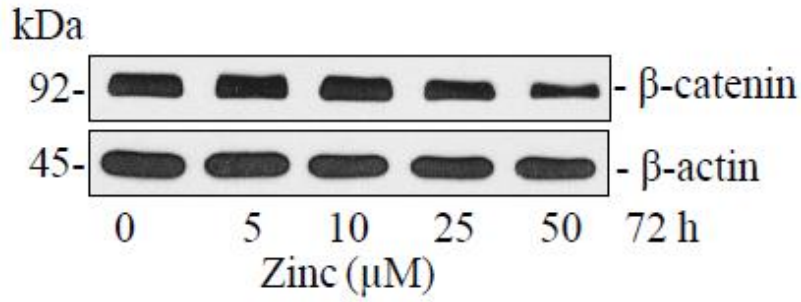
kDa
92-
- β-catenin
45-
- β-actin
0
5
10
25
50
72 h
Zinc (μM)

D

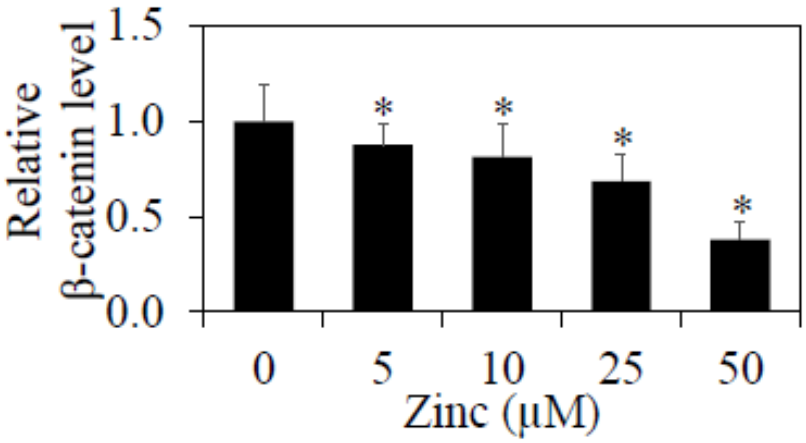
Relative
β-catenin level
1.5
1.0
0.5
0.0
*
*
*
*
0
5
10
25
50
Zinc (μM)

Figure 4.23 Effect of zinc ion on ß-catenin expression. (A, C) Cells were treated with zinc ion (0-50 μM) for 24 or 72 h. The treated cells were subjected to western blot analysis to determine the expression levels of ß-catenin. The blots were re-probed with ß-actin to confirm equal loading of the samples. (B, D) The blots were quantified by densitometry and mean data from three independent experiments were normalized to the results. The bars are the means ± S.E.M. of independent triplicate experiments. *p<0.05 versus untreated control.

6.2 Effect of zinc ion on ß-catenin degradasion.

As the decrease of ß-catenin via the ubiquitin-proteasomal mechanism is the determining step of ß-catenin signaling (Holland et al., 2013), the proteasome inhibitor was used to prove whether such degradation was responsible for the zinc ion-mediated ß-catenin depletion. The cells were treated with 50 μM of zinc ion for 24 h in the absence or presence of 10 μM of clasto-lactacystin ß-lactone (specific proteasome inhibitor).

The results indicated that treatment of the cells with zinc ion resulted in a significant decrease in ß-catenin level. Interestingly, such a phenomenon was prevented by the addition of proteasome inhibitor (Figure 4.24), suggesting that zinc ion could affect proteasome degradation of ß-catenin.

Further, ubiquitination of ß-catenin was analyzed in response to zinc ion treatment using immunoprecipitation. The cells were treated with zinc ion (0-50

μM) for 0-3 h and cell lysates were prepared and immunoprecipitated using an anti- ß-catenin antibody.

The resulting immune complexes were then analyzed for ubiquitin by western blot using an anti-ubiquitin antibody. Fugues 4.25 shows that the levels of ß-catenin-ubiquitin complexes were found to be increase in zinc ion-treated group in dose- and time-dependent manner, suggesting that zinc ion was able to induce ubiquitination of ß-catenin

Taken together, zinc ion mediated ß-catenin down-regulation via a proteasome-dependent mechanism.

A

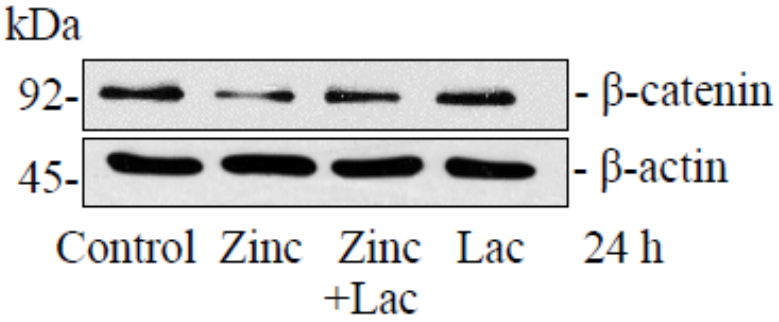

B

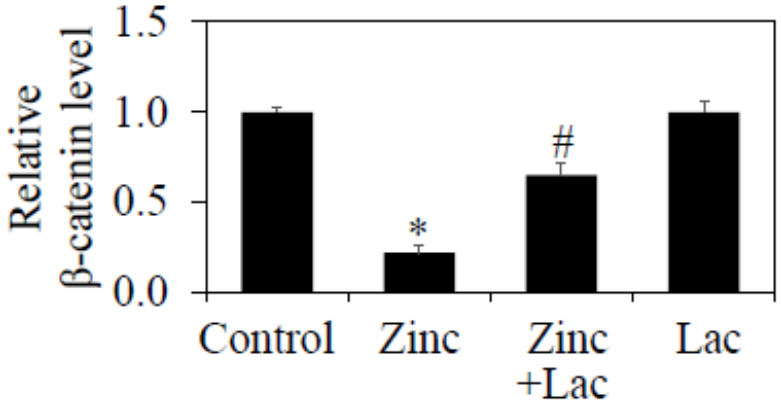

Figure 4.24 Effect of zinc ion on proteasome degradation of β-catenin**.** Cells were treated with zinc ion (50 μM) in the presence or absence of clasto-lactacystin β-lactone (Lac 10 μM) for 24 h. Expression level of β-catenin was determined by western blot analysis. The blots were quantified by densitometry and mean data from three independent experiments were normalized to the results. The bars are the means ± S.E.M. of independent triplicate experiments. *P<0.05 versus non-treated control; #P<0.05 versus 50 μM zinc ion-treated cells.

A

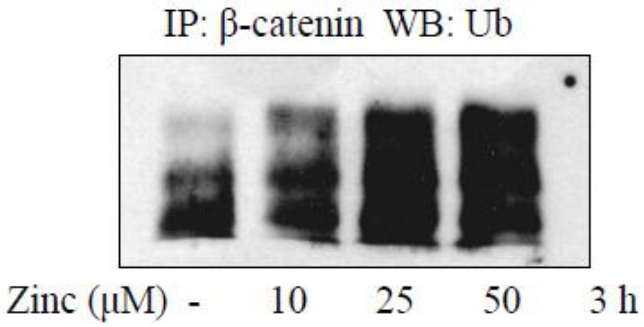

B

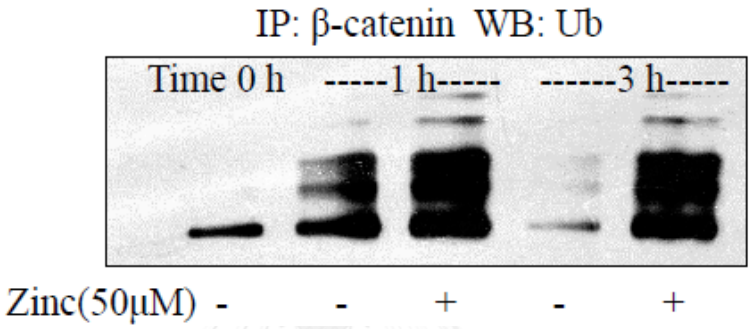

Figure 4.25 Effect of zinc on β-catenin ubiquitination**.** After 1-3 h of treatment the cells with zinc ion (0-50 μM) in the presence of Lac (10 μM), cells lysates were prepared and immunoprecipitated (IP) with anti-β-catenin antibody. The resulting immune complexes were then analyzed for β-catenin ubiquitination by western blotting (WB) using anti-ubiquitin antibody.

6.3 Effect of zinc ion on PKCα activation.PKCα is an important negative regulator of β-catenin as it was phosphorylated and subjected to proteasomal degradation (Gwak et al., 2006).

Active PKCα (phosphorylated PKCα) and its total form were evaluated by western blot analysis in the cells treated with zinc ion (0-50 μM) for 12 h. Figures 26A and B show that treatment of the cells with zinc ion resulted in a substantial increase in phosphorylated PKCα, while the total PKCα remained unaffected.

A

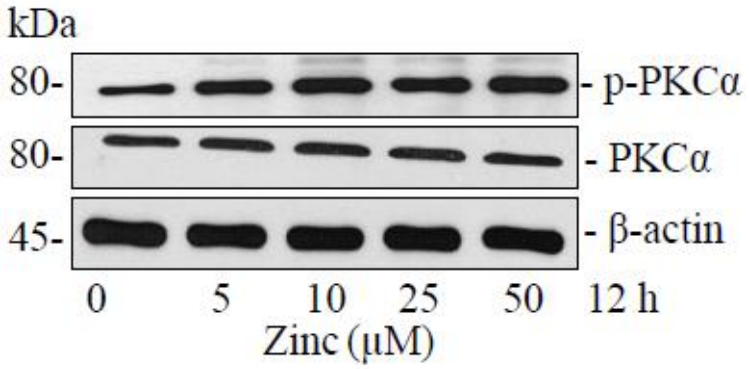

B

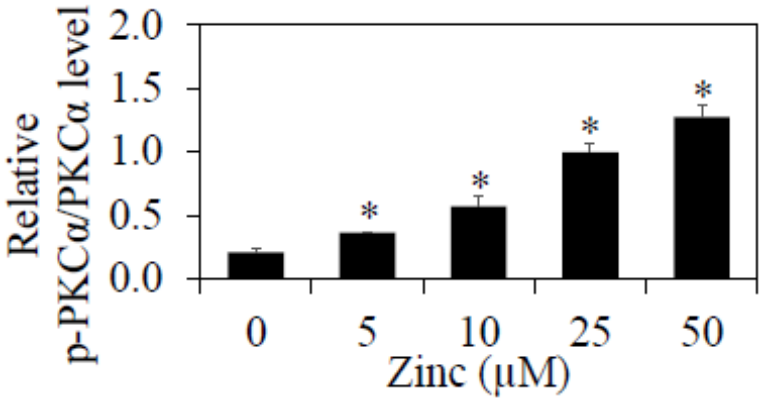

Figure 4.26 Effect of zinc ion on PKCα activation in H460 cells. (A) Cells were treated with zinc ion (0-50 μM) for 12 h. The treated cells were subjected to western blot analysis to determine the expression levels of PKCα. The blots were re-probed with β-actin to confirm equal loading of the samples. (B) The blots were quantified by densitometry and mean data from three independent experiments were normalized to the results. The bars are the means ± S.E.M. of independent triplicate experiments. *p<0.05 versus non-treated control.

6.4 Effect of PKCα on CSC phenotypes

To investigate the effects of PKC on CSC markers, we next utilized a highly selective PKCα inhibitor bisindolylmaleimide I (BIM; 5 μM) and PKCα activator A23187 (0.1 μM). The cells were treated with zinc ion for 3 days in the absence or presence of BIM, and the key spheroid forming behavior was tested with spheroid formation assay and CSC markers were analyzed by western blotting.

Figure 4.27 shows that treatment of the cells with zinc ion alone reduced the expressions of all CSC-related proteins including CD133, ß-catenin, ALDH1A1, Oct4, Nanog, and Sox2. The addition of the PKCα inhibitor (BIM) obviously prevented such decrease of CSC markers. Consistantly, the attenuated spheroid formation induced by zinc ion could be reversed by the treatment of PKCα inhibitor as indicated in figure 4.28.

In like fashion, treatment of the cells with PKCα activator resulted in a significant reduction of CSC properties of lung cancer cells, such as the down-regulation of CSC markers (CD133, ß-catenin, and ALDH1A1) and the decrease in spheroid formation as shown in figures 4.29 and 4.30, respectively.

Taken together, these finding provided the evidence that zinc ion exerted its inhibitory effect on CSC regulation of lung cancer cells via PKCα activation and mediated ß-catenin degradation via a PKCα-dependent mechanism.

A

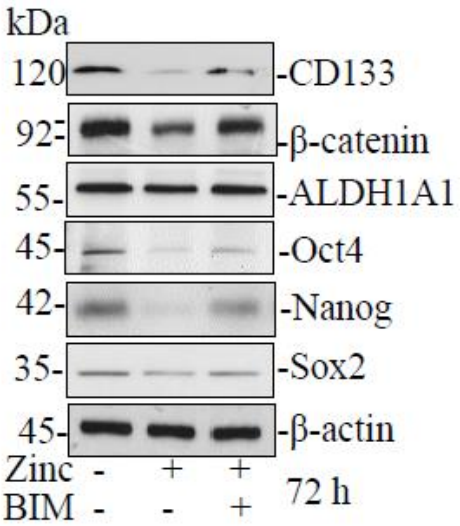

B

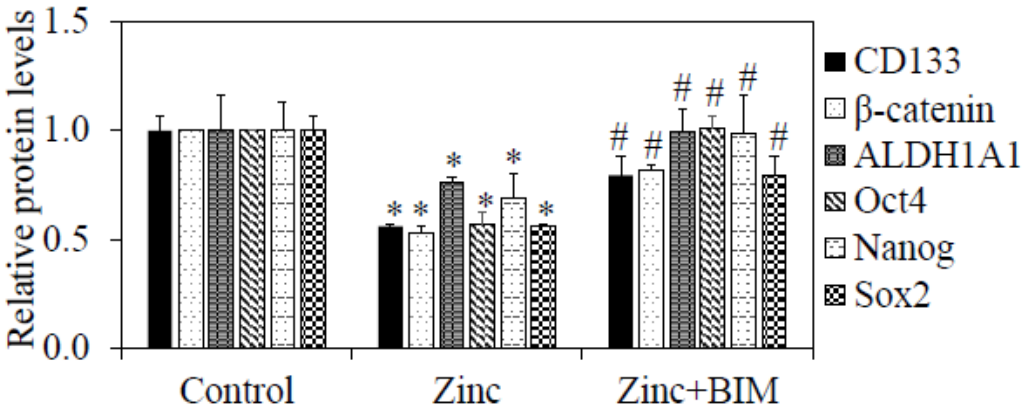

Figure 4.27 Effect of PKCα on expression of CSC markers verified by PKCα inhibitor. (A) Cells were treated with zinc ion (50 μM), in the presence or absence of 5 μM bisindolylmaleimide I (BIM; PKCα inhibitor) for 72 h. The treated cells were subjected to western blot analysis to determine the expression levels of CSC markers. The blots were re-probed with β-actin to confirm equal loading of the samples. (B) The blots were quantified by densitometry and mean data from three independent experiments were normalized to the results. The bars are the means ± S.E.M. of independent triplicate experiments. *p<0.05 versus non-treated control cells. #p<0.05 versus zinc ion-treated cells.

A

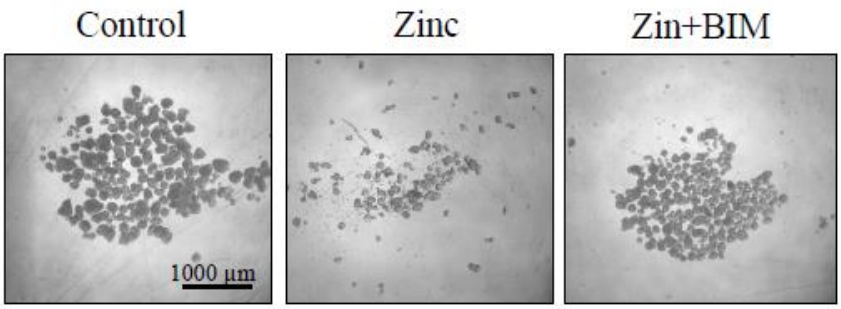

B

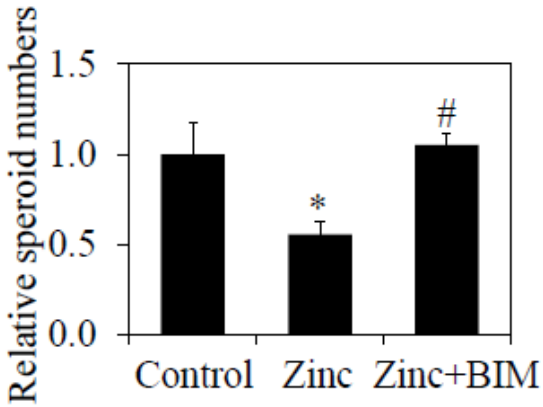

C

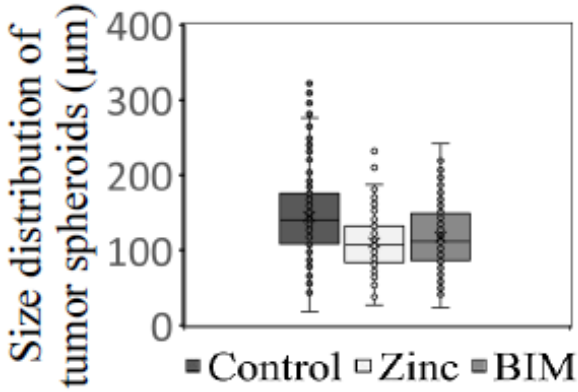

Figure 4.28 Effect of PKCα on spheroid formation verified by PKCα inhibitor. (A) Cells were treated with zinc ion (50 µM) in the presence or absence of 5 µM BIM for 3 days. Tumor sphere formation was determined. Cells were cultured under non-attached and serum-starved conditions and tumor spheroids were visualized under a phase contrast

microscope after 4 weeks of culture, scale bar = 1000 μm. (B, C) The tumor spheroids were quantified. Values are means ± S.E.M. of triplicate independent experiments. *p<0.05 versus non-treated control cells. #p<0.05 versus zinc ion-treated cells.

A

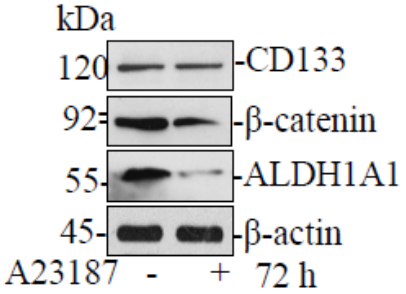

B

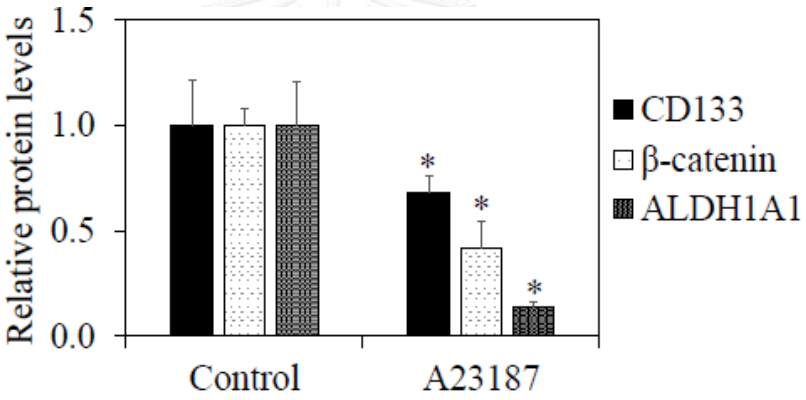

Figure 4.29 Effect of PKCα on expression of CSC markers verified by PKCα inducer. (A) Cells were treated with 0.1 μM A23187 (PKC activator) for 72 h. The treated cells were subjected to western blot analysis to determine the expression levels of CSC markers. The blots were re-probed with β-actin to confirm equal loading of the samples. (B) The blots were quantified by densitometry and mean data from three independent experiments were normalized to the results. The bars are the means ± S.E.M. of independent triplicate experiments. *p<0.05 versus non-treated control cells.

A

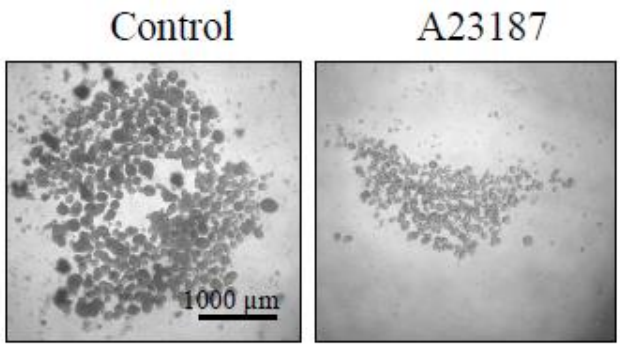

B

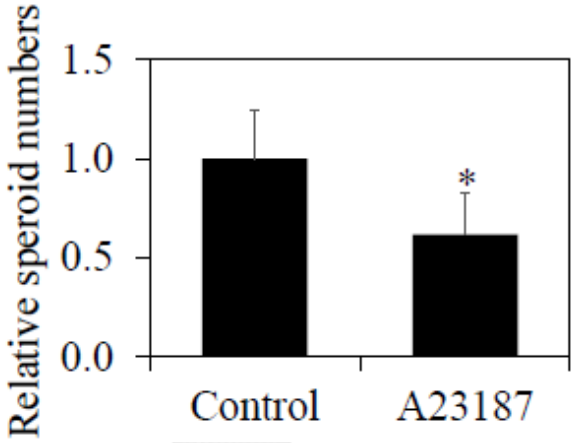

C

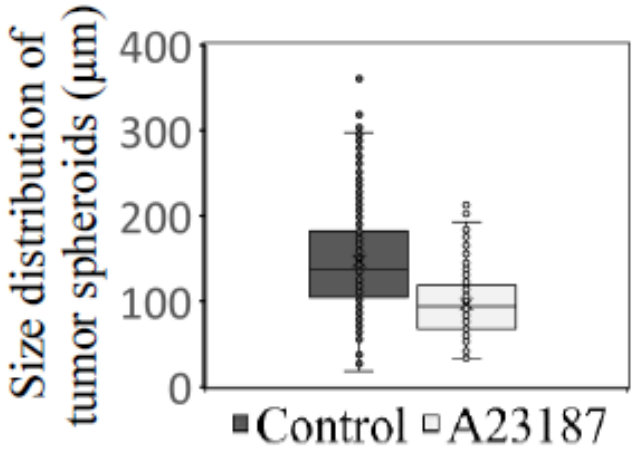

Figure 4.30 Effect of PKCα on spheroid formation verified by PKCα inducer. (A) Cells were treated with 0.1 µM A23187 for 3 days. Tumor sphere formation was determined. Cells were cultured under non-attached and serum-starved conditions and tumor spheroids were visualized under a phase contrast microscope after 4 weeks of culture,

scale bar = 1000 μm. (B, C) The tumor spheroids were quantified. Values are means ± S.EM. of triplicate independent experiments. *p<0.05 versus non-treated control cells.

7. Effect of superoxide anion on CSC phenotypes

7.1 Effect of superoxide anion on CSC markers.

For CSC marker evaluation, cells were treated with zinc ion (50 μM) in the absence or presence of superoxide anion scavenger (MnTBAP; 50 μM) and evaluated for CSC markers. Additionally, a superoxide anion generator DNMQ (5 μM) was used to indicate the effect of superoxide anion on CSCs.

The results indicated that treatment of the cells with zinc ion or DMNQ alone had a negative effect on CSC markers expressed in these cells, and this effect of zinc ion could be abolished by the addition of MnTBAP (Figure 4.31).

7.2 Effect of superoxide anion on spheroid formation.

Cells were treated with DMNQ or zinc ion, in the absence or presence of MnTBAP (50 μM) and evaluated for spheroid formation capability.

Figure 4.32 demonstates that MnTBAP completely inhibited zinc ion-suppressed spheroid formation as shown by the number of spheroids in zinc+MnTBAP groups reversed to the control level. Also, a superoxide anion inducer significantly reduced the number of spheroids formed, indicating the role of superoxide anion in inhibiting this CSC behavior.

A

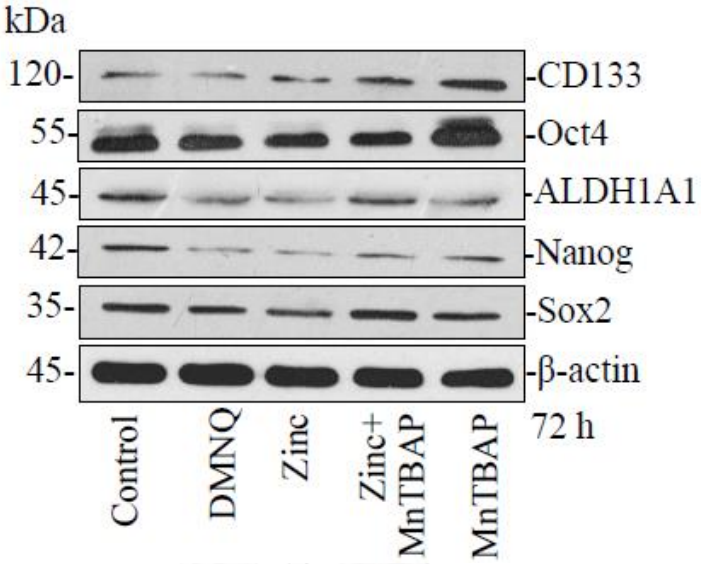

B

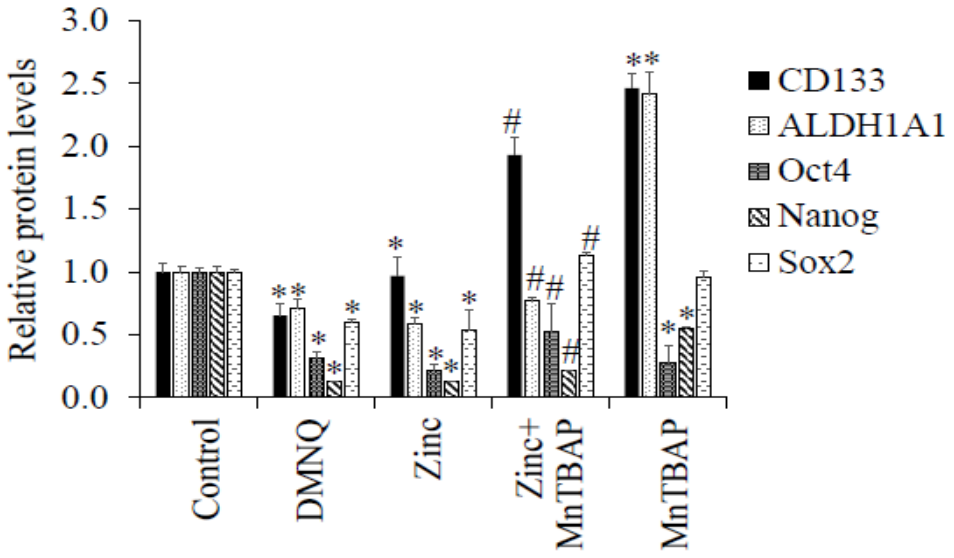

Figure 4.31 Effect of superoxide anion on CSC markers of H460 cells. Cells were incubated with 5 μM DMNQ or 50 μM zinc ion, in the presence or absence of MnTBAP (50 μM) for 3 days. (A) The treated-cells were collected and analyzed for the expression levels of CSC markers by Western blotting. The blots were re-probed with β-actin to confirm equal loading. (B) The immunoblot signals were quantified by densitometry and mean data from independent experiments were normalized to the results. The

bars are the means ± S.E.M. of independent triplicate experiments. *p<0.05 versus non-treated control cells. #p<0.05 versus zinc ion-treated cells.

A

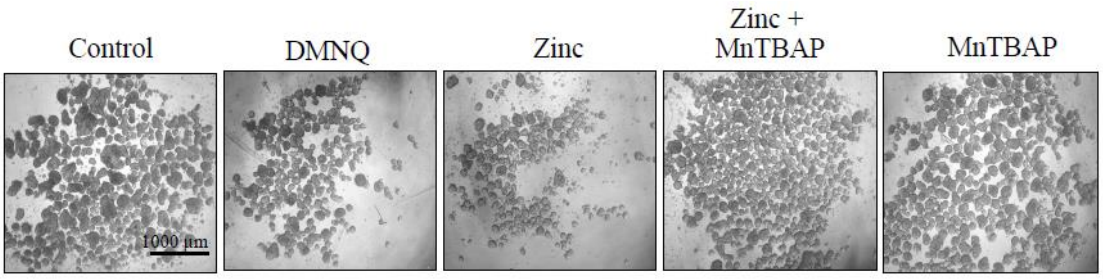

B

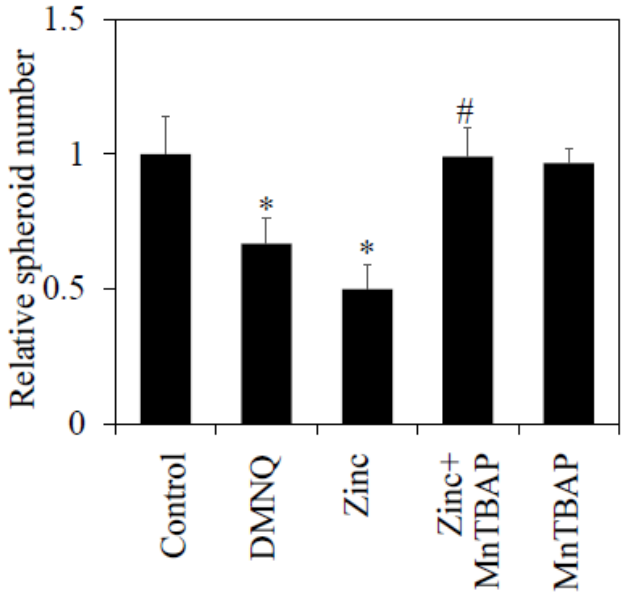

C

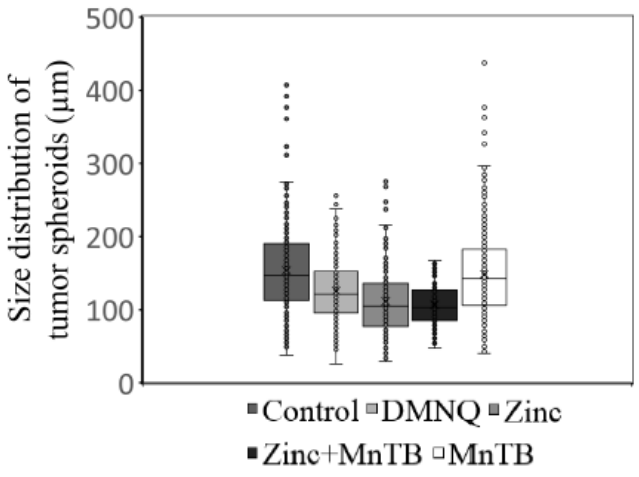

Figure 4.32 Effect of superoxide anion on tumor spheroid formation of H460 cells. H460 cells were incubated with 5 μM DMNQ or 50 μM zinc ion, in the presence or absence of MnTBAP (50 μM) for 3 days. (A) Tumor spheroids were visualized under a phase contrast microscope after 4 weeks of culture; scale bar = 1000 μm. (B-C) Quantitative analysis of tumor spheroids. Values are means ± S.E.M. of triplicate independent experiments. *p<0.05 versus non-treated control cells. #p<0.05 versus zinc ion-treated cells.

7.3 Effect of superoxide anion on on ß-catenin degradation.

Further, cells were similarly treated with DMNQ or zinc ion, in the presence or absence of MnTBAP and subjected to western blot analysis for ß-catenin determination after 24 h of treatment and immunoprecipitation for ß-catenin-ubiquitin complex evaluation after 3 h of treatment.

Figures 4.33A and B show that the intracellular ß-catenin levels were reduced by DMNQ and zinc ion treatments. Significantly zinc-induced ß-catenin reduction can be reversed by MnTBAP treatment. Besides, the evidence also poined to the possibility that the increase of ß-catenin-ubiquitin complex in zinc-treated cells can be inhibited by treatment with MnTBAP (Figure 4.33C). These finding implied that superoxide anion generated by zinc ion could regulate ß-catenin degradation via ubiquitin-proteasome pathway.

A

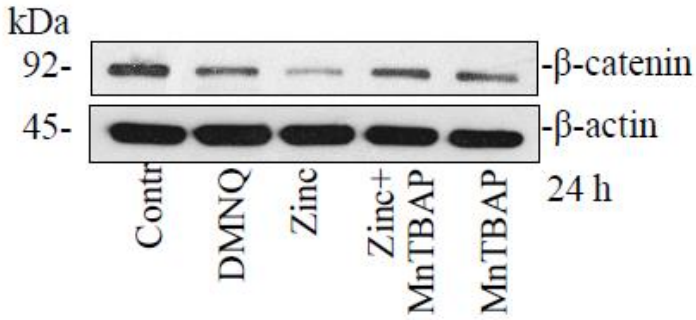

B

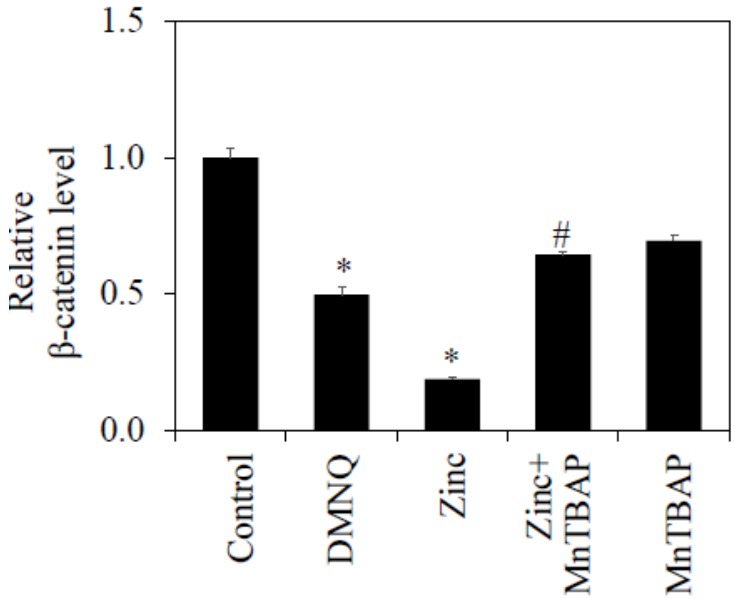

C

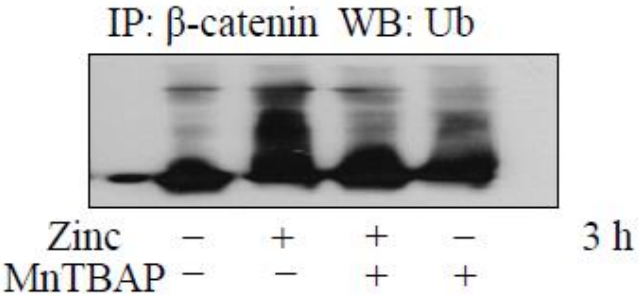

Figure 4.33 The effects of superoxide anion on β-catenin degradation**.** Cells were incubated with 5 μM DMNQ or 50 μM of zinc ion in the presence or absence of 50 μM MnTBAP. (A) the expression levels of β-catenin was determined by western blotting after 24 h of incubation. The blots were re-probed with β-actin to confirm equal

loading of the samples. (B) The immunoblot signals were quantified by densitometry and mean data from three independent experiments were normalized to the results. The bars are the means ± S.E.M. of triplicate independent experiments. *p<0.05 versus non-treated control cells. #p<0.05 versus zinc ion-treated cells. (C) After 3 h of treatment, cell lysates were prepared and immunoprecipitated (IP) with anti-β-catenin antibody. The resulting immune complexes were then analyzed for β-catenin ubiquitination by western blotting (WB) using anti-ubiquitin antibody.

8. Effect of superoxide anion on PKCα expression.

Evidence indicated that ROS as a signaling messenger have a capability to oxidize the crucial target molecules, including PKCα (Wu and Wu, 2010). Importantly, PKCα contains multiple cysteine residues which can be oxidized and activated by ROS (Gomez et al., 1999). This study next investigated the effect of superoxide anion on PKCα activation. Cells were treated with zinc ion in the presence or absence of MnTBAP (50 μM) for 12 h and the expression level of activated PKCα and total PKCα were measured by western blot analysis.

Figure 4.34 shows the increased activation of PKCα by zinc ion could be significantly inhibited by MnTBAP treatment, suggesting the role of zinc ion-induced superoxide anion generation in PKCα activation.

Taken together, these results support the earlier findings and indicate the regulatory roles of zinc and superoxide anion in CSC regulation and PKCα -mediated β-catenin degradation.

A

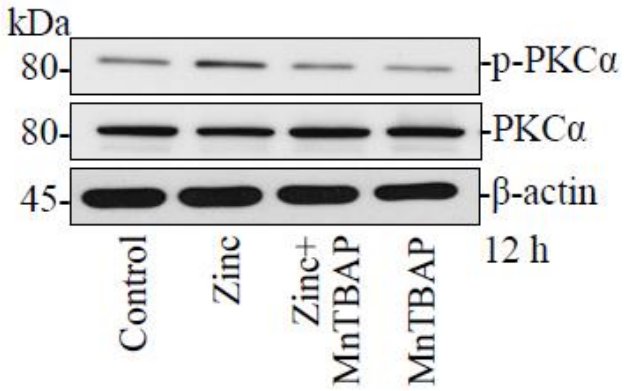

B

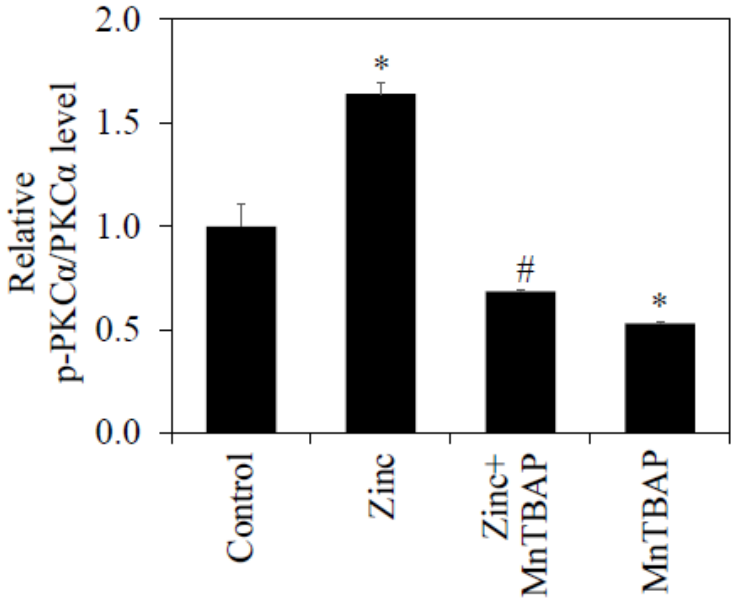

Figure 4.34 The effect of superoxide anion on PKC**α** activation**.** Cells were incubated with 50 μM of zinc ion in the presence or absence of 50 μM MnTBAP for 12 h. (A) Expression levels of active PKC**α** and total PKC**α** were analyzed by western blotting. (B) The blots were re-probed with β-actin to confirm equal loading of the samples. The immunoblot signals were quantified by densitometry and mean data from three independent experiments were normalized to the results. The bars are the means ± S.E.M. of triplicate independent experiments. *p<0.05 versus non-treated control cells. #p<0.05 versus zinc ion-treated cells.

9. Effect of zinc ion on stem cell program in other lung cancer cells

Having shown the suppressive role of zinc on CSC traits of H460 lung cancer cells, this study further confirmed such findings in other lung cancer cell lines. Human lung cancer H292 and H23 cells were treated with various non-toxic concentrations of zinc ion (0-50 μM) and CSC characteristics as well as key molecular mechanism, such as CSC markers, spheroid inductive ability, intracellular superoxide anion generation, and PKCα activation were evaluated as previously described.

The results demonstrated that in both H292 and H23 cell lines, zinc ion exhibited a negative regulatory effect on CSC phenotypes which were similar to those of H460 cells.

9.1 Effect of zinc on CSC in lung cancer H292 cells

Figures 4.35 and 4.36 show that zinc ion depleted expression levels of CSC markers (CD133, ß-catenin, and ALDH1A1) and suppressed the ability to form spheroids of H292 lung cancer cells. Also, zinc ion caused an elevation of superoxide anion level (Figure 4.37) and a significant increase in phosphorylated PKCα expression (Figure 4.38) in H292 cell lines.

9.1.1 Effect of zinc on CSC markers in H292 cells.

A

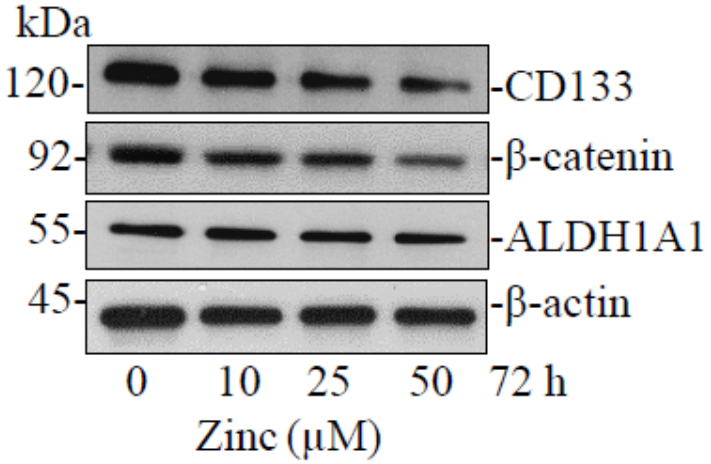

B

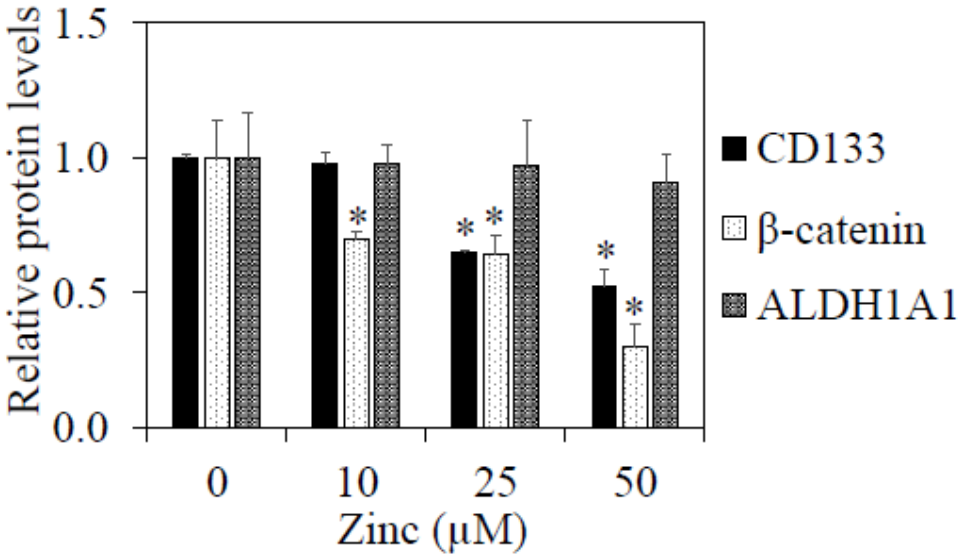

C

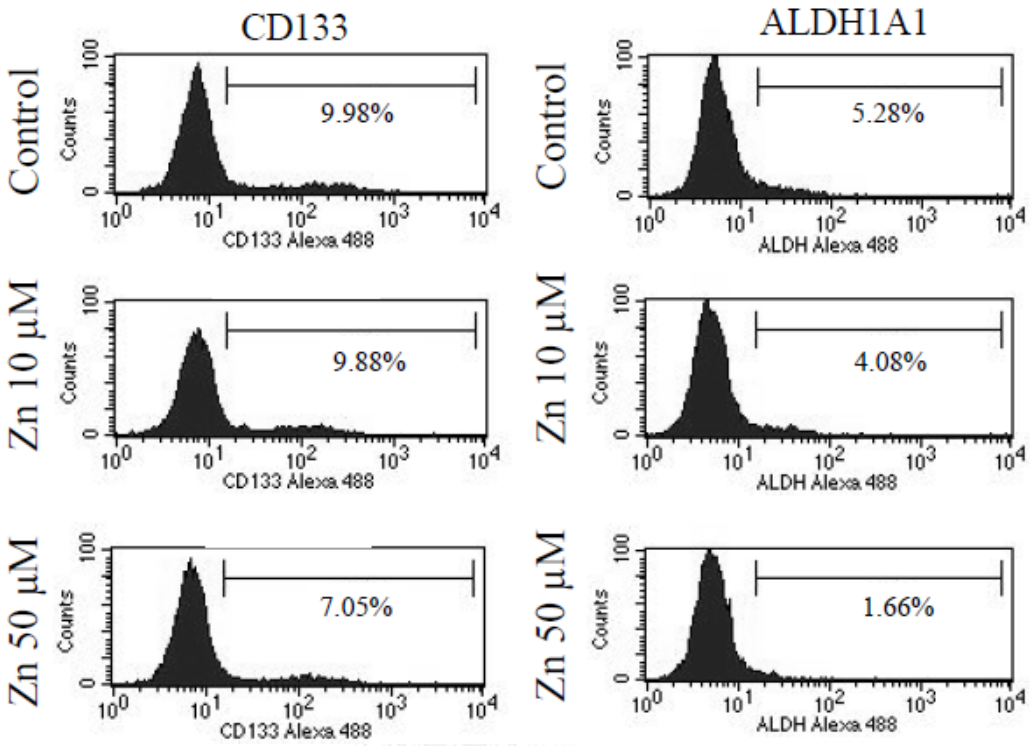

Figure 4.35 Effect of zinc ion on CSC markers of lung cancer H292 cells**.** Zinc ion-exposed cells (0-50 µM) for 3 days were analyzed for the expression levels of CSC markers (A) Expression levels of CSC markers were analyzed by western blotting. The blots were re-probed with ß-actin to confirm equal loading of the samples. (B) The blots were quantified by densitometry and mean data from three independent experiments were normalized to the results. The bars are the means ± S.E.M. of independent triplicate experiments. *P<0.05 versus non-treated control. (C) The expression of CD133 and ALDH1A1 was measured by flow cytometry for treated and non-treated cells at 72 h of zinc ion treatment. Flow cytometry was performed using rabbit anti-CD133 and ALDH1A1 monoclonal antibodies followed by Alexa Fluor 488-labeled secondary antibody to visualize CD133 and ALDH1A1 expression.

9.1.2 Effect of zinc ion on spheroid formation in H292 cells.

A

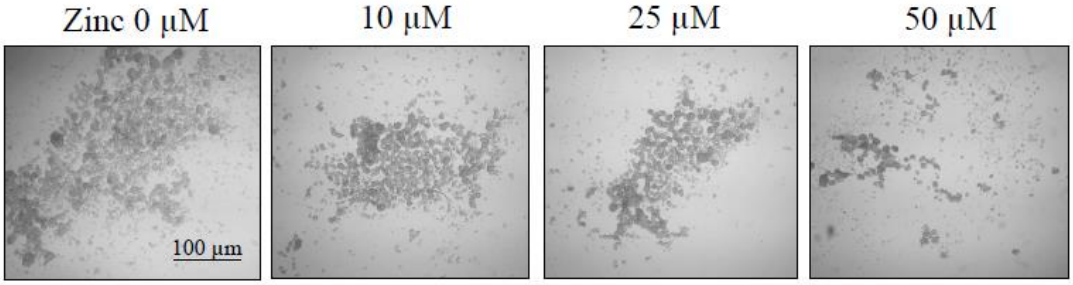

B

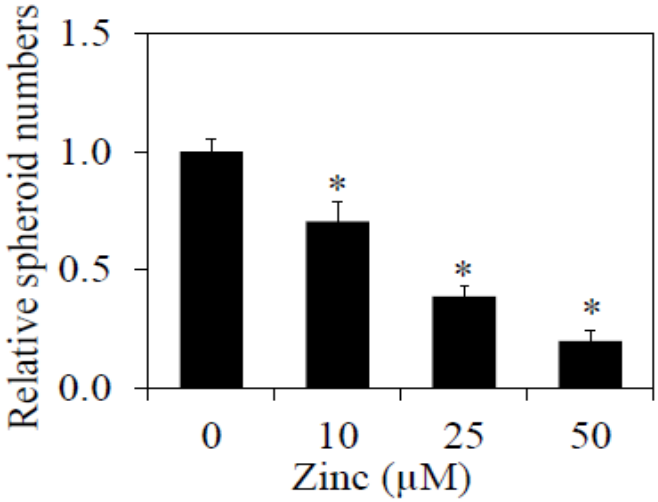

C

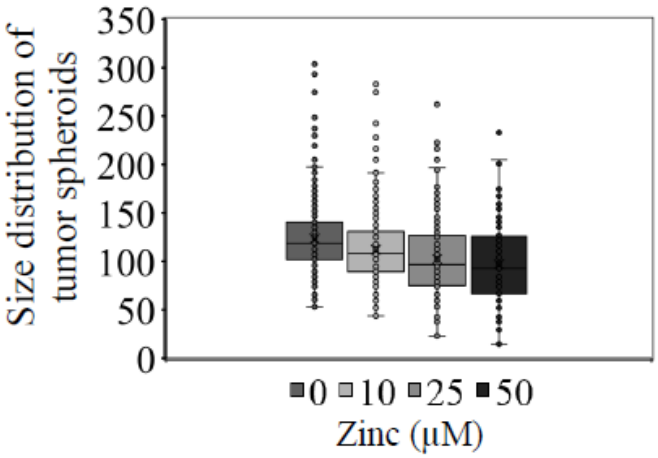

Figure 4.36 Effects of zinc ion on tumor spheroid formation in H292 cells. (A) Zinc ion-exposed cells (0-50 µM) for 3 days were analyzed for tumor sphere formation. Tumor

spheroids were visualized under a phase contrast microscope after 4 weeks of culture; scale bar = 1000 μm. (B-C) Quantitative analysis of tumor spheroids. Values are means ± S.E.M of triplicate independent experiments. * P<0.05 versus non-treated control.

9.1.3 Effect of zinc ion on superoxide anion generation in H292 cells.

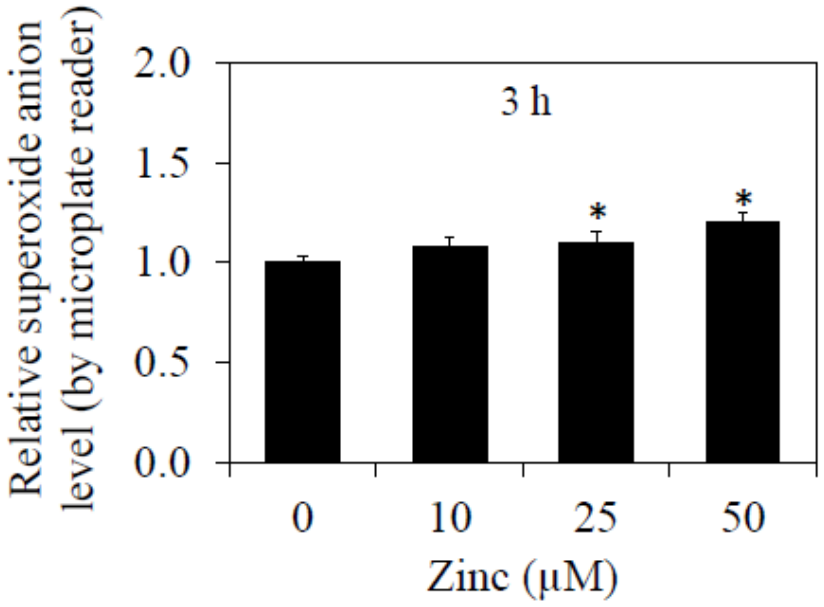

Figure 4.37 Effects of zinc ion on superoxide anion generation in H292 cells in dose-dependent manner analyzed by microplate reader. The cells were incubated with DHE at 4°C for 30 min prior to the treatment with zinc (0–50 μM) for 3 h and the fluorescence intensity was analyzed by a microplate reader. Mean intensity was normalized to untreated control cells and represented as relative superoxide anion level. Values are means ± S.E.M. of independent triplicate experiments. *p<0.05 versus non-treated control.

9.1.4 Effect of zinc ion on PKCα activation in H292 cells

A

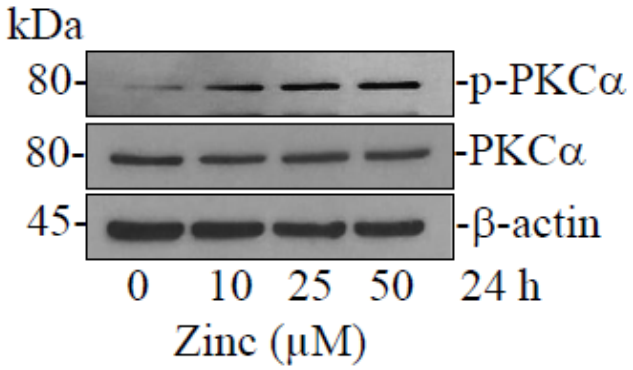

B

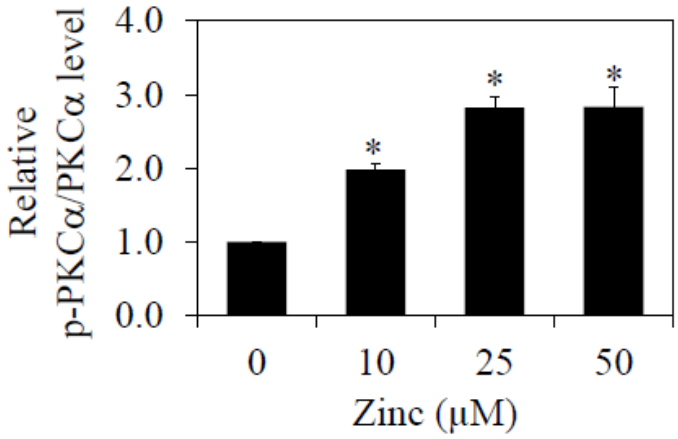

Figure 4.38 Effect of zinc ion on PKCα activation in H292 cells. (A) Cells were treated with zinc ion (0-50 μM) for 24 h. The treated cells were subjected to western blot analysis to determine the expression levels of PKCα. The blots were re-probed with β-actin to confirm equal loading of the samples. (B) The blots were quantified by densitometry and mean data from three independent experiments were normalized to the results. The bars are the means ± S.E.M. of independent triplicate experiments. *$p<0.05$ versus non-treated control.

9.2 Effect of zinc on CSC in lung cancer H23 cells

Figures 4.39 and 4.40 indicate that zinc ion reduced the expression levels of CSC markers (CD133, β-catenin, and ALDH1A1) and attenuated the ability to form spheroids of H23 lung cancer cells. In addition, zinc ion resulted in an elevation of superoxide anion level (Figure 4.41) and a significant increase in phosphorylated PKCα expression (Figure 4.42) in H23 cell lines.

9.2.1 Effect of zinc on CSC markers in H23 cells.

A

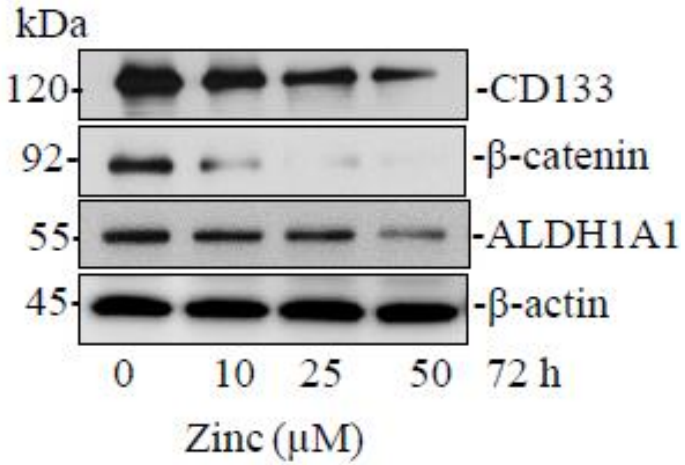

B

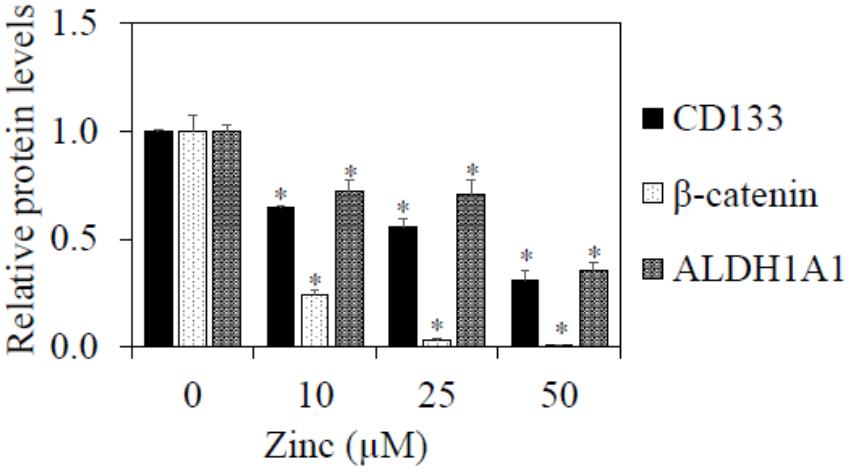

C

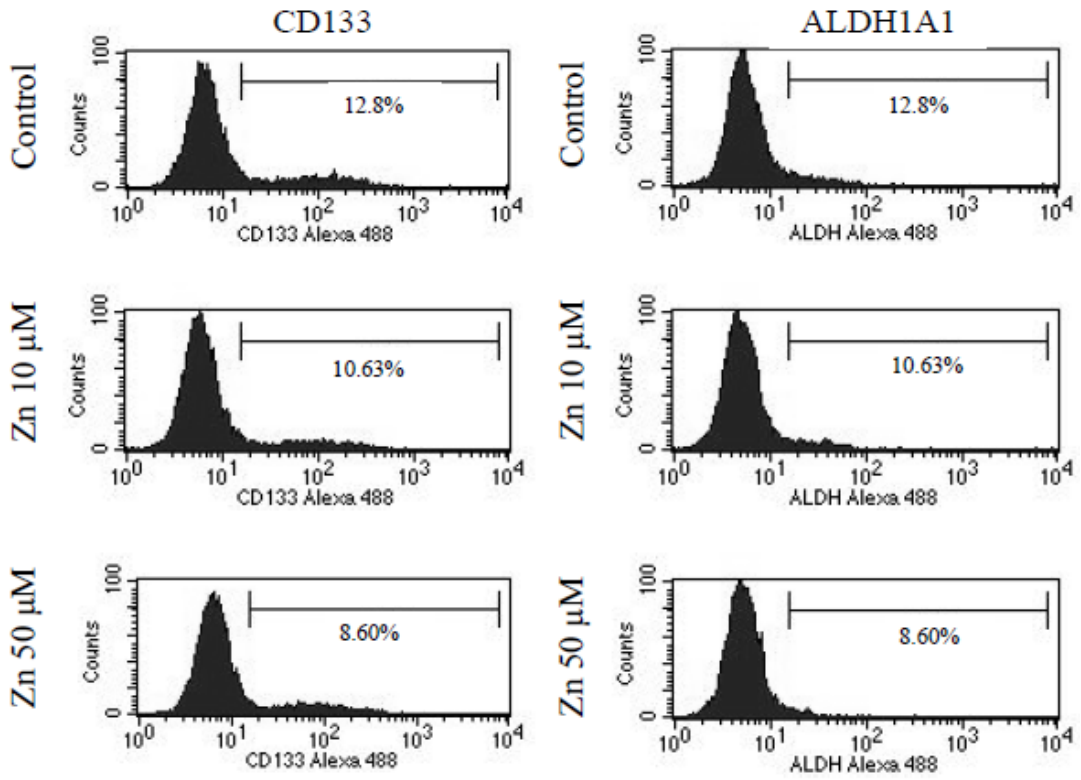

Figure 4.39 Effect of zinc on CSC markers of lung cancer H23 cells**.** Zinc ion-exposed cells (0-50 µM) for 3 days were analyzed for the expression levels of CSC markers (A) Expression levels of CSC markers were analyzed by western blotting. The blots were re-probed with β-actin to confirm equal loading of the samples. (B) The blots were quantified by densitometry and mean data from three independent experiments were normalized to the results. The bars are the means ± S.E.M. of independent triplicate experiments. *P<0.05 versus non-treated control. (C) The expression of CD133 and ALDH1A1 was measured by flow cytometry for treated and non-treated cells at 72 h of zinc ion treatment. Flow cytometry was performed using rabbit anti-CD133 and ALDH1A1 monoclonal antibodies followed by Alexa Fluor 488-labeled secondary antibody to visualize CD133 and ALDH1A1 expression.

9.2.2 Effect of zinc ion on spheroid formation in H23 cells.

A

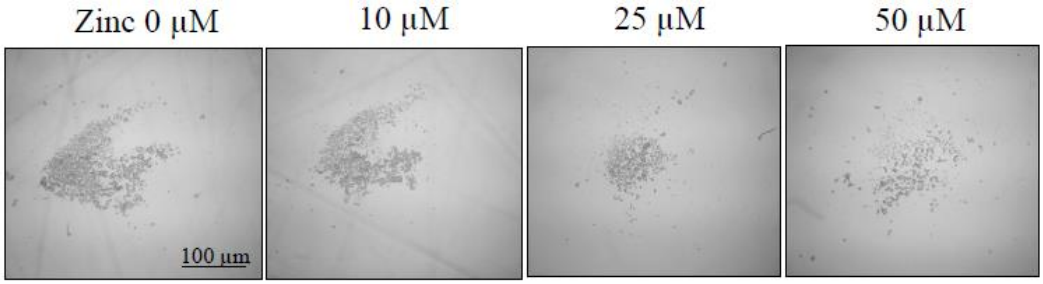

B

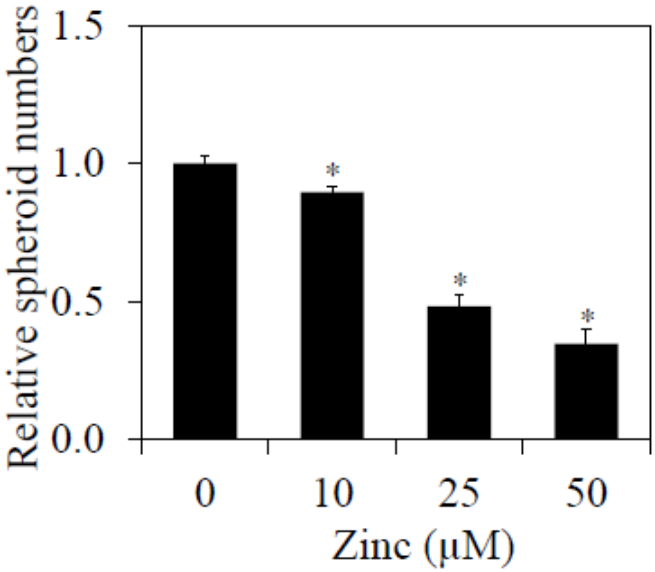

C

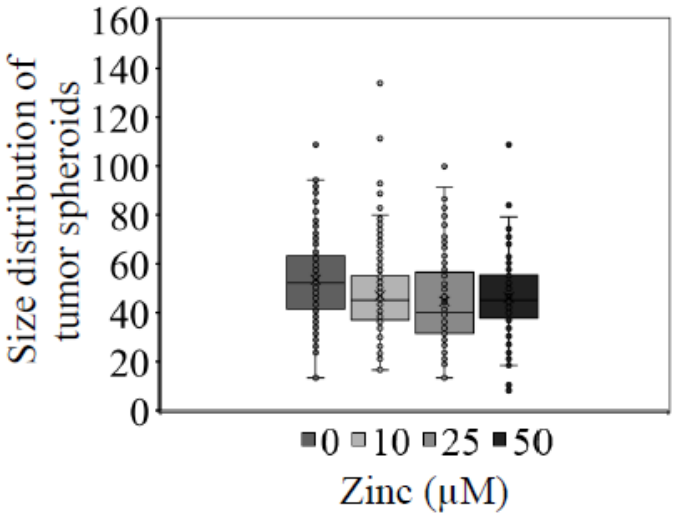

Figure 4.40 Effects of zinc on tumor spheroid formation in H23 cells. (A) Zinc ion-exposed cells (0-50 μM) for 3 days were analyzed for tumor sphere formation. Tumor spheroids were visualized under a phase contrast microscope after 4 weeks of culture; scale bar = 1000 μm. (B-C) Quantitative analysis of tumor spheroids. Values are means ± S.E.M. of triplicate independent experiments. * P<0.05 versus non-treated control.

9.2.3 Effect of zinc ion on superoxide anion generation in H23 cells.

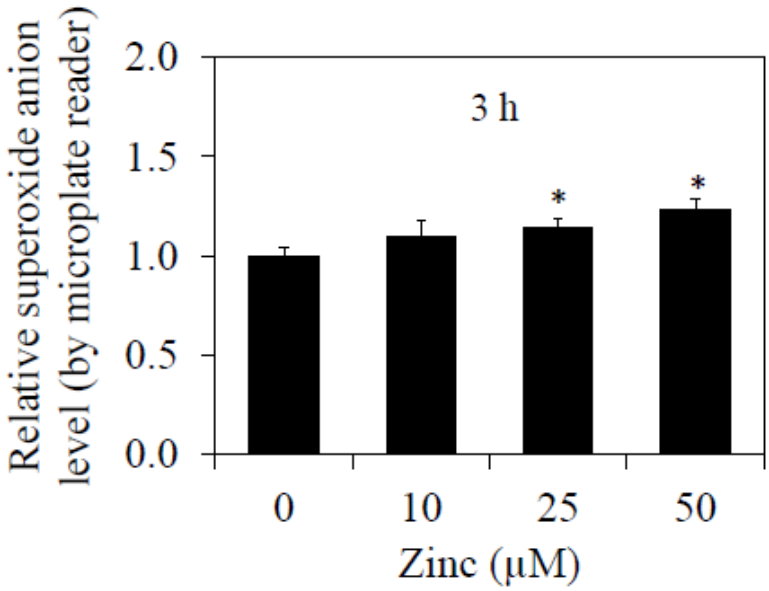

Figure 4.41 Effects of zinc on superoxide anion generation in H23 cells in dose-dependent manner analyzed by microplate reader. The cells were incubated with DHE at 4°C for 30 min prior to the treatment with zinc (0–50 μM) for 3 h and the fluorescence intensity was analyzed by a microplate reader. Mean intensity was normalized to untreated control cells and represented as relative superoxide anion levels. Values are means ± S.E.M. of independent triplicate experiments. *p<0.05 versus non-treated control.

9.2.4 Effect of zinc ion on PKCα activation in H23 cells

A

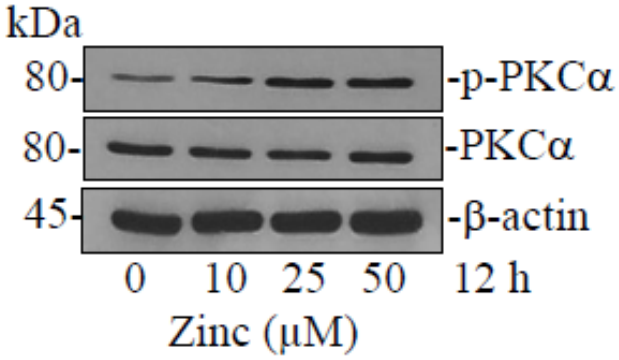

B

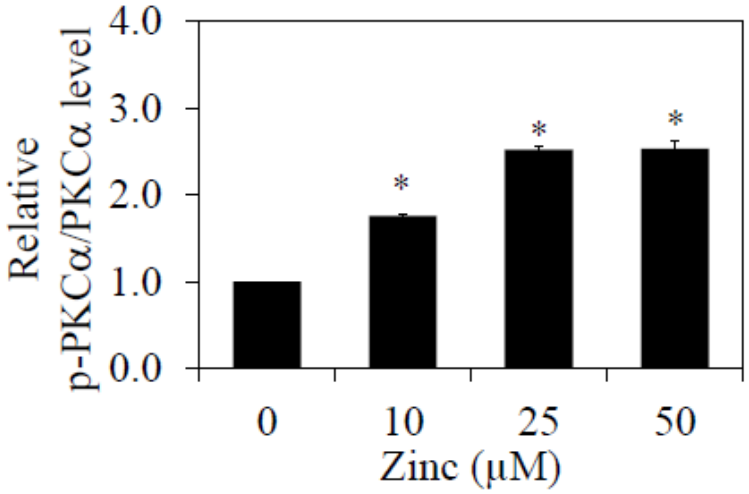

Figure 4.42 Effect of zinc on PKCα activation in H23 cells. (A) Cells were treated with zinc ion (0-50 μM) for 24 h. The treated cells were subjected to western blot analysis to determine the expression levels of PKCα. The blots were re-probed with β-actin to confirm equal loading of the samples. (B) The blots were quantified by densitometry and mean data from three independent experiments were normalized to the results. The bars are the means ± S.E.M. of independent triplicate experiments. *p<0.05 versus non-treated control.

Taken together, these results have supported the earier conclusion that zinc ion has a negative regulatory effect on CSC control in lung cancer cells by regulating of PKCα via a superoxide-mediated mechanism.

CHAPTER V
DISCUSSION AND CONCLUSIONS

Zinc ion is an essential trace element that is incorporated in many enzymes and transcription factors regulating several cell functions, such as cell replication, tissue or cell growth, immunity, and bone formation (Hajo and Wolfgang, 2010; Wu et al., 2013). Zinc ion has a capability to bind directly to amino acid residues at the catalytic site and participates in reaction activity of enzymes, leading to affect several life processes (Kuwahara and Coleman, 1990). Commonly, zinc ion is transported by two major proteins, including Zrt/Irt-like protein (ZIP) and zinc transporter protein (ZnT). ZIP transports extracellular zinc ion to the cytosol, while ZnT transports cytosolic zinc ion out of the cells or moves it into vesicle or organelle (Haase and Maret, 2003; Cousins et al., 2006).

Interestingly, previous evidence indicated that several zinc ion influx transporters such as ZIP 6 (Hogstrand et al., 2013), ZIP7 (Taylor et al., 2012) and ZIP10 (Kagara et al., 2007) were shown to be up-regulated in some cancer cells and their high levels correlate with aggressive behaviors and poor prognosis. Besides, the aberrant level of zinc ion has been found in the condition of cancer. The reduced plasma zinc ion level was found in patients with gallbladder, prostate, and lung cancers (Gupta et al., 2005; Gumulec et al., 2014), while the elevated level of zinc ion in plasma or tissues was detected in liver and breast cancers (Wright and Dormandy, 1972; Margalioth et al., 1983; Kollmeier et al., 1992). The different plasma levels of zinc ion among cancer types may be due to the different expressions of zinc ion transporter proteins in each kinds of cancer (Kagara et al., 2007; Taylor et al., 2012; Hogstrand et

al., 2013). Furthermore, recent study has shown that zinc ion treatment succeeds in sensitizing lung cancer cells for anoikis (Pramchu-Em et al., 2016). Such information has suggested that zinc ion may play important parts on the basis of cancer cell biology.

For clinical application, in case of zinc supplement, clinical data revealed a significant increase in plasma zinc ion level approximately 23 μM after supplemented with 150 mg of elemental zinc for 6 weeks (Samman and Roberts, 1987). The concentration of zinc ion in various conditions was considered in this work. The results illustrated that although concentrations of zinc ion used in this study caused no cytotoxic effect on lung cancer cells, they clearly have intracellular effects on cell functions.

An amount of evidence has indicated the roles of EMT and CSCs in cancer progression and metastasis (Hermann et al., 2007; Yang and Weinberg, 2008; Iwatsuki et al., 2010; Merlos-Suarez et al., 2011; Perona et al., 2011; Craene and Berx, 2013). Until recently, the knowledge of zinc ion on the molecular mechanisms of cancer metastasis is still not fully understood especially those regulating EMT and CSCs. EMT is considered to be a critical augmenting process of cancer metastasis as it facilitates cancer dissemination in many ways (Yang and Weinberg, 2008; Iwatsuki et al., 2010; Craene and Berx, 2013).

In the process of EMT, cellular phenotypes are altered together with the distinguished expressions of protein markers being changed from epithelial toward mesenchymal types (Yang and Weinberg, 2008; Thiery et al., 2009; Iwatsuki et al., 2010; Craene and Berx, 2013). The process facilitates the loss of cell adhesion and increases cell motility and survival in detached condition (Yang and Weinberg, 2008; Thiery et

al., 2009; Iwatsuki et al., 2010; Craene and Berx, 2013). During EMT, an elongated fibroblast-like morphology of the cells is frequently observed. However, indicators like the switching between E-cadherin and N-cadherin, as well as EMT transcription factors snail and slug are more acceptable as hallmarks of EMT (Yang and Weinberg, 2008; Thiery et al., 2009; Iwatsuki et al., 2010; Craene and Berx, 2013). EMT features of H460 cells were characterized by (i) the change of cell morphology from epithelial to fibroblast-liked mesenchymal shape, (ii) the increased EMT markers N-cadherin, vimentin, snail, and slug, together with the reduction of epithelial marker E-cadherin, and (iii) EMT behaviors, including increased migration, invasion and tumorigenic potential (Gomez et al., 1999; Fernando et al., 2010; Kim et al., 2014; Lin et al., 2014; Winitthana et al., 2014; Yao et al., 2015). In consistent with such studies, the results of this work showed that zinc ion-treated lung cancer cells displayed the elongated mesenchymal-like shape with the significant increase of EMT markers namely N-cadherin, vimentin, snail and slug. Also, this study found that the E-cadherin was dramatically reduced in response to zinc ion treatment.

Previous studies have indicated that EMT facilitates the cell motility by decreasing cell-cell interaction via E-cadherin, while increases in N-cadherin-mediated steady-state of active Rac1 (Nieman et al., 1999; Wheelock et al., 2008). Similar to N-cadherin, vimentin was shown to increase FAK and Rac1 activities (Mendez et al., 2010; Havel et al., 2015). This study found that zinc ion could induce EMT, resulting in the increase of cancer cell migration and invasion. The proteins regulating cell motility like FAK, RhoA, and Rac1 were found to be activated in response to such up-stream signals. Like lung cancer, zinc ion seems to be involved in an enhancement of migratory ability in breast cancer cells (Kagara et al., 2007; Levenson and Somers, 2008; Taylor et al.,

2012; Hogstrand et al., 2013) and increased cell migration ability of normal keratinocyte in regulation of wound repair (Tenaud et al., 2000).

In addition, the EMT event was shown to be a key factor that enhances ability of cancer cells to metastasis by increasing the survival after cell detachment and ability to form tumors (Chunhacha et al., 2013; Winitthana et al., 2014). It has been previously reported that the ability of cancer cells in forming new tumor can be enhanced by EMT as a result of snail augmentation (Hwang et al., 2011; Voon et al., 2013; Zhou et al., 2014). We have supported this fact by the demonstration that treatment of the cells with zinc ion induced EMT with significant up-regulation of snail expression increased number and size of tumor colonies in 3D culturing anchorage-independent condition.

Signaling pathways activated by ROS and impairment of redox control are involved in various processes of carcinogenesis and cancer progression (Luanpitpong et al., 2010; Rungtabnapa et al., 2011; Chanvorachote and Luanpitpong, 2016). In general, ROS are continuously produced as a byproduct of mitochondrial chain reaction and detoxified by antioxidants and enzymes to keep them at nonharmful levels (Chance et al., 1979). The accumulated evidence reveals the role of low-to-moderate levels of ROS in maintaining several cell activities including proliferation and motility (Luanpitpong et al., 2010). Such behaviors of cancer cells as migration, apoptosis, and adhesion to endothelial cells were shown to be regulated through ROS-dependent mechanisms (Chanvorachote and Chunhacha, 2013). In particular, hydrogen peroxide was shown to mediate anoikis resistance in lung cancer cells by inhibiting caveolin-1 degradation (Rungtabnapa et al., 2011). The involvement of ROS signaling

on cancer metastasis and EMT has garnered increasing attentions (Wu, 2006; Wang et al., 2010; Wu and Wu, 2010; Lee et al., 2013). The EMT-related transcription factor snail was shown to be directly regulated by the balance of cellular ROS status (Lee et al., 2013; Cichon and Radisky, 2014).

Zinc ion have a pivotal role in redox metabolism. In spite of its antioxidant role as an essential cofactor of superoxide dismutase (Ivanovska et al.), an enzyme that catalyzes the conversion of superoxide anion to hydrogen peroxide (Rakhit and Chakrabartty, 2006), zinc ion can act as a prooxidant. In neurons, intracellular zinc ion was shown to be tightly associated with the change in cellular ROS. When neurons are damaged, the bound zinc ion is released into the cytoplasm as a free form and this form of zinc ion triggers further ROS production (Aizenman et al., 2000; Zhang et al., 2004). In addition, the increase in intracellular zinc ion was demonstrated to promote superoxide anion generation from the function of the enzyme 12-lipoxygenase (12-LOX) (Aizenman et al., 2000; Zhang et al., 2004). Interestingly, zinc ion was shown to induce Hep-2 cancer cell apoptosis by stimulating ROS production (Rudolf et al., 2005). These observations are consistent with the results of this study showing that treatment of lung cancer cells with zinc ion resulted in the induction of ROS, superoxide anion in this condition.

Importantly, this current study has reported for the first time that zinc ion significantly induced EMT characteristics in lung cancer cells through the enhancement of cellular superoxide anion level. Superoxide anion has been implicated in various biological and pathological processes (Yang et al., 2002; Brandes, 2003; Buetler et al., 2004). Evidence has shown that the level of superoxide anion is frequently upregulated

in cancer cells and regulates cancer cell proliferation, migration and metastasis (Safford et al., 1994; Suh et al., 1999; Yang et al., 2002; Lopez-Lazaro, 2007; Banskota et al., 2015). Regarding of EMT process, although some studies have indicated that hydrogen peroxide can also mediate EMT in human malignant mesothelioma and human ovarian cancer cells (Cheng et al., 2010; Kim et al., 2013) , treatment of the zinc ion in our system caused no effect on the cellular level of hydrogen peroxide. This study has first revealed the role of superoxide anion in regulation of EMT in cancer cells, as the EMT could be induced by addition of superoxide anion generator DMNQ.

DMNQ is known to induce superoxide anion generation via NADPH oxidase activity (Watanabe and Forman, 2003; Ishihara et al., 2006). This study found that treatment of the cells with DMNQ significantly increased the protein hallmarks of EMT as well as metastatic potentials. Such roles of superoxide anion on EMT were linked with the results of zinc ion, suggesting that zinc ion mediates the EMT phenotypes via the production of cellular superoxide anion. These results were confirmed by the ROS inhibitory experiment. Addition of superoxide anion inhibitor MnTBAP in the zinc ion-treated cells was shown to abolish superoxide anion induction as well as EMT phenotypes in response to zinc ion treatment, strongly indicating that the effect of zinc ion on EMT was regulated via superoxide-dependent mechanism. These findings not only provide the evidence of endogenous element in regulation of cancer biology, but also add the fact involving specific ROS roles on EMT process of cancer cells. The schematic mechanism of zinc ion-induced EMT in lung cancer cells is indicated in figure 5.1

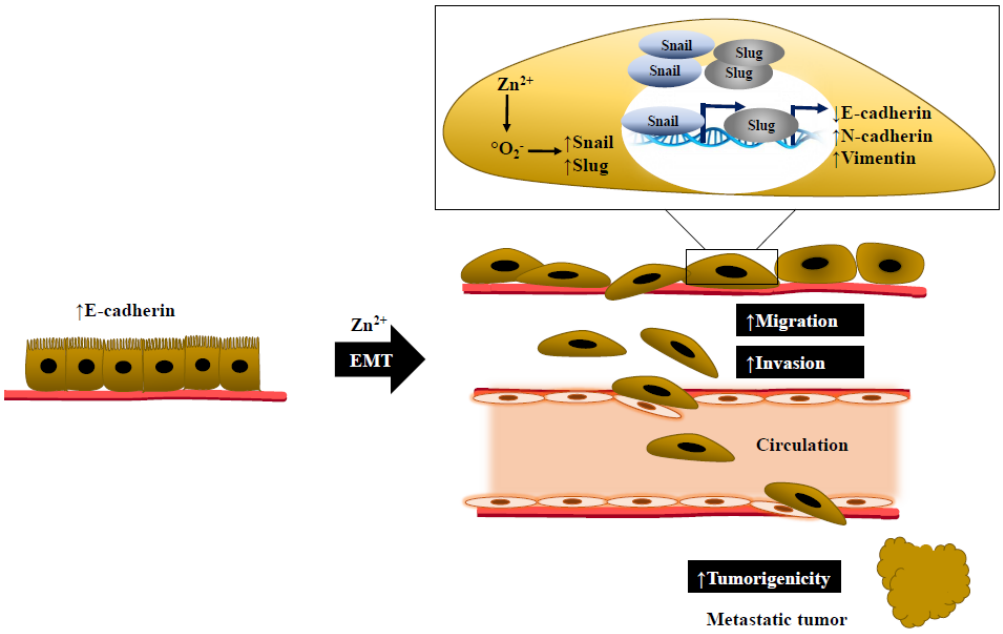

Figure 5.1 The schematic mechanism of zinc ion-induced EMT in lung cancer cells

Recent biological studies focusing on the aggressive behaviors of cancer cells have posited the CSC paradigm as initiating and driving such malignant diseases (Hermann et al., 2007; Merlos-Suarez et al., 2011; Perona et al., 2011). In lung cancer, certain populations of CSCs have been identified and associated with chemotherapeutic resistance, cancer progression, metastasis, and relapse (Eramo et al., 2010; Singh et al., 2012; Zakaria et al., 2015). Therefore, all factors influencing CSC characteristics are of great interest as they may deepen insight into cancer cell biology leading to the development of novel anticancer strategies.

Furthermore, evidence stated that EMT could play a role in an acquisition of CSC phenotypes (Kurrey et al., 2009; Scheel and Weinberg, 2012; Zhou et al., 2014; Luanpitpong et al., 2016), since EMT-regulatory transcription factors, including snail and slug are known to mediate CSC properties (Kurrey et al., 2009; Zhou et al., 2014; Luanpitpong et al., 2016). Snail have been reported to enhance stemness properties,

such as self-renewal, tumorigenicity and therapeutic resistance (Kurrey et al., 2009; Zhou et al., 2014), while slug have been found to stabilize CSC transcription factor in controlling of CSC phenotypes (Luanpitpong et al., 2016). On the other hand, some studies suggested that CSCs often exhibited EMT characteristics and share some behaviors with EMT cells (Yongsanguanchai et al., 2015). As zinc ion has the effect on EMT process of lung cancer, therefore, this study further evaluated whether zinc ion may affect CSC program. Surprisingly, the present study revealed that EMT was not critical for the role of zinc ion in regulation of lung CSC program in the tested system, which consistent with certain studies that EMT and CSCs are not always associated (Biddle et al., 2011; Gavert et al., 2011; Phiboonchaiyanan et al., 2016)

It has been recently shown that expression levels of ALDH1A1 and CD133 have a significant prognostic value strongly related to poor survival in non-small cell lung cancer (Alamgeer et al., 2013). Also, these two markers have been shown to be well-accepted indicators for CSCs, in particular in lung cancer (Ginestier et al., 2007; Eramo et al., 2008; Jiang et al., 2009). The present study revealed that zinc ion treatment reduced ALDH1A1 and CD133 expression in the three different NSCLC cells. The pluripotency markers Oct4, Sox2, and Nanog have been shown to be augmented in various CSCs (Jeter et al., 2011; Liu et al., 2013; Boumahdi et al., 2014; Koo et al., 2015) and such proteins were shown to be important to maintain CSC characteristics in such cancers (Chiou et al., 2010; Jeter et al., 2011; Liu et al., 2013; Boumahdi et al., 2014; Koo et al., 2015). The treatment of zinc ion resulted in Oct4, Sox2, and Nanog down-regulation, leading to attenuate self-renewal property of lung cancer cells. Consistently, in three different cell lines, zinc ion succeeded in suppressing spheroid formation under anchorage and serum-starved condition which has been shown to

reflect self-renewal ability of CSCs (Levina et al., 2010; Cao et al., 2011; Singh et al., 2012; Kantara et al., 2014; Condello et al., 2015; Chanvorachote and Luanpitpong, 2016; Grun et al., 2016; Luanpitpong et al., 2016; Zhou et al., 2016)..

Evidence has shown that the Wingless (Wnt)/ß-catenin pathway is an important regulator of pluripotency embryonic stem cells and the role of the Wnt pathway in regulation of CSCs is also widely accepted (Cai and Zhu, 2012; Holland et al., 2013; Zhang et al., 2015). In lung cancer, the Wnt/ß-catenin has been shown as a potential target for the development of novel anticancer drugs (Zhang et al., 2015; Yang et al., 2016). Another evidence has indicated a link between the Wnt/ß-catenin signaling and CSCs that ß-Catenin is a component of the cadherin cell adhesion complex playing a key role in the Wnt/ß-catenin pathway (Clevers, 2006; Cai and Zhu, 2012; Su et al., 2015). In addition, the link between ß-catenin and such pluripotency markers has been previously demonstrated in several studies (Cai and Zhu, 2012; Holland et al., 2013; Li et al., 2013; Zhang et al., 2015; Kim et al., 2016). Regarding of lung cancer, Wnt/ß-catenin mediated increased expression of Oct4 (Zhang et al., 2015; Kim et al., 2016), Nanog (Li et al., 2013; Zhang et al., 2015; Kim et al., 2016), and Sox2 (Kim et al., 2016). Moreover, the Wnt antagonist was shown to reduce the expression of Nanog and Oct4 (Zhang et al., 2015) in lung cancer. Consistent with the results of this study, the decrease in CSC-related transcription factors Oct4, Sox2, and Nanog was found subsequent to the downregulation of ß-catenin.

Previously, PKCα was demonstrated to diminish cellular ß-catenin levels by phosphorylating the protein at the position of serine 33 and 37 and threonine 41,

which actuated ß-catenin degradation through ubiquitin-proteasomal degradation (van Noort et al., 2002; Gwak et al., 2006; Luna-Ulloa et al., 2011). The results of this study not only advocated the role of PKCα in ß-catenin regulation but also firstly provided a link between PKCα activation and cancer stemness in lung cancer cells. The increased activation of PKCα by PKCα activator and zinc ion treatments can reduce ß-catenin level together with suppressing other determinants of spheroid formation and CSC-related factors, and such event in zinc ion-treated cells was ameliorated by PKCα inhibitor. As activity of ß-catenin strictly depends on its presence in the cells, the PKCα-mediated degradation of ß-catenin presented in this study, would be, at least in part, a mechanism by which zinc ion suppresses CSC program of lung cancer cells.

Moreover, having shown that superoxide anion generated by zinc ion play a kay role in regulation of EMT. Focusing on CSC biology, iron was shown to induce CSC phenotypes in lung cancer cells via the generation of hydroxyl radical (Chanvorachote and Luanpitpong, 2016). This study provided the detail that the principal ROS generated in response to zinc ion exposure is superoxide anion, which subsequently linked the superoxide anion triggered by zinc ion with the activation of PKCα, a known determinant of ß-catenin stability, as it has been previously shown that PKCα can be activated by ROS (Lee et al., 2004).

Again, DMNQ and MnTBAP were used to clarify that superoxide anion could be critical for CSC regulation. This study found that treatment of the cells with DMNQ significantly decreased the CSC markers as well as spheroid initiation, unveiling the roles of superoxide anion in CSC program. Besides, the results of the ROS inhibitory

experiment provided the information that addition of superoxide anion inhibitor MnTBAP in the zinc ion-treated cells was shown to reduce the activation of PKCα and the accumulation of β-catenin-ubiquitin complex as well as reverse CSC characteristics in response to zinc ion treatment, indicating that the negative effect of zinc ion on lung CSC features was regulated via superoxide anion/PKCα/β-catenin dependent mechanism. The schematic mechanism of zinc ion-suppressed CSC phenotype in lung cancer cells is shown in figure 5.2

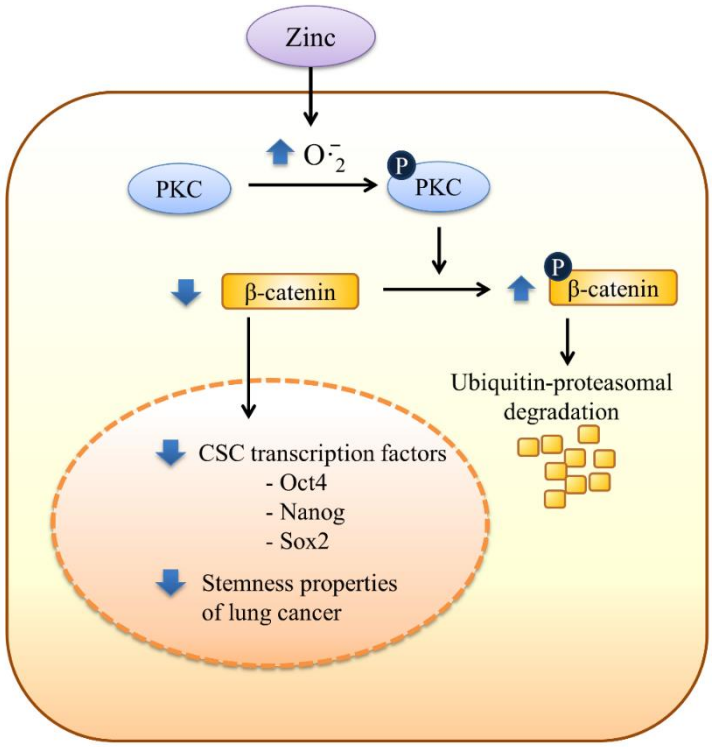

Figure 5.2 The schematic mechanism of zinc ion-suppressed CSC phenotype in lung cancer cells

The inverse effect of zinc ion on EMT and cancer stemness was disclosed in this study may be due to the heterogeneity of cancer cells in cell model. The effect of zinc ion on EMT was clearly detected because it mainly affected the major

population of the cells (non-CSC cells), while the role of zinc ion in stemness was occurred in sub-population of cancer cells (CSCs) which were found only 0.01-3% of total population (Klonisch et al., 2008; Visvader and Lindeman, 2008; Bao et al., 2013; Enderling et al., 2013; Sottoriva et al., 2013).

Previous studies have indicated the regulatory role of Wnt/ß-catenin signaling in CSCs and EMT (Jiang et al., 2007; Cai and Zhu, 2012; Wu et al., 2012; Holland et al., 2013; Su et al., 2015; Zhang et al., 2015). Although zinc ion reduced intracellular ß-catenin level, such decreased ß-catenin did not affect EMT process in this condition, which could be due to the fact that (i) ß-catenin signaling might not to be a key mechanism in lung cancer EMT regulation since ß-catenin signal seems to be a down-stream effect of snail/slug transcription repressor of E-cadherin and cadherin switching (Nelson and Nusse, 2004) and (ii) superoxide anion generated by zinc ion can directly induce the up-regulation of EMT transcription factors.

In conclusions, our finding provided the evidence that zinc ion has inverse effects on EMT and CSCs of lung cancer cells. While zinc ion induces EMT phenotypes, it was shown to suppresses CSC characteristics as indicated in figure 5.3**.** The increase in EMT markers and the reduction of epithelial marker were observed in zinc ion-treated cells, indicating the induction of EMT with mesenchymal-like morphology and increased cancer cell motility. In contrast, zinc ion reduced tumor spheroid forming with the decrease in CSC markers**.** Such the regulation was dependent on zinc ion-induced superoxide anion generation which increased the EMT proteins and promoted cell motility. Also, this study found that superoxide anion generated by zinc ion

suppressed CSCs through the PKCα/β-catenin dependent mechanism by activating PKCα which subsequently phosphorylated and mediated β-catenin degradation via the ubiquitin-proteasomal mechanism. The novel finding derived from insight on EMT and CSC regulation of lung cancer cells may lead to the better understanding of cancer cell biology regarding this essential endogenous element on cancer aggressive behaviors and have important implications for anti-cancer strategies, cancer chemotherapy and prevention.

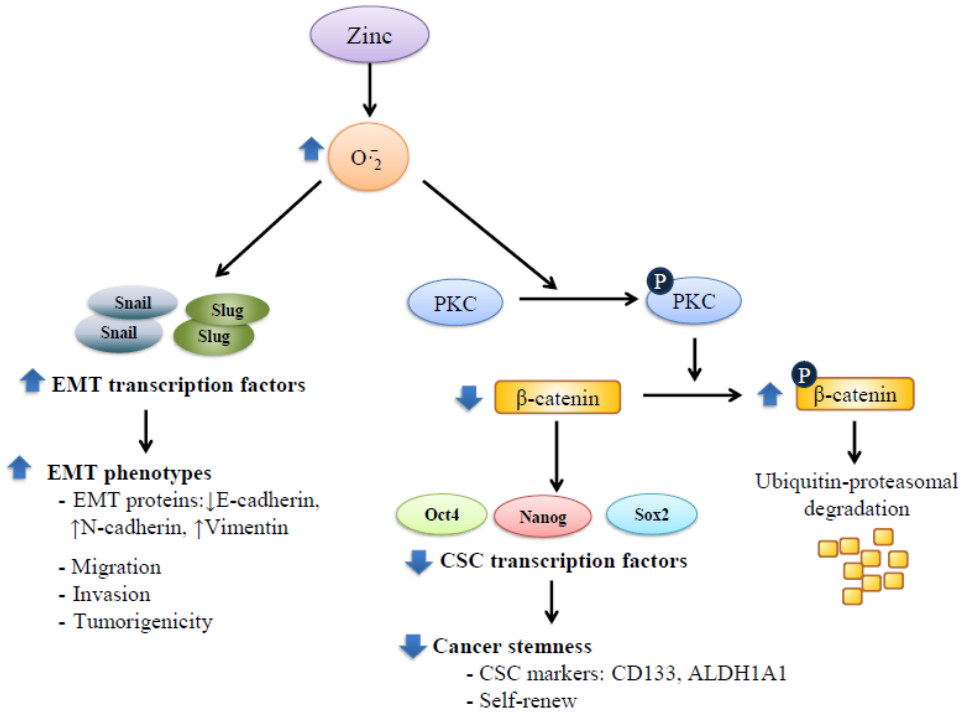

Figure 5.3 The schematic diagram summarizes the effect of zinc ion on EMT and cancer stemess of lung cancer cells.

REFERENCES

Alamgeer, M., et al. 2013. The prognostic significance of aldehyde dehydrogenase 1A1 (ALDH1A1) and CD133 expression in early stage non-small cell lung cancer. Thorax, 68: 1095-1104.

Andreoli, S. P. 1991. Reactive oxygen molecules, oxidant injury and renal disease. Pediatr Nephrol, 5: 733-742.

Bachelder, R. E., Yoon, S. O., Franci, C., de Herreros, A. G. and Mercurio, A. M. 2005. Glycogen synthase kinase-3 is an endogenous inhibitor of Snail transcription: implications for the epithelial-mesenchymal transition. J Cell Biol, 168: 29-33.

Bao, B., Prasad, A. S., Beck, F. W. and Sarkar, F. H. 2007. Zinc up-regulates NF-kappaB activation via phosphorylation of IkappaB in HUT-78 (Th0) cells. FEBS Lett, 581: 4507-4511.

Barbera, M. J., et al. 2004. Regulation of Snail transcription during epithelial to mesenchymal transition of tumor cells. Oncogene, 23: 7345-7354.

Bertolini, G., et al. 2009. Highly tumorigenic lung cancer CD133+ cells display stem-like features and are spared by cisplatin treatment. Proc Natl Acad Sci U S A, 106: 16281-16286.

Bolos, V., Blanco, M., Medina, V., Aparicio, G., Diaz-Prado, S. and Grande, E. 2009. Notch signalling in cancer stem cells. Clin Transl Oncol, 11: 11-19.

Brabletz, T., et al. 2005. Invasion and metastasis in colorectal cancer: epithelial-mesenchymal transition, mesenchymal-epithelial transition, stem cells and beta-catenin. Cells Tissues Organs, 179: 56-65.

Brautigan, D. L., Bornstein, P. and Gallis, B. 1981. Phosphotyrosyl-protein phosphatase. Specific inhibition by Zn. J Biol Chem, 256: 6519-6522.

Brown, A. M., et al. 2000. Zn2+ inhibits alpha-ketoglutarate-stimulated mitochondrial respiration and the isolated alpha-ketoglutarate dehydrogenase complex. J Biol Chem, 275: 13441-13447.

Cai, C. and Zhu, X. 2012. The Wnt/beta-catenin pathway regulates self-renewal of cancer stem-like cells in human gastric cancer. Mol Med Rep, 5: 1191-1196.

Cao, L., et al. 2011. Sphere-forming cell subpopulations with cancer stem cell properties in human hepatoma cell lines. BMC Gastroenterol, 11: 71.

Carter, C. A. and Kane, C. J. 2004. Therapeutic potential of natural compounds that regulate the activity of protein kinase C. Curr Med Chem, 11: 2883-2902.

Chanvorachote, P. and Luanpitpong, S. 2016. Iron induces cancer stem cells and aggressive phenotypes in human lung cancer cells. Am J Physiol Cell Physiol, 310: C728-739.

Cheng, J. C., Auersperg, N. and Leung, P. C. 2012. EGF-induced EMT and invasiveness in serous borderline ovarian tumor cells: a possible step in the transition to low-grade serous carcinoma cells? PLoS One, 7: e34071.

Cheng, J. C., Klausen, C. and Leung, P. C. 2010. Hydrogen peroxide mediates EGF-induced down-regulation of E-cadherin expression via p38 MAPK and snail in human ovarian cancer cells. Mol Endocrinol, 24: 1569-1580.

Cichon, M. A. and Radisky, D. C. 2014. ROS-induced epithelial-mesenchymal transition in mammary epithelial cells is mediated by NF-kB-dependent activation of Snail. Oncotarget, 5: 2827-2838.

Clevers, H. 2006. Wnt/ß-Catenin Signaling in Development and Disease. Cell, 127: 469-480.

Cochrane, C. R., Szczepny, A., Watkins, D. N. and Cain, J. E. 2015. Hedgehog Signaling in the Maintenance of Cancer Stem Cells. Cancers, 7: 1554-1585.

Condello, S., et al. 2015. [beta]-Catenin-regulated ALDH1A1 is a target in ovarian cancer spheroids. Oncogene, 34: 2297-2308.

Cousins, R. J., Liuzzi, J. P. and Lichten, L. A. 2006. Mammalian zinc transport, trafficking, and signals. J Biol Chem, 281: 24085-24089.

Craene, B. D. and Berx, G. 2013. Regulatory networks defining EMT during cancer initiation and progression. Nat Rev Cancer, 13: 97-110.

Csermely, P., Szamel, M., Resch, K. and Somogyi, J. 1988. Zinc increases the affinity of phorbol ester receptor in T lymphocytes. Biochemical and Biophysical Research Communications, 154: 578-583.

da Silva, S. D., et al. 2015. Epithelial-mesenchymal transition (EMT) markers have prognostic impact in multiple primary oral squamous cell carcinoma. Clin Exp Metastasis, 32: 55-63.

Dineley, K. E., Richards, L. L., Votyakova, T. V. and Reynolds, I. J. 2005. Zinc causes loss of membrane potential and elevates reactive oxygen species in rat brain mitochondria. Mitochondrion, 5: 55-65.

Edme, N., Downward, J., Thiery, J. P. and Boyer, B. 2002. Ras induces NBT-II epithelial cell scattering through the coordinate activities of Rac and MAPK pathways. J Cell Sci, 115: 2591-2601.

Eramo, A., et al. 2008. Identification and expansion of the tumorigenic lung cancer stem cell population. Cell Death Differ, 15: 504-514.

Fang, D., et al. 2007. Phosphorylation of beta-catenin by AKT promotes beta-catenin transcriptional activity. J Biol Chem, 282: 11221-11229.

Fantozzi, A., et al. 2014. VEGF-mediated angiogenesis links EMT-induced cancer stemness to tumor initiation. Cancer Res, 74: 1566-1575.

Farrell, J., et al. 2014. HGF induces epithelial-to-mesenchymal transition by modulating the mammalian hippo/MST2 and ISG15 pathways. J Proteome Res, 13: 2874-2886.

Forbes, I. J., Zalewski, P. D., Giannakis, C. and Betts, W. H. 1990. Zinc induces specific association of PKC with membrane cytoskeleton. Biochem Int, 22: 741-748.

Frederickson, C. J., Koh, J. Y. and Bush, A. I. 2005. The neurobiology of zinc in health and disease. Nat Rev Neurosci, 6: 449-462.

Fukada, T., Yamasaki, S., Nishida, K., Murakami, M. and Hirano, T. 2011. Zinc homeostasis and signaling in health and diseases: Zinc signaling. J Biol Inorg Chem, 16: 1123-1134.

Fukawa, T., Kajiya, H., Ozeki, S., Ikebe, T. and Okabe, K. 2012. Reactive oxygen species stimulates epithelial mesenchymal transition in normal human epidermal keratinocytes via TGF-beta secretion. Exp Cell Res, 318: 1926-1932.

Gil, D., Ciolczyk-Wierzbicka, D., Dulinska-Litewka, J., Zwawa, K., McCubrey, J. A. and Laidler, P. 2011. The mechanism of contribution of integrin linked kinase (ILK) to epithelial-mesenchymal transition (EMT). Adv Enzyme Regul, 51: 195-207.

Ginestier, C., et al. 2007. ALDH1 is a marker of normal and malignant human mammary stem cells and a predictor of poor clinical outcome. Cell Stem Cell, 1: 555-567.

Gomez, D. E., Skilton, G., Alonso, D. F. and Kazanietz, M. G. 1999. The role of protein kinase C and novel phorbol ester receptors in tumor cell invasion and metastasis (Review). Oncol Rep, 6: 1363-1370.

Grosse-Gehling, P., et al. 2013. CD133 as a biomarker for putative cancer stem cells in solid tumours: limitations, problems and challenges. J Pathol, 229: 355-378.

Grun, D., Adhikary, G. and Eckert, R. L. 2016. VEGF-A acts via neuropilin-1 to enhance epidermal cancer stem cell survival and formation of aggressive and highly vascularized tumors. Oncogene.

Gumulec, J., Masarik, M., Adam, V., Eckschlager, T., Provaznik, I. and Kizek, R. 2014. Serum and Tissue Zinc in Epithelial Malignancies: A Meta-Analysis. PLoS ONE, 9: e99790.

Gupta, S. K., Singh, S. P. and Shukla, V. K. 2005. Copper, zinc, and Cu/Zn ratio in carcinoma of the gallbladder. J Surg Oncol, 91: 204-208.

Gwak, J., et al. 2006. Protein-kinase-C-mediated beta-catenin phosphorylation negatively regulates the Wnt/beta-catenin pathway. J Cell Sci, 119: 4702-4709.

Haase, H. and Maret, W. 2003. Intracellular zinc fluctuations modulate protein tyrosine phosphatase activity in insulin/insulin-like growth factor-1 signaling. Exp Cell Res, 291: 289-298.

Hajo, H. and Wolfgang, M. 2010. The Regulatory and Signaling Functions of Zinc Ions in Human Cellular Physiology. Cellular and Molecular Biology of Metals, CRC Press**:** 181-212.

Hancock, J. T., Desikan, R. and Neill, S. J. 2001. Role of reactive oxygen species in cell signalling pathways. Biochem Soc Trans, 29: 345-350.

Hansson, A. 1996. Extracellular zinc ions induces mitogen-activated protein kinase activity and protein tyrosine phosphorylation in bombesin-sensitive Swiss 3T3 fibroblasts. Arch Biochem Biophys, 328: 233-238.

Havel, L. S., Kline, E. R., Salgueiro, A. M. and Marcus, A. I. 2015. Vimentin regulates lung cancer cell adhesion through a VAV2-Rac1 pathway to control focal adhesion kinase activity. Oncogene, 34: 1979-1990.

Hermann, P. C., et al. 2007. Distinct populations of cancer stem cells determine tumor growth and metastatic activity in human pancreatic cancer. Cell Stem Cell, 1: 313-323.

Hirano, T., Murakami, M., Fukada, T., Nishida, K., Yamasaki, S. and Suzuki, T. 2008. Roles of zinc and zinc signaling in immunity: zinc as an intracellular signaling molecule. Adv Immunol, 97: 149-176.

Hogstrand, C., Kille, P., Ackland, Margaret L., Hiscox, S. and Taylor, Kathryn M. 2013. A mechanism for epithelial–mesenchymal transition and anoikis resistance in breast cancer triggered by zinc channel ZIP6 and STAT3 (signal transducer and activator of transcription 3). Biochemical Journal, 455: 229-237.

Holland, J. D., Klaus, A., Garratt, A. N. and Birchmeier, W. 2013. Wnt signaling in stem and cancer stem cells. Curr Opin Cell Biol, 25: 254-264.

Hwang, W. L., et al. 2011. SNAIL regulates interleukin-8 expression, stem cell-like activity, and tumorigenicity of human colorectal carcinoma cells. Gastroenterology, 141: 279-291, 291 e271-275.

Ivanovska, J., et al. 2015. DAPK loss in colon cancer tumor buds – implications for migration capacity of disseminating tumor cells. Oncotarget.

Iwatsuki, M., et al. 2010. Epithelial-mesenchymal transition in cancer development and its clinical significance. Cancer Sci, 101: 293-299.

Jiang, F., et al. 2009. Aldehyde dehydrogenase 1 is a tumor stem cell-associated marker in lung cancer. Mol Cancer Res, 7: 330-338.

Jiang, Y. G., et al. 2007. Role of Wnt/beta-catenin signaling pathway in epithelial-mesenchymal transition of human prostate cancer induced by hypoxia-inducible factor-1alpha. Int J Urol, 14: 1034-1039.

Ju, L. and Zhou, C. 2013. Integrin beta 1 enhances the epithelial-mesenchymal transition in association with gefitinib resistance of non-small cell lung cancer. Cancer Biomark, 13: 329-336.

Kagara, N., Tanaka, N., Noguchi, S. and Hirano, T. 2007. Zinc and its transporter ZIP10 are involved in invasive behavior of breast cancer cells. Cancer Sci, 98: 692-697.

Kambe, T. 2014. Introduction: “Zinc Signaling”–The Blossoming Field of Zinc Biology. Zinc Signals in Cellular Functions and Disorders. T. Fukada and T. Kambe, Springer Japan: 1-5.

Kantara, C., O'Connell, M., Sarkar, S., Moya, S., Ullrich, R. and Singh, P. 2014. Curcumin promotes autophagic survival of a subset of colon cancer stem cells, which are ablated by DCLK1-siRNA. Cancer Res, 74: 2487-2498.

Karamboulas, C. and Ailles, L. 2013. Developmental signaling pathways in cancer stem cells of solid tumors. Biochim Biophys Acta, 1830: 2481-2495.

Katsuno, Y., Lamouille, S. and Derynck, R. 2013. TGF-beta signaling and epithelial-mesenchymal transition in cancer progression. Curr Opin Oncol, 25: 76-84.

Khoury, H., et al. 2005. HGF Converts ErbB2/Neu Epithelial Morphogenesis to Cell Invasion. Molecular Biology of the Cell, 16: 550-561.

Kim, M. C., Cui, F. J. and Kim, Y. 2013. Hydrogen peroxide promotes epithelial to mesenchymal transition and stemness in human malignant mesothelioma cells. Asian Pac J Cancer Prev, 14: 3625-3630.

Kim, Y. M., et al. 2007. Zn2+-induced NF-kappaB-dependent transcriptional activity involves site-specific p65/RelA phosphorylation. Cell Signal, 19: 538-546.

Kimlin, L. C., Casagrande, G. and Virador, V. M. 2013. In vitro three-dimensional (3D) models in cancer research: an update. Mol Carcinog, 52: 167-182.

Knowles, L. M., Gurski, L. A., Engel, C., Gnarra, J. R., Maranchie, J. K. and Pilch, J. 2013. Integrin alphavbeta3 and fibronectin upregulate Slug in cancer cells to promote clot invasion and metastasis. Cancer Res, 73: 6175-6184.

Kollmeier, H., Seemann, J., Wittig, P., Rothe, G. and Witting, C. 1992. Zinc concentrations in human tissues. Liver zinc in carcinoma and severe liver disease. Pathol Res Pract, 188: 942-945.

Kuwahara, J. and Coleman, J. E. 1990. Role of the zinc(II) ions in the structure of the three-finger DNA binding domain of the Sp1 transcription factor. Biochemistry, 29: 8627-8631.

Lamouille, S., Xu, J. and Derynck, R. 2014. Molecular mechanisms of epithelial–mesenchymal transition. Nat Rev Mol Cell Biol, 15: 178-196.

Lansdown, A. B. 1996. Zinc in the healing wound. Lancet, 347: 706-707.

Lansdown, A. B., Mirastschijski, U., Stubbs, N., Scanlon, E. and Agren, M. S. 2007. Zinc in wound healing: theoretical, experimental, and clinical aspects. Wound Repair Regen, 15: 2-16.

Larue, L. and Bellacosa, A. 2005. Epithelial-mesenchymal transition in development and cancer: role of phosphatidylinositol 3' kinase/AKT pathways. Oncogene, 24: 7443-7454.

Lee, S. S., Tsai, C. H., Yu, C. C. and Chang, Y. C. 2013. Elevated snail expression mediates tumor progression in areca quid chewing-associated oral squamous cell carcinoma via reactive oxygen species. PLoS One, 8: e67985.

Lee, Y.-I., Kwon, Y.-J. and Joo, C.-K. 2004. Integrin-linked kinase function is required for transforming growth factor ß-mediated epithelial to mesenchymal transition. Biochemical and Biophysical Research Communications, 316: 997-1001.

Levenson, C. W. and Somers, R. C. 2008. Nutritionally regulated biomarkers for breast cancer. Nutr Rev, 66: 163-166.

Levina, V., et al. 2010. Elimination of human lung cancer stem cells through targeting of the stem cell factor-c-kit autocrine signaling loop. Cancer Res, 70: 338-346.

Li, T., et al. 2010. ALDH1A1 is a marker for malignant prostate stem cells and predictor of prostate cancer patients' outcome. Lab Invest, 90: 234-244.

Liao, G., Wang, M., Ou, Y. and Zhao, Y. 2014. IGF-1-induced epithelial-mesenchymal transition in MCF-7 cells is mediated by MUC1. Cell Signal, 26: 2131-2137.

Link, T. A. and von Jagow, G. 1995. Zinc ions inhibit the QP center of bovine heart mitochondrial bc1 complex by blocking a protonatable group. J Biol Chem, 270: 25001-25006.

Liu, A., Yu, X. and Liu, S. 2013. Pluripotency transcription factors and cancer stem cells: small genes make a big difference. Chin J Cancer, 32: 483-487.

Lobo, N. A., Shimono, Y., Qian, D. and Clarke, M. F. 2007. The biology of cancer stem cells. Annu Rev Cell Dev Biol, 23: 675-699.

Luanpitpong, S., et al. 2016. SLUG is required for SOX9 stabilization and functions to promote cancer stem cells and metastasis in human lung carcinoma. Oncogene, 35: 2824-2833.

Luanpitpong, S., Wang, L., Stueckle, T. A., Tse, W., Chen, Y. C. and Rojanasakul, Y. 2014. Caveolin-1 regulates lung cancer stem-like cell induction and p53 inactivation in carbon nanotube-driven tumorigenesis. Oncotarget, 5: 3541-3554.

Luna-Ulloa, L. B., Hernandez-Maqueda, J. G., Castaneda-Patlan, M. C. and Robles-Flores, M. 2011. Protein kinase C in Wnt signaling: implications in cancer initiation and progression. IUBMB Life, 63: 915-921.

MacDonald, B. T., Tamai, K. and He, X. 2009. Wnt/β-catenin signaling: components, mechanisms, and diseases. Developmental cell, 17: 9-26.

MacDonald, R. S. 2000. The role of zinc in growth and cell proliferation. J Nutr, 130: 1500S-1508S.

Maitland, N. J. and Collins, A. T. 2008. Prostate cancer stem cells: a new target for therapy. J Clin Oncol, 26: 2862-2870.

Mamuya, F. A. and Duncan, M. K. 2012. aV integrins and TGF-beta-induced EMT: a circle of regulation. J Cell Mol Med, 16: 445-455.

Mao, J., et al. 2014. Roles of Wnt/beta-catenin signaling in the gastric cancer stem cells proliferation and salinomycin treatment. Cell Death Dis, 5: e1039.

Margalioth, E. J., Schenker, J. G. and Chevion, M. 1983. Copper and zinc levels in normal and malignant tissues. Cancer, 52: 868-872.

Maschler, S., et al. 2005. Tumor cell invasiveness correlates with changes in integrin expression and localization. Oncogene, 24: 2032-2041.

McDermott, S. P. and Wicha, M. S. 2010. Targeting breast cancer stem cells. Molecular Oncology, 4: 404-419.

Mehlen, P. and Puisieux, A. 2006. Metastasis: a question of life or death. Nat Rev Cancer, 6: 449-458.

Mendez, M. G., Kojima, S. and Goldman, R. D. 2010. Vimentin induces changes in cell shape, motility, and adhesion during the epithelial to mesenchymal transition. FASEB J, 24: 1838-1851.

Merlos-Suarez, A., et al. 2011. The intestinal stem cell signature identifies colorectal cancer stem cells and predicts disease relapse. Cell Stem Cell, 8: 511-524.

Miyazono, K. 2009. Transforming growth factor-beta signaling in epithelial-mesenchymal transition and progression of cancer. Proc Jpn Acad Ser B Phys Biol Sci, 85: 314-323.

Newton, A. C. 1995. Protein kinase C: structure, function, and regulation. J Biol Chem, 270: 28495-28498.

Nguyen, D. X., Bos, P. D. and Massague, J. 2009. Metastasis: from dissemination to organ-specific colonization. Nat Rev Cancer, 9: 274-284.

Nieman, M. T., Prudoff, R. S., Johnson, K. R. and Wheelock, M. J. 1999. N-cadherin promotes motility in human breast cancer cells regardless of their E-cadherin expression. J Cell Biol, 147: 631-644.

Nimmanon, T. and Taylor, K. 2014. Zinc Signaling and Cancer. Zinc Signals in Cellular Functions and Disorders. T. Fukada and T. Kambe, Springer Japan**:** 285-313.

Noh, K. M. and Koh, J. Y. 2000. Induction and activation by zinc of NADPH oxidase in cultured cortical neurons and astrocytes. J Neurosci, 20: RC111.

Oloumi, A., McPhee, T. and Dedhar, S. 2004. Regulation of E-cadherin expression and β-catenin/Tcf transcriptional activity by the integrin-linked kinase. Biochimica et Biophysica Acta (BBA) - Molecular Cell Research, 1691: 1-15.

Onder, T. T., Gupta, P. B., Mani, S. A., Yang, J., Lander, E. S. and Weinberg, R. A. 2008. Loss of E-cadherin promotes metastasis via multiple downstream transcriptional pathways. Cancer Res, 68: 3645-3654.

Parker, P. J., et al. 1986. The complete primary structure of protein kinase C--the major phorbol ester receptor. Science, 233: 853-859.

Pattabiraman, D. R. and Weinberg, R. A. 2014. Tackling the cancer stem cells – what challenges do they pose? Nature reviews. Drug discovery, 13: 497-512.

Perona, R., Lopez-Ayllon, B. D., de Castro Carpeno, J. and Belda-Iniesta, C. 2011. A role for cancer stem cells in drug resistance and metastasis in non-small-cell lung cancer. Clin Transl Oncol, 13: 289-293.

Pramchu-Em, C., Meksawan, K. and Chanvorachote, P. 2016. Zinc Sensitizes Lung Cancer Cells to Anoikis through Down-Regulation of Akt and Caveolin-1. Nutr Cancer, 68: 312-319.

Prasad, A. S., Bao, B., Beck, F. W. and Sarkar, F. H. 2001. Zinc activates NF-kappaB in HUT-78 cells. J Lab Clin Med, 138: 250-256.

Radisky, D. C., et al. 2005. Rac1b and reactive oxygen species mediate MMP-3-induced EMT and genomic instability. Nature, 436: 123-127.

Rahuel-Clermont, S. and Dunn, M. F. 1998. The biological chemistry of zinc. Copper and Zinc in Inflammatory and Degenerative Diseases. K. D. Rainsford, R. Milanino, J. R. J. Sorenson and G. P. Velo, Springer Netherlands: 47-59.

Rudolf, E. 2007. Depletion of ATP and oxidative stress underlie zinc-induced cell injury. Acta Medica (Hradec Kralove), 50: 43-49.

Rudolf, E. and Cervinka, M. 2010. Zinc pyrithione induces cellular stress signaling and apoptosis in Hep-2 cervical tumor cells: the role of mitochondria and lysosomes. Biometals, 23: 339-354.

Rudolf, E., Rudolf, K. and Cervinka, M. 2005. Zinc induced apoptosis in HEP-2 cancer cells: the role of oxidative stress and mitochondria. Biofactors, 23: 107-120.

Samet, J. M., Dewar, B. J., Wu, W. and Graves, L. M. 2003. Mechanisms of Zn(2+)-induced signal initiation through the epidermal growth factor receptor. Toxicol Appl Pharmacol, 191: 86-93.

Samet, J. M., et al. 1998. Activation of MAPKs in human bronchial epithelial cells exposed to metals. Am J Physiol, 275: L551-558.

Scheel, C. and Weinberg, R. A. 2012. Cancer stem cells and epithelial-mesenchymal transition: concepts and molecular links. Semin Cancer Biol, 22: 396-403.

Shi, X., Zhang, Y., Zheng, J. and Pan, J. 2012. Reactive oxygen species in cancer stem cells. Antioxid Redox Signal, 16: 1215-1228.

Siegel, R. L., Miller, K. D. and Jemal, A. 2015. Cancer statistics, 2015. CA: A Cancer Journal for Clinicians, 65: 5-29.

Siegel, R. L., Miller, K. D. and Jemal, A. 2017. Cancer statistics, 2017. CA: A Cancer Journal for Clinicians, 67: 7-30.

Singh, S., et al. 2012. EGFR/Src/Akt signaling modulates Sox2 expression and self-renewal of stem-like side-population cells in non-small cell lung cancer. Mol Cancer, 11: 73.

Sliva, D. 2004. Signaling pathways responsible for cancer cell invasion as targets for cancer therapy. Curr Cancer Drug Targets, 4: 327-336.

Strutz, F., et al. 2002. Role of basic fibroblast growth factor-2 in epithelial-mesenchymal transformation. Kidney Int, 61: 1714-1728.

Taki, M., Kamata, N., Yokoyama, K., Fujimoto, R., Tsutsumi, S. and Nagayama, M. 2003. Downregulation of Wnt4 and upregulation of Wnt5a expression by epithelialmesenchymal transition in human squamous carcinoma cells. Cancer Science, 94: 593-597.

Tanaka, Y., et al. 2013. Prognostic impact of EMT (epithelial-mesenchymal-transition)-related protein expression in endometrial cancer. Cancer Biol Ther, 14: 13-19.

Taylor, K. M., Hiscox, S., Nicholson, R. I., Hogstrand, C. and Kille, P. 2012. Protein kinase CK2 triggers cytosolic zinc signaling pathways by phosphorylation of zinc channel ZIP7. Sci Signal, 5: ra11.

Thannickal, V. J. and Fanburg, B. L. 2000. Reactive oxygen species in cell signaling. Am J Physiol Lung Cell Mol Physiol, 279: L1005-1028.

Thiery, J. P., Acloque, H., Huang, R. Y. and Nieto, M. A. 2009. Epithelial-mesenchymal transitions in development and disease. Cell, 139: 871-890.

Voon, D. C., et al. 2013. EMT-induced stemness and tumorigenicity are fueled by the EGFR/Ras pathway. PLoS One, 8: e70427.

Wang, Z., Li, Y. and Sarkar, F. H. 2010. Signaling Mechanism(S) of Reactive Oxygen Species in Epithelial-Mesenchymal Transition Reminiscent of Cancer Stem Cells in Tumor Progression. Curr Stem Cell Res Ther, 5: 74-80.

Wheelock, M. J., Shintani, Y., Maeda, M., Fukumoto, Y. and Johnson, K. R. 2008. Cadherin switching. J Cell Sci, 121: 727-735.

Wong, A. S. and Gumbiner, B. M. 2003. Adhesion-independent mechanism for suppression of tumor cell invasion by E-cadherin. J Cell Biol, 161: 1191-1203.

Wright, E. B. and Dormandy, T. L. 1972. Liver zinc in carcinoma. Nature, 237: 166.

Wu, W.-S. 2006. The signaling mechanism of ROS in tumor progression. Cancer and Metastasis Reviews, 25: 695-705.

Wu, W.-S. and Wu, J.-R. 2010. The Role of ROS Signaling in Tumor Progression. Signal Transduction in Cancer Metastasis. W.-S. Wu and C.-T. Hu, Springer Netherlands. **15:** 103-118.

Wu, W., Bromberg, P. A. and Samet, J. M. 2013. Zinc ions as effectors of environmental oxidative lung injury. Free Radic Biol Med, 65: 57-69.

Wu, W., Graves, L. M., Gill, G. N., Parsons, S. J. and Samet, J. M. 2002. Src-dependent phosphorylation of the epidermal growth factor receptor on tyrosine 845 is required for zinc-induced Ras activation. J Biol Chem, 277: 24252-24257.

Wu, W., et al. 2003. Zinc-induced PTEN protein degradation through the proteasome pathway in human airway epithelial cells. J Biol Chem, 278: 28258-28263.

Wu, Z. Q., Li, X. Y., Hu, C. Y., Ford, M., Kleer, C. G. and Weiss, S. J. 2012. Canonical Wnt signaling regulates Slug activity and links epithelial-mesenchymal transition with epigenetic Breast Cancer 1, Early Onset (BRCA1) repression. Proc Natl Acad Sci U S A, 109: 16654-16659.

Xu, J., Lamouille, S. and Derynck, R. 2009. TGF-beta-induced epithelial to mesenchymal transition. Cell Res, 19: 156-172.

Yang, J. and Weinberg, R. A. 2008. Epithelial-mesenchymal transition: at the crossroads of development and tumor metastasis. Dev Cell, 14: 818-829.

Yongsanguanchai, N., Pongrakhananon, V., Mutirangura, A., Rojanasakul, Y. and Chanvorachote, P. 2015. Nitric oxide induces cancer stem cell-like phenotypes in human lung cancer cells. Am J Physiol Cell Physiol, 308: C89-100.

Yook, J. I., Li, X. Y., Ota, I., Fearon, E. R. and Weiss, S. J. 2005. Wnt-dependent regulation of the E-cadherin repressor snail. J Biol Chem, 280: 11740-11748.

Zhao, C., et al. 2009. Hedgehog signalling is essential for maintenance of cancer stem cells in myeloid leukaemia. Nature, 458: 776-779.

Zhou, D., et al. 2016. RBP2 induces stem-like cancer cells by promoting EMT and is a prognostic marker for renal cell carcinoma. Exp Mol Med, 48: e238.

Zhou, W., et al. 2014. Snail contributes to the maintenance of stem cell-like phenotype cells in human pancreatic cancer. PLoS One, 9: e87409.

APPENDIX

APPENDIX

TABLES OF EXPERIMENTAL RESULTS

Table 1 The percentage of H460 cell viability was determined by MTT assay after treatment with various concentrations of zinc ion for 24 h.

Zinc (μM)	% Cell viability
0	100.00 ± 0.00
5	99.05 ± 5.47
10	95.88 ± 3.40
25	93.08 ± 3.23
50	91.86 ± 3.57
100	86.62 ± 9.29*

Value represents means ± S.E.M. of four-independent experiments, *P<0.05 versus non-treated control.

Table 2 The percentage of apoptotic cells of H460 cells was determined by Hoechst 33342 staining after treatment with various concentrations of zinc ion for 24 h.

Zinc (μM)	% Apoptosis
0	0.00 ± 0.00
5	1.33 ± 1.53
10	4.00 ± 4.36
25	7.67 ± 3.51
50	9.00 ± 5.57
100	19.67 ± 3.51*

Value represents means ± S.E.M. of three-independent experiments, *P<0.05 versus non-treated control.

Table 3 Relative cell proliferation of H460 cells was determined by MTT assay after treatment with various concentrations of zinc ion for 0-72 h.

Zinc (μM)	Relative cell proliferation			
	0h	24h	48h	72h
0	1.00 ± 0.00	2.07 ± 0.18	3.18 ± 0.46	5.26 ± 0.35
5	1.00 ± 0.00	2.07 ± 0.21	2.91 ± 0.33	5.00 ± 0.12
10	1.00 ± 0.00	2.01 ± 0.23	3.01 ± 0.37	5.06 ± 0.21
25	1.00 ± 0.00	1.99 ± 0.19	2.81 ± 0.32	4.83 ± 0.08
50	1.00 ± 0.00	1.91 ± 0.22	2.56 ± 0.26	4.46 ± 0.15

Value represents means ± S.E.M. of four-independent experiments, *P<0.05 versus non-treated control.

Table 4 Relative protein levels of EMT markers of H460 cells were determined by western blot analysis after treatment with various concentrations of zinc ion for 24 h.

Zinc (μM)	Relative protein levels				
	N-cadherin	E-cadherin	Vimentin	Slug	Snail
0	1.00 ± 0.00	1.00 ± 0.00	1.00 ± 0.00	1.00 ± 0.00	1.00 ± 0.00
5	1.17 ± 0.15*	0.71 ± 0.01*	4.50 ± 0.74*	1.27 ± 0.13*	2.42 ± 0.53*
10	1.27 ± 0.20*	0.51 ± 0.03*	5.56 ± 0.09*	1.28 ± 0.12*	4.50 ± 0.15*
25	1,54 ± 0.10*	0.49 ± 0.00*	5.88 ±0.52*	1.55 ± 0.16*	5.45 ± 0.14*
50	2.01 ± 0.19*	0.18 ± 0.01*	6.09 ± 0.29*	1.76 ± 0.12*	5.92 ± 0.69*

Value represents means ± S.E.M. of three-independent experiments, *P<0.05 versus non-treated control.

Table 5 Relative migration levels of H460 cells were determined by wound healing migration assay after treatment with various concentrations of zinc ion for 24 h.

Zinc (μM)	Relative migration level
0	1.00 ± 0.00
5	1.31 ± 0.10*
10	1.40 ± 0.14*
25	1.57 ± 0.12*
50	1.88 ± 0.10*

Value represents means ± S.E.M. of three-independent experiments, *P<0.05 versus non-treated control.

Table 6 Relative migration levels of H460 cells were determined by transwell migration assay after treatment with various concentrations of zinc ion for 24 h.

Zinc (μM)	Relative migration level
0	1.00 ± 0.00
5	1.29 ± 0.16
10	1.31 ± 0.12*
25	1.50 ± 0.12*
50	1.84 ± 0.35*

Value represents means ± S.E.M. of three-independent experiments, *P<0.05 versus non-treated control.

Table 7 Relative invasion levels of H460 cells were determined by transwell invasion assay after treatment with various concentrations of zinc ion for 24 h.

Zinc (μM)	Relative invasion level
0	1.00 ± 0.00
5	1.23 ± 0.20
10	1.79 ± 0.44*
25	2.06 ± 0.60 *
50	2.60 ± 0.37*

Value represents means ± S.E.M. of three-independent experiments, *P<0.05 versus non-treated control.

Table 8 Relative protein levels of motility-regulatory proteins of H460 cells were determined by western blot analysis after treatment with various concentrations of zinc ion for 24 h.

Zinc (μM)	Relative protein levels		
	p-FAK/FAK	Rac1-GTP	RhoA-GTP
0	1.00 ± 0.00	1.00 ± 0.00	1.00 ± 0.00
5	1.45 ± 0.11*	1.28 ± 0.11*	1.38 ± 0.10*
10	3.70 ± 0.24*	1.64 ± 0.10*	1.64 ± 0.18*
25	4.78 ± 0.56*	1.77 ± 0.22*	1.80 ± 0.20*
50	5.02 ± 0.42*	1.97 ± 0.17*	2.11 ± 0.26*

Value represents means ± S.E.M. of three-independent experiments, *P<0.05 versus non-treated control.

Table 9 Relative colony numbers and size of H460 cells were determined by *in vitro* tumorigenicity assay after treatment with various concentrations of zinc ion for 24 h.

Zinc (μM)	Relative colony numbers	Relative colony size
0	1.00 ± 0.00	1.00 ± 0.00
5	0.95 ± 0.06	1.03 ± 0.03
10	1.12 ± 0.08	1.08 ± 0.08
25	1.38 ± 0.12*	1.30 ± 0.20*
50	1.76 ± 0.18*	1.41 ± 0.20*

Value represents means ± S.E.M. of three-independent experiments, *P<0.05 versus non-treated control.

Table 10 Relative superoxide anion level in time-dependent manner determined by microplate reader after treatment with zinc ion (50 μM) for 0-3 h.

Zinc (μM)	Relative superoxide anion levels		
	0 h	1 h	3 h
50	1.00 ± 0.00	1.35 ± 0.20*	2.05 ± 0.57*

Value represents means ± S.E.M. of three-independent experiments, *P<0.05 versus non-treated control.

Table 11 Relative hydrogen peroxide level in time-dependent manner determined by microplate reader after treatment with zinc ion (50 μM) for 0-3 h.

Zinc (μM)	Relative hydrogen peroxide levels		
	0 h	1 h	3 h
50	1.00 ± 0.00	1.03 ± 0.07	1.09 ± 0.09

Value represents means ± S.E.M. of three-independent experiments, *P<0.05 versus non-treated control.

Table 12 Relative hydroxyl radical level in time-dependent manner determined by microplate reader after treatment with zinc ion (50 μM) for 0-3 h.

Zinc (μM)	Relative hydroxyl radical levels		
	0 h	1 h	3 h
50	1.00 ± 0.00	1.07 ± 0.04	1.10 ± 0.06

Value represents means ± S.E.M. of three-independent experiments, *P<0.05 versus non-treated control.

Table 13 Relative superoxide anion level in dose-dependent manner determined by microplate reader after treatment with various concentrations of zinc ion for 3 h.

Zinc (μM)	Relative superoxide anion levels
0	1.00 ± 0.00
5	1.62 ± 0.23*
10	1.64 ± 0.23*
25	1.67 ± 0.22*
50	1.80 ± 0.12*

Value represents means ± S.E.M. of three-independent experiments, *P<0.05 versus non-treated control.

Table 14 Relative hydrogen peroxide level in dose-dependent manner determined by microplate reader after treatment with various concentrations of zinc ion for 3 h.

Zinc (μM)	Relative hydrogen peroxide levels
0	1.00 ± 0.00
5	1.04 ± 0.07
10	1.02 ± 0.17
25	1.06 ± 0.18
50	1.14 ± 0.13

Value represents means ± S.E.M. of three-independent experiments, *P<0.05 versus non-treated control.

Table 15 Relative hydroxyl radical level in dose-dependent manner determined by microplate reader after treatment with various concentrations of zinc ion for 3 h.

Zinc (μM)	Relative hydroxyl radical levels
0	1.00 ± 0.00
5	1.04 ± 0.17
10	1.05 ± 0.06
25	1.04 ± 0.12
50	1.08 ± 0.05

Value represents means ± S.E.M. of three-independent experiments, *P<0.05 versus non-treated control.

Table 16 Relative superoxide anion level in time-dependent manner determined by flow cytometry after treatment with zinc ion (50 μM) for 0-3 h.

Zinc (μM)	Relative superoxide anion levels		
	0 h	1 h	3 h
50	1.00 ± 0.00	1.33 ± 0.02*	1.60 ± 0.10*

Value represents means ± S.E.M. of three-independent experiments, *P<0.05 versus non-treated control.

Table 17 Relative hydrogen peroxide levels in time-dependent manner determined by flow cytometry after treatment with zinc ion (50 μM) for 0-3 h.

Zinc (μM)	Relative hydrogen peroxide levels		
	0 h	1 h	3 h
50	1.00 ± 0.00	1.10 ± 0.11	1.06 ± 0.04

Value represents means ± S.E.M. of three-independent experiments, *P<0.05 versus non-treated control.

Table 18 Relative hydroxyl radical level in time-dependent manner determined by flow cytometry after treatment with zinc ion (50 μM) for 0-3 h.

Zinc (μM)	Relative hydroxyl radical levels		
	0 h	1 h	3 h
50	1.00 ± 0.00	1.07 ± 0.09	1.04 ± 0.05

Value represents means ± S.E.M. of three-independent experiments, *P<0.05 versus non-treated control.

Table 19 Relative superoxide anion levels in response to zinc ion and superoxide anion modulators determined by microplate reader after treatment for 3 h.

Treatment	Relative superoxide anion levels
Control	1.00 ± 0.00
Zinc	1.99 ± 0.18*
Zinc+MnTBAP	1.38 ± 0.31#
MnTBAP	1.21 ± 0.58

Value represents means ± S.E.M. of three-independent experiments, *P<0.05 versus non-treated control, #P<0.05 versus zinc ion-treated group.

Table 20 Relative protein levels of EMT markers of H460 cells in response to zinc ion and superoxide anion modulators were determined by western blot analysis after treatment for 24 h.

Treatment	Relative protein levels				
	N-cadherin	E-cadherin	Vimentin	Slug	Snail
Control	1.00 ± 0.00	1.00 ± 0.00	1.00 ± 0.00	1.00 ± 0.00	1.00 ± 0.00
DMNQ	1.15 ± 0.12*	0.29 ± 0.04*	7.83 ± 0.26*	1.19 ± 0.07*	2.94 ± 0.49*
Zinc	1.76 ± 0.08*	0.24 ± 0.03*	10.04 ± 0.35*	1.10 ± 0.02*	3.44 ± 0.70*
Zinc+MnTBAP	0.53 ± 0.02#	1.52 ± 0.09#	4.99 ± 0.39#	0.84 ± 0.02#	0.47 ± 0.02#
MnTBAP	0.41 ± 0.02	1.37 ± 0.08	3.23 ± 0.57	0.81 ± 0.03	0.24 ± 0.10

Value represents means ± S.E.M. of three-independent experiments, *P<0.05 versus non-treated control, #P<0.05 versus zinc ion-treated group.

Table 21 Relative migration level of H460 cells in response to zinc ion and superoxide anion modulators were determined by wound healing assay after treatment for 24 h.

Treatment	Relative migration level
Control	1.00 ± 0.00
DMNQ	1.41 ± 0.13*
Zinc	1.53 ± 0.19*
Zinc+MnTBAP	1.14 ± 0.12#
MnTBAP	1.00 ± 0.07

Value represents means ± S.E.M. of three-independent experiments, *P<0.05 versus non-treated control, #P<0.05 versus zinc ion-treated group.

Table 22 Relative invasion level of H460 cells in response to zinc ion and superoxide anion modulators were determined by transwell invasion assay after treatment for 24 h.

Treatment	Relative invasion level
Control	1.00 ± 0.00
DMNQ	1.31 ± 0.02*
Zinc	1.66 ± 0.25*
Zinc+MnTBAP	1.17 ± 0.09#
MnTBAP	1.16 ± 0.01

Value represents means ± S.E.M. of three-independent experiments, *P<0.05 versus non-treated control, #P<0.05 versus zinc ion-treated group.

Table 23 Relative colony numbers and size of H460 cells in response to zinc ion and superoxide anion modulators were determined by *in vitro* tumorigenicity assay after treatment for 24 h.

Treatment	Relative colony numbers	Relative colony size
Control	1.00 ± 0.00	1.00 ± 0.00
DMNQ	1.87 ± 0.26*	2.51 ± 0.00*
Zinc	2.00 ± 0.25*	2.69 ± 0.24*
Zinc+MnTBAP	1.23 ± 0.08#	1.72 ± 0.10#
MnTBAP	1.25 ± 0.11	1.47 ± 0.44

Value represents means ± S.E.M. of three-independent experiments, *P<0.05 versus non-treated control, #P<0.05 versus zinc ion-treated group.

Table 24 Relative superoxide anion level in response to DMNQ and zinc ion determined by microplate reader after treatment for 3 h.

Treatment	Relative superoxide anion levels
Control	1.00 ± 0.00
DMNQ	1.42 ± 0.09*
Zinc	1.60 ± 0.12*

Value represents means ± S.E.M. of three-independent experiments, *P<0.05 versus non-treated control.

Table 25 Relative protein levels of CSC markers in H460 cells were determined by western blot analysis after treatment with various concentrations of zinc ion for 72 h.

Zinc (μM)	Relative protein levels				
	CD133	ALDH1A1	Oct4	Nanog	Sox2
0	1.00 ± 0.00	1.00 ± 0.11	1.00 ± 0.02	1.00 ± 0.03	1.00 ± 0.04
5	0.89 ± 0.00*	0.75 ± 0.00*	0.89 ± 0.04*	0.30 ± 0.01*	0.75 ± 0.03*
10	0.89 ± 0.05*	0.73 ± 0.12*	0.87 ± 0.01*	0.22 ± 0.02*	0.63 ± 0.02*
25	0.83 ± 0.02*	0.44 ± 0.00*	0.35 ± 0.00*	0.21 ± 0.03*	0.41 ± 0.04*
50	0.44 ± 0.01*	0.36 ± 0.07*	0.20 ± 0.02*	0.10 ± 0.02*	0.27 ± 0.01*

Value represents means ± S.E.M. of three-independent experiments, *P<0.05 versus non-treated control.

Table 26 Relative protein levels of CD133 and ALDH1A1 in CSC-rich population determined by western blot analysis.

Treatment	Relative protein levels	
	CD133	ALDH1A1
H460 WT cells	1.00 ± 0.00	1.00 ± 0.00
CSC-rich cells	3.66 ± 0.02*	2.74 ± 0.07*

Value represents means ± S.E.M. of three-independent experiments, *P<0.05 versus H460 WT cells.

Table 27 Relative spheroid numbers of H460 cells was determined by tumor spheroid assay after treatment with various concentrations of zinc ion for 72 h.

Zinc (μM)	Relative spheroid numbers
0	1.00 ± 0.02
5	0.54 ± 0.05*
10	0.40 ± 0.06*
25	0.22 ± 0.01*
50	0.10 ± 0.02*

Value represents means ± S.E.M. of three-independent experiments, *P<0.05 versus non-treated control.

Table 28 Relative β-catenin level was determined by western blot analysis after treatment with various concentrations of zinc ion for 24 and 72 h.

Zinc (μM)	Relative β-catenin level	
	24 h	72 h
0	1.00 ± 0.12	1.00 ± 0.19
5	0.80 ± 0.07*	0.88 ± 0.11*
10	0.33 ± 0.11*	0.81 ± 0.17*
25	0.33 ± 0.06*	0.69 ± 0.14*
50	0.33 ± 0.01*	0.38 ± 0.10*

Value represents means ± S.E.M. of three-independent experiments, *P<0.05 versus non-treated control.

Table 29 Relative β-catenin level was determined by western blot analysis after treatment with zinc ion in the present and absence of proteasome inhibitor for 24 h.

Treatment	Relative β-catenin level
Control	1.00 ± 0.03
Zinc	0.22 ± 0.04*
Zinc+Lac	0.65 ± 0.07#
Lac	1.00 ± 0.06

Value represents means ± S.E.M. of three-independent experiments, *P<0.05 versus non-treated control, #P<0.05 versus zinc ion-treated group.

Table 30 Relative p-PKCα/ PKCα level was determined by western blot analysis after treatment with various concentrations of zinc ion for 12 h.

Zinc (μM)	Relative p-PKCα/PKCα level
0	0.21 ± 0.03
5	0.37 ± 0.01*
10	0.57 ± 0.08*
25	1.00 ± 0.07*
50	1.28 ± 0.10*

Value represents means ± S.E.M. of three-independent experiments, *P<0.05 versus non-treated control.

Table 31 Relative protein levels of CSC markers in response to zinc ion treatment in the present and absence of PKCα inhibitor were determined by western blot analysis after treatment for 72 h.

Treatment	Relative protein levels					
	CD133	β-catenin	ALDH1A1	Oct4	Nanog	Sox2
Control	1.00 ± 0.06	1.00 ± 0.00	1.00 ± 0.17	1.00 ± 0.00	1.00 ± 0.13	1.00 ± 0.06
Zinc	0.56 ± 0.01*	0.53 ± 0.03*	0.76 ± 0.03*	0.57 ± 0.06*	0.69 ± 0.12*	0.56 ± 0.01*
Zinc+BIM	0.79 ± 0.09#	0.81 ± 0.03#	1.00 ± 0.10#	1.01 ± 0.05#	0.98 ± 0.18#	0.79 ± 0.09#

Value represents means ± S.E.M. of three-independent experiments, *P<0.05 versus non-treated control, #P<0.05 versus zinc ion-treated group.

Table 32 Relative spheroid numbers in response to zinc ion treatment in the present and absence of PKCα inhibitor determined by spheroid formation assay after treatment for 72 h.

Treatment	Relative spheroid numbers
Control	1.00 ± 0.17
Zinc	0.56 ± 0.07*
Zinc+BIM	1.05 ± 0.06#

Value represents means ± S.E.M. of three-independent experiments, *P<0.05 versus non-treated control, #P<0.05 versus zinc ion-treated group.

Table 33 Relative protein levels of CSC markers in response to PKCα activator were determined by western blot analysis after treatment for 72 h.

Treatment	Relative protein levels		
	CD133	β-catenin	ALDH1A1
Control	1.00 ± 0.21	1.00 ± 0.08	1.00 ± 0.21
A23187	0.68 ± 0.08*	0.42 ± 0.12*	0.14 ± 0.02*

Value represents means ± S.E.M. of three-independent experiments, *P<0.05 versus non-treated control.

Table 34 Relative spheroid numbers in response to PKCα activator determined by spheroid formation assay after treatment for 72 h.

Treatment	Relative spheroid numbers
Control	1.00 ± 0.25
A23187	0.62 ± 0.21*

Value represents means ± S.E.M. of three-independent experiments, *P<0.05 versus non-treated control.

Table 35 Relative protein levels of CSC markers in response to zinc ion and superoxide anion modulators were determined by western blot analysis after treatment for 72 h.

Treatment	Relative protein levels				
	CD133	ALDH1A1	Oct4	Nanog	Sox2
Control	1.00 ± 0.07	1.00 ± 0.04	1.00 ± 0.03	1.00 ± 0.04	1.00 ± 0.02
DMNQ	0.65 ± 0.09*	0.71 ± 0.07*	0.31 ± 0.06*	0.13 ± 0.00*	0.60 ± 0.02*
Zinc	0.97 ± 0.15*	0.59 ± 0.05*	0.22 ± 0.05*	0.13 ± 0.00*	0.54 ± 0.16*
Zinc+MnTBAP	1.93 ± 0.14#	0.77 ± 0.03#	0.52 ± 0.22#	0.21 ± 0.01#	1.13 ± 0.04#
MnTBAP	2.46 ± 0.12*	2.42 ± 0.17*	0.28 ± 0.13*	0.55 ± 0.01*	0.95 ± 0.05

Value represents means ± S.E.M. of three-independent experiments, *P<0.05 versus non-treated control, #P<0.05 versus zinc ion-treated group.

Table 36 Relative spheroid numbers in response to zinc ion zinc ion and superoxide anion modulators determined by spheroid formation assay after treatment for 72 h.

Treatment	Relative spheroid numbers
Control	1.00 ± 0.14
DMNQ	0.67 ± 0.09*
Zinc	0.50 ± 0.09*
Zinc+MnTBAP	0.99 ± 0.11#
MnTBAP	0.97 ± 0.05

Value represents means ± S.E.M. of three-independent experiments, *P<0.05 versus non-treated control, #P<0.05 versus zinc ion-treated group.

Table 37 Relative β-catenin level in response to zinc ion and superoxide anion modulators treatment was determined by western blot analysis after treatment for 24 h.

Treatment	Relative β-catenin level
Control	1.00 ± 0.03
DMNQ	0.50 ± 0.03*
Zinc	0.19 ± 0.01*
Zinc+MnTBAP	0.65 ± 0.01#
MnTBAP	0.70 ± 0.02

Value represents means ± S.E.M. of three-independent experiments, *P<0.05 versus non-treated control.

Table 38 Relative p-PKCα/PKCα level in response to zinc ion and superoxide anion modulators treatment was determined by western blot analysis after treatment for 72 h.

Treatment	Relative p-PKCα/PKCα level
Control	1.00 ± 0.10
Zinc	1.64 ± 0.06*
Zinc+MnTBAP	0.69 ± 0.00#
MnTBAP	0.53 ± 0.00*

Value represents means ± S.E.M. of three-independent experiments, *P<0.05 versus non-treated control.

Table 39 Relative protein levels of CSC markers in H292 cells were determined by western blot analysis after treatment with various concentrations of zinc ion for 72 h.

Zinc (μM)	Relative protein levels		
	CD133	β-catenin	ALDH1A1
0	1.00 ± 0.01	1.00 ± 0.14	1.00 ± 0.17
10	0.98 ± 0.04	0.70 ± 0.03*	0.98 ± 0.07
25	0.65 ± 0.01*	0.64 ± 0.08*	0.97 ± 0.17
50	0.52 ± 0.07*	0.30 ± 0.08*	0.91 ± 0.10

Value represents means ± S.E.M. of three-independent experiments, *P<0.05 versus non-treated control.

Table 40 Relative spheroid numbers of H292 cells was determined by tumor spheroid assay after treatment with various concentrations of zinc ion for 72 h.

Zinc (μM)	Relative spheroid numbers
0	1.00 ± 0.05
10	071 ± 0.08*
25	0.39 ± 0.04*
50	0.20 ± 0.04*

Value represents means ± S.E.M. of three-independent experiments, *P<0.05 versus non-treated control.

Table 41 Relative superoxide anion level in dose-dependent manner in H292 cells was determined by microplate reader after treatment for 3 h.

Zinc (μM)	Relative superoxide anion level
0	1.00 ± 0.04
10	1.08 ± 0.05
25	1.10 ± 0.06 *
50	1.21 ± 0.04 *

Value represents means ± S.E.M. of three-independent experiments, *P<0.05 versus non-treated control.

Table 42 Relative p-PKCα/PKCα level in H292 cells were determined by western blot analysis after treatment with various concentrations of zinc ion for 24 h.

Zinc (μM)	Relative p-PKCα/PKCα level
0	1.00 ± 0.00
10	1.98 ± 0.07 *
25	2.82 ± 0.16 *
50	2.83 ± 0.27 *

Value represents means ± S.E.M. of three-independent experiments, *P<0.05 versus non-treated control.

Table 43 Relative protein levels of CSC markers in H23 cells were determined by western blot analysis after treatment with various concentrations of zinc ion for 72 h.

Zinc (μM)	Relative protein levels		
	CD133	β-catenin	ALDH1A1
0	1.00 ± 0.01	1.00 ± 0.07	1.00 ± 0.03
10	0.64 ± 0.01*	0.24 ± 0.02*	0.72 ± 0.05*
25	0.56 ± 0.04*	0.03 ± 0.00*	0.70 ± 0.07*
50	0.31 ± 0.05*	0.01 ± 0.00*	0.35 ± 0.03*

Value represents means ± S.E.M. of three-independent experiments, *P<0.05 versus non-treated control.

Table 44 Relative spheroid numbers of H23 cells was determined by tumor spheroid assay after treatment with various concentrations of zinc ion for 72 h.

Zinc (μM)	Relative spheroid numbers
0	1.00 ± 0.03
10	0.90 ± 0.02*
25	0.48 ± 0.04*
50	0.35 ± 0.05*

Value represents means ± S.E.M. of three-independent experiments, *P<0.05 versus non-treated control.

Table 45 Relative superoxide anion level in dose-dependent manner in H23 cells determined by microplate reader after treatment for 3 h.

Zinc (μM)	Relative superoxide anion level
0	1.00 ± 0.05
10	1.10 ± 0.08
25	1.14 ± 0.04*
50	1.23 ± 0.06*

Value represents means ± S.E.M. of three-independent experiments, *P<0.05 versus non-treated control.

Table 46 Relative p-PKCα/PKCα level in H23 cells were determined by western blot analysis after treatment with various concentrations of zinc ion for 12 h.

Zinc (μM)	Relative p-PKCα/PKCα level
0	1.00 ± 0.00
10	1.76 ± 0.03*
25	2.52 ± 0.04*
50	2.53 ± 0.09*

Value represents means ± S.E.M. of three-independent experiments, *P<0.05 versus non-treated control.

VITA

Miss. Chuanpit Ninsontia was born on August 29, 1985 in Nakhonratchasima. She received her B. Pharm (2nd honor) from the faculty of Pharmacy, Chiang Mai university, Chiang Mai, Thailand in 2006. In 2009, she enrolled in the Master of Science in Pharmacy Program in Pharmacology and Toxicology, Faculty of Pharmaceutical Sciences, Chulalongkorn University, Bangkok, Thailand and received her Master Degree in 2011. In 2013, she entered the Doctor of Philosophy in Pharmacology and Toxicology, Faculty of Pharmaceutical Sciences, Chulalongkorn University, Bangkok, Thailand.